Title
Targeted Therapies for Acute Leukemia

Author
Aldana Masangkay, Grace Idalia

Publication Date
2013

Peer reviewed|Thesis/dissertation

UNIVERSITY OF CALIFORNIA

Los Angeles

Targeted Therapies for Acute Leukemia

A dissertation submitted to the faculty of UCLA

in partial fulfillment of the requirements for the degree

Doctor of Philosophy in Biochemistry and Molecular Biology

by

Grace Idalia Aldana Masangkay

2013

ABSTRACT OF THE DISSERTATION

Targeted Therapies for Acute Leukemia

by

Grace Idalia Aldana Masangkay
Doctor of Philosophy in Biochemistry and Molecular Biology
University of California, Los Angeles
2013

Professor Catherine Clarke, Chair

Small molecules that can disrupt cell signaling by inhibiting protein-protein interactions hold promise for the development of therapeutics against leukemia. This study tested the effect of two compounds, XX-650-23 and tubacin, on cell survival and proliferation of acute myeloid leukemia (AML) and acute lymphoblastic leukemia (ALL) cells, respectively.

The cAMP response element-binding protein (CREB) is a nuclear transcription factor involved in cell proliferation, differentiation, and survival. Phosphorylated CREB recruits histone acetyltransferase, CREB-binding protein (CBP), and subsequent target gene expression occurs. The small molecule XX-650-23, identified through *in silico* screening methods, disrupts the CREB:CBP complex. We tested its effects on various AML cell lines using MTT and trypan blue exclusion assays. XX-650-23 preferentially

targets AML cells, yielding 50 percent inhibitory concentrations (IC50s) ranging from 910 nM to 2.3 μM; we found that it synergizes with cytarabine. XX-650-23 delays the cell cycle in the G1/S phase and downregulates CREB target genes, such as cyclins A and D. Our results suggest that XX-650-23 delays the cell cycle, which stresses the cell, activating caspases involved in apoptosis, as indicated by PARP cleavage of HL60 cells.

Histone deacetylase 6 (HDAC6), which deacetylates α-tubulin, has become a target for developing drugs to treat cancer. Previous studies demonstrated that inhibition of HDAC6 in multiple myeloma (MM) cells results in apoptosis. The small molecule tubacin (a tubulin acetylation inducer) inhibits HDAC6. We observed a higher antiproliferative effect of tubacin in ALL cells than in normal hematopoietic cells. Treatment with tubacin suppresses proliferation in ALL cells, with IC50s ranging from 1.2 μM to 2 μM. We found that it increased acetylation of α-tubulin within 30 minutes of treatment. Our study revealed that tubacin alone inhibits the aggresome pathway, resulting in an accumulation of polyubiquitinated proteins and apoptosis. Furthermore, unlike in MMs, it activated signaling pathways that do not involve JNK/SAP. We demonstrated that it indirectly inhibits the Na^+/K^+-ATPase pump, yielding lower K^+ and higher Ca^+ concentrations in the cytosol. Our results suggest that targeting CREB or HDAC6 alone or in combination with chemotherapy could provide a novel approach to treat AML and ALL, respectively.

The dissertation of Grace Idalia Aldana Masangkay is approved.

_____
Robert Clubb

_____
John Colicelli

_____
Steven Clarke

_____
Kathleen Sakamoto

_____
Catherine Clarke, Committee Chair

University of California, Los Angeles

2013

DEDICATION

I dedicate this dissertation to my beloved family: to my father, Mauricio, who has always wanted the best for me and has motivated me to achieve my professional goals; to my mother, Luz Idalia, who rests in peace due to cancer — Mom, I will contribute to the fight against this disease; to my husband, Reynaldo, for his great love and support during this long academic journey; to my beautiful and wonderful daughters, Grace Gabriella and Daniella Rae, for their words of encouragement that helped me work hard and do my best; to my mother-in-law, Virginia, my sister, Maritza, and my niece, Michelle, for helping me take care of my daughters when I could not give them my attention; to my nephew, Aldo, for his unconditional support when I most needed it; to my aunts and uncles for their love and words of wisdom. To all my sisters, brothers, cousins, and their families for believing in me. Thank you all for your encouragement and love. I love all of you very much, and I could not have done it without God and all of you in my life. We did it!

TABLE OF CONTENTS

LIST OF FIGURES

Chapter 1

Chapter 2

LIST OF TABLES

Chapter 1

ACKNOWLEDGEMENTS

I want to thank my Principal Investigator, Dr. Kathleen Sakamoto, and the members of my doctoral committee, Drs. Catherine Clarke, John Colicelli, Steven Clarke, and Robert Clubb for their valuable guidance throughout my graduate career.

I want to thank Dr. Elliot M. Landaw for his statistical collaboration with the CalcuSyn experiments, Dr. Agustin Rodriguez-Gonzalez for allowing me to work with him in the tubacin project, Dr. Kazuo Okemoto for performing the calcium influx study in the presence of tubacin. Dr. Kazunari Yamada for determining the IC50s of XX-650-23 in MV-4-11 and molm-13 cells. Rongqing Guo for performing the *in vivo* experiments with XX-650-23, Dr. Bryan Mitton and Ritika Dutta for measuring the Renilla luciferase activity of HEK-293T cells transiently transfected with a CRE-*Renilla* luciferase plasmid in the presence of XX-650-23, Dr. Hee-Don Chae for his guidance with the cell cycle analysis of HL60 cells that were treated with XX-650-23. Rachel Ochoa, Elena Bibikova and the rest of the members of the Sakamoto Laboratory for their friendship and time spent discussing my project and potential experiments.

I want to thank my chemistry teacher from LACC, Mrs. Elaine Carter, and my professors from California State University, Los Angeles: Drs. Linda Tunstad, Jamil Momand, Carlos Gutierrez, Scott Grover, and Raymond Garcia for their wonderful mentorship.

Finally, I want to acknowledge the funding sources that made my studies possible during this dissertation: the graduate student minority supplement for NIH grant

(GRS) R01 HL075826 and the Eugene Cota-Robles Fellowship, Chemistry and Biochemistry Department, UCLA.

Vita

2002–2005	B.S., Biochemistry. California State University, Los Angeles, Los Angeles, CA
2005–2007	M.S., Chemistry with option in Biochemistry California State University, Los Angeles, Los Angeles, CA
2007–2009	Eugene Cota-Robles Fellowship University of California, Los Angeles Department of Chemistry
2008–2011	Teaching Assistant University of California, Los Angeles Department of Chemistry Chem 253A (3 quarters) Chem 253B (2 quarters) Chem 153L (1 quarter)
2011–2013	Graduate research supplement (GRS) R01 HL075826
2011	The American Society of Hematology (ASH) Minority Graduate Student Abstract Achievement Award Winner, $1500 prize Abstract #3607, 53rd ASH annual meeting in San Diego, CA

PUBLICATIONS AND PRESENTATIONS

Mitton, B., E.-C., Cho., **Aldana-Masangkay, G. I**., Sakamoto, K. M. *The function of cyclic-adenosine monophosphate responsive element-binding protein in hematologic malignancies.* Leukemia and Lymphoma 2011; 52(11):2057–2063.

Aldana-Masangkay, G. I., Rodriguez-Gonzalez, A., Lin, T., Ikeda, A. K., Hsieh, Y.-T., Kim, Y-.M., Lomenick, Brett., Okemoto, K., Landaw, E., Wang, D., Mazitschek, R., Bradner, J. E., Sakamoto, K. M. *Tubacin suppresses proliferation and induces apoptosis of acute lymphoblastic leukemia cells.* Leukemia and Lymphoma 2011; 52(8):1544–1555.

Aldana-Masangkay, G. I., Sakamoto, K. M. *The Role of HDAC6 in Cancer.* J. Biomed and Biotech. 2011; 2011:875824.

Sakamoto, K. M., **Aldana-Masangkay, G.** *MDC-3100, a small-molecule androgen antagonist, for the oral treatment of prostate cancer.* Drug Profile; in press.

Wu, W. K., Sakamoto, K. M., Milani, M., **Aldana-Masankgay, G**., Fan, D., Wu, K., Lee, C. W., Cho, C. H., Yu, J., Sung, J. J. *Macroautophagy modulates cellular response to proteasome inhibitors in cancer therapy.* Drug Resist Updat. 2010; 13(3):87–92.

A small molecule inhibitor targeting CREB and CBP inhibits proliferation of AML cells in vitro and in vivo. Abstract #3607, 53rd ASH annual meeting in San Diego, CA., 2011.

CHAPTER 1

A Small-Molecule Inhibitor Targeting CREB and CBP Suppresses Proliferation of AML Cells *In Vitro* and *In Vivo*

1-1 Introduction

Leukemia

Leukemia, a cancer of the blood and bone marrow (BM), is characterized by the failure of abnormal cells to differentiate into mature cells. It is a heterogeneous set of diseases with differences in morphology, cytochemistry, immunophenotype, cytogenetics, and molecular abnormalities that may arise from either mutations or gene overexpression [1]. Leukemia can have a lymphoid or myeloid origin and, depending on the rate of cell growth, is classified into four main groups: acute lymphocytic (ALL), chronic lymphocytic (CLL), acute myeloid (AML), and chronic myeloid (CML) [2]. ALL accounts for approximately 75 percent of childhood leukemia, while patients with AML, the most common cancer among adults, have a median age in the late 60s [1–3]. In ALL and AML, an overproliferation of immature blast cells and a reduction of normal

cells in the BM and other organs result in anemia, granulocytopenia, and thrombocytopenia [4].

For the past 20 years, the accepted standard of care for induction treatment against leukemia has been cytarabine, a 2-ß-OH analogue of deoxycytidine, combined with an anthracycline, usually daunorubicin [1, 5]. Cytarabine inhibits DNA synthesis by competitive inhibition of DNA polymerase. It is active against proliferating cells during the S-phase [4]. Daunorubicin inhibits DNA replication by intercalation of base pairs; inhibits topoisomerase II activity, resulting in single- and double-strand DNA breaks; affects regulation of genes expression; and produces free radical damage to DNA [6]. These chemotherapeutic agents target leukemic cells, as well as normal cells, resulting in easy bleeding, immunodeficiency, and infections. In addition, the patients at highest risk can undergo allogeneic stem-cell transplantation [1, 4, 5]. Problems with bone marrow transplantation include recurrent leukemia, graft-versus-host disease, interstitial pneumonitis, and immunodeficiency [4]. Despite the current aggressive chemotherapy treatments and BM transplantation, leukemia has five-year event-free survival rates of approximately 80 percent in pediatric ALL, almost 60 percent for childhood AML, and 20 percent in adults with AML [3]. These statistics demonstrate the need to develop new drugs, new targets, and new approaches.

The role of CREB transcription factor in AML

Acute leukemia develops as a consequence of a combination of genetic mutations that alter proliferation, differentiation, and survival functions that, in turn, can lead to loss of apoptosis in cells and culminate in leukemic transformation. The most

frequent targets of chromosomal translocations in AML are genes that encode transcription factors [7]. These transcription factors play an essential role in normal cellular behavior; they integrate extracellular signals that help regulate gene expression, and alterations in their functions have been observed to contribute to AML [3, 8]. Cyclic-AMP-response element-binding protein (CREB) is a nuclear transcription factor that was first observed to contribute to cancer due to a chromosomal t(12;22)(q13;q12) translocation in clear cell sarcomas of soft tissue. This chromosomal translocation yields a constitutively active fusion protein — Ewing's sarcoma fused with the C-terminal DNA-binding domain of ATF1 (EWS-ATF1) — that binds to the promoters of CREB target genes [9].

CREB was also found to contribute to AML. Previous studies in our lab found an overexpression of CREB in the majority of tissue samples from leukemia patients with ALL and AML. This result was associated with an increased risk of relapse and worse prognosis for event-free survival in AML patients [10, 11]. CREB transgenic mice developed myeloproliferative disease after one year, but CREB by itself was not sufficient to cause acute leukemia [11]. Our previous studies also showed that CREB stimulates abnormal proliferation and survival of myeloid cells *in vitro* and *in vivo* through upregulation of cyclin A1 [11, 12]. Cyclins A and D are both CREB target genes involved in the regulation of G/S transition [13, 14]. In a liquid culture, CREB downregulation in the TF-1 and K562 AML cell lines decreased proliferation and fewer cells reach the S phase; this finding correlated with a decrease in the expression of cyclins A1 and D [11]. Furthermore, CREB knockdown *in vitro* and *in vivo* inhibits leukemic progression without affecting normal hematopoietic stem cell function [15].

These findings indicate that CREB acts as a proto-oncogene, making it a potential target to treat AML patients [11, 12, 15].

Characteristics of CREB

The CREB belongs to the ATF/CREB family of proteins. It is expressed and conserved in most tissues as a 43 KDa basic/leucine zipper (bZIP) nuclear transcription factor that regulates proliferation, differentiation, and survival of a variety of cells, including neuronal and hematopoietic cells [11, 16–19]. In humans and mice, the CREB contains 11 exons, with an alternative splicing of one exon that encodes the α peptide, yielding CREBΔ or CREBα. CREB also has another main isoform, CREBβ, that contains alternative splicings of several 5' exons, yielding a CREB protein that lacks the first 40 residues of the other two main isoforms. All three forms are ubiquitously expressed in all tissues and can activate CRE-dependent transcription in response to high levels of cAMP [16, 19].

CREBs bind constitutively as dimers to promoters that contain CREs that can be either palindromic (TGACGTCA) or half-site (TGACG or CGTCA) sequences [20–22]. The Kd of the CREB-CRE interaction has been reported to range from 1 to 180 nM [16]. Structural studies of the CREB bZIP domain-CRE complex reveal that the bZIP domain folds into a continuous single helix [19]. The CREB DNA-binding domain contains basic domain residues asparagine 293 (Asn293) and arginine 301 (Arg301) that are critical for base recognition. Dimerization between CREB family members is promoted by intersubunit salt bridges and hydrogen-bonded interactions [19].

Genome-wide approaches have revealed the presence of CREB in approximately 4,000 promoter sites *in vivo*, depending on the methylation state of CREs near the promoter. In transformed human embryonic kidney 293 (HEK293T) cells, CRE methylation frequency was 70 percent in intergenic regions, where CREB is considered nonfunctional, and 20 percent in promoters. CREB occupied most unmethylated CREs at the promoter in HEK293T cells; this finding indicates that DNA methylation restricts CREB binding in the genome [23]. CREB-binding sites are most active when close to the TATA box [19].

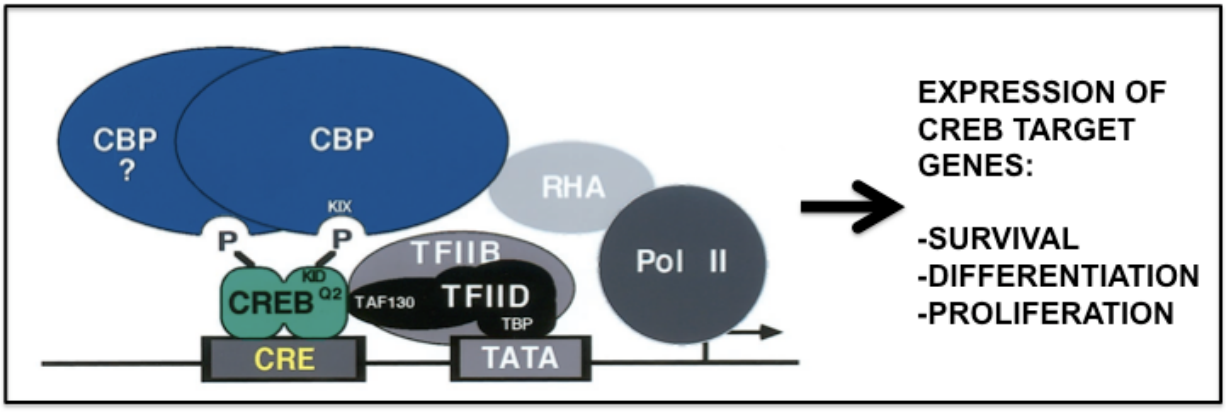

Figure 1.1. Activation of CREB leads to CBP recruitment and stabilization of RNA polymerase II. CREB is constitutively bound to the CRE element of a CREB target gene. Downstream from CRE, the TATA box binds transcription factors that interact with the Q2 domain of CREB, generating basal transcription. Phosphorylation of Ser133 in the KID domain induces the recruitment and binding of CBP through its KIX domain. Whether CBP binds as a dimer remains unclear. CBP can stabilize RNA polymerase II indirectly through RNA helicase A (RHA) and induces expression of CREB target genes involved in survival, differentiation, and proliferation (adapted from [16]).

CREB contains an amino-terminal transactivation domain (TAD) and a carboxy-terminal basic leucine zipper (bZIP) DNA-binding and dimerization domain. TAD contains a 60-amino-acid kinase-inducible domain (KID) which contains the PKA phosphorylation site (RRPSY) and a glutamine-rich (Q2) constitutive activation domain.

Q2 is involved in basal transcription, and KID plays a key role in induced phosphorylation-dependent transcription [16, 24, 25].

Activation of CREB leads to binding with CBP

Phosphorylation of CREB at serine 133 (Ser133) in the KID domain promotes the association with transducers of regulated CREB activity (TORCs), the KIX domain of CREB-binding protein (CBP), and its paralog p300. CBP is a 265-kDa nuclear coactivator that stimulates transcription by modulating chromatin through histone acetylation and the recruitment of RNA polymerase II complexes [16, 26–28] (**Fig. 1.1**).

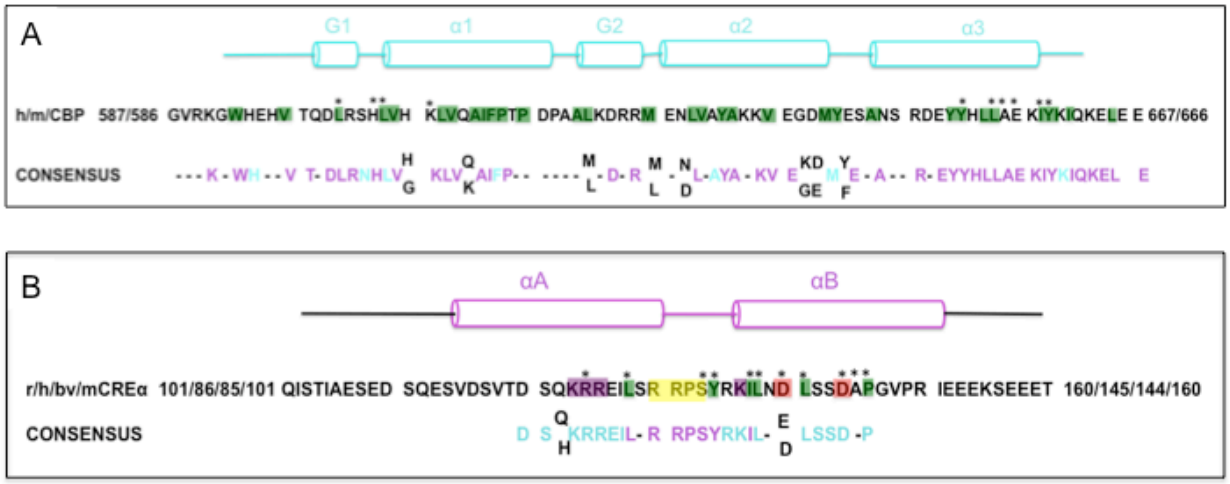

Figure 1.2. Sequence alignments of KIX-CBP and pKID-CREB domains. Alignments of **(A)** KIX and **(B)** pKID domain sequences from different species (prefix abbreviations: bv for bovine; h, human; m, mouse; r, rat). KIX and pKID coding: green: conserved hydrophobic residues; stars: residues involved in the interaction between KIX and pKID; purple: conserved basic residues; red: acidic residues; yellow: residues that form the invariant phosphorylation motif. Consensus sequences color coding: purple: invariant residues; cyan: positions that are invariant in 70% of the cases; black: positions always occupied by either one of two residues. Alignments were performed using the program BLAST for protein sequences in the NCBI database (adapted from [28]).
*Reprinted by permission from Nature Publishing Group: [Nature], **(401)**, copyright (1999).*

P-CREB requires the core KIX domain, a 94-residue sequence, for interaction and transcriptional activation [16, 29, 30]. The KIX and KID domains are highly conserved among mice, rats, humans, and other species [28] (**Fig. 1.2**).

CREB is the first transcription factor whose activity was shown to be regulated by phosphorylation [19]. Phosphorylation at Ser133 may be mediated by serine-threonine kinases, including cAMP-dependent protein kinase A (PKA), protein kinase C (PKC), and calcium- and calmodulin-dependent kinases. Protein kinase B/AKT, mitogen- and stress-activated protein kinase (MSK-1), and pp90 ribosomal S6 kinase (pp90 RSK) [16, 31, 32]. Neurotransmitters and growth factors, such as the granulocyte macrophage colony-stimulating factor (GM-CSF), can also induce phosphorylation [11]. The GM-CSF and interleukin-3 (IL-3) can stimulate the proliferation and maturation of myeloid progenitor cells and can also induce transcription of the early growth response-1 gene (egr-1) [33]. The GM-CSF induces phosphorylation of CREB by pp90RSK in human myeloid cell line TF-1 [17, 33, 34]. The activation of CREB and its association with CBP leads to the transcription of more than 5000 genes, including the proto-oncogene c-Fos and other genes involved in the cell cycle, growth survival, and such neuronal activities as memory and learning [35].

Interaction between the PKID of CREB and the KIX domain of CBP

The structure of the CREB:CBP complex reveals that the KIX domain folds into a three-helix structure, where α1 and α3 are nearly parallel to each other and form a shallow hydrophobic groove that interacts with the KID domain (**Fig. 1.3**) [19, 28, 36].

The critical hydrogen bond between phosphorylated Ser133 (pSer133) with tyrosine 658 (Tyr658) and an ion pair with lysine 662 (Lys662) of the KIX domain induce a coil-to-helix folding transition in the KID domain that further stabilizes the complex through interactions with the hydrophobic groove in the KIX domain [28]. Helices αA and αB are arranged at an angle of approximately 90°, and the amphipathic αB contains the critical pSer133 and performs most of the interactions with KIX [28]. A surface distal to the CREB-binding site of KIX includes a critical residue, arginine 600 (Arg600), that is required for the CREB:CBP complex. Mutagenesis of Arg600 to glutamine (Gln) and methylation of KIX at Arg600 by the methyltransferase CARM1/PRMT4 reduce complex formation [30, 37].

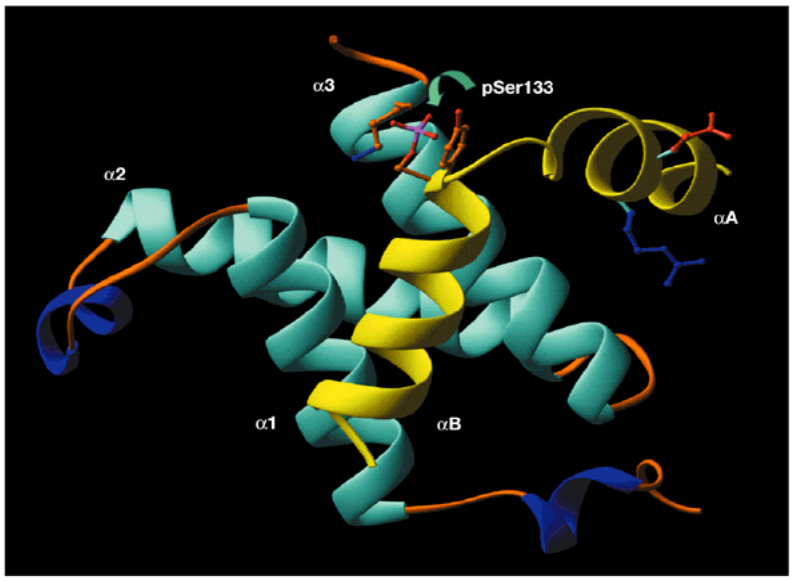

Figure 1.3. The KID-CREB:KIX-CPB complex interaction. Upon binding to the KIX domain (cyan), the pSer133-KID domain (yellow) undergoes a structural change from a coil to helix conformation, yielding two helices, αA and αB, that are positioned almost perpendicular to each other. The KIX domain consists of three helices, α1–α3. Helices 1 and 3 form a hydrophobic groove that makes most contacts with the amphipathic αB. Ser133 forms an ion pair with Lys662 and a hydrogen bond with Tyr658 in KIX (adapted from [19]).
*Reprinted by permission from Nature Publishing Group: [Nature Reviews Molecular Cell Biology], **(2)**, copyright (2001).*

XX-650-23 inhibits the CREB:CBP complex

An NMR-based screening approach for compounds that bind to KIX was performed by using a preselected small-molecule library of 762 compounds identified KG-501 (2-napthol-AS-E-phosphate), a compound that targets the surface distal to the CREB-binding site that includes Arg600 [38]. The preselected library had been used previously to discover ligands and to identify binding sites. The samples were ranked according to the extent of amide chemical shift changes, using 2D ^{15}N-^{1}H heteronuclear single quantum coherence spectra that monitored compound binding to ^{15}N-labeled KIX. We found that KG-501 significantly affected the backbone amides at sites along helices 1 and 2 and the area containing the Arg600 (**Fig. 1.4**).

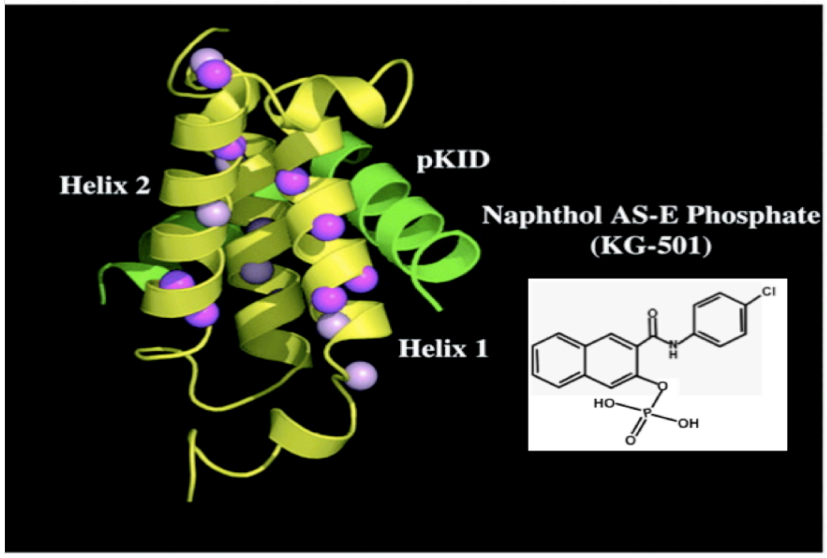

Figure 1.4. 2D ^{15}N-^{1}H heteronuclear single quantum coherence spectra of CREB:CBP complex in the presence of KG-501. KG-501 shifts the backbone amide (purple spheres) along helices 1 and 2 of the KIX domain (yellow). It also shifts Lys662 and Arg600, critical amino acids involved in CREB binding. The pKID domain of CREB is displayed in green. Inset: the molecular structure of KG-501 (adapted from [38]).
*Reprinted by permission from National Academy of Sciences of the USA: [National Academy of Sciences], **(51)**, copyright (2004).*

KG-501 affected the KIX domain and downregulated CREB target genes. *In vitro* binding assays using purified recombinant phospho-CREB and GST-KIX protein revealed that KG-501 disrupted the binding of phospho-CREB to KIX, with a K_i of approximately 90 μM. KG-501 also disrupted the CREB:p300 — without, however, inhibiting its histone acetylation (HAT) activity. TORCs bind to the leucine zipper region of CREB, which has no sequence similarity with KIX; KG-501 was found not to inhibit TORCs. Together, these results indicated that KG501 acts specifically on the KIX domain [38]. We also found that KG-501 inhibits CREB target genes, such as NR4A2, αCG, c-Fos, and RGS2. *In vivo* mammalian two-hybrid assays revealed a CREB-dependent transcription K_i of about 10 μM [38].

Dr. Xiao and colleagues [39] found that the huge discrepancy between the K_i values was due to KG-501 undergoing *in situ* dephosphorylation, yielding napthol AS-E (**Fig. 1.5**), a cell-permeable compound. Using a *Renilla* luciferase (RLuc) complementation assay — with the C-terminal RLuc fragment fused to the KIX and KID fused to the N-terminal fragment of RLuc via a flexible linker — they found that napthol AS-E inhibits the CREB:CBP. In HEK-293T cells, napthol AS-E was found to inhibit RLuc with an IC50 of 2.26 $\pm$ 0.65 μM. An *in vitro* assay using a His_6-tagged RLucC-KIX protein was expressed and purified from *E. coli*, and phosphorylated KID-RLucN was expressed from HEK293T cells. Crude cell lysates were used for the complementation study and luciferase activity was decreased with an IC50 of 2.90 $\pm$ 0.81 μM. Dr. Xiao and colleagues [39] observed no significant inhibition with KG-501 at concentrations of up to 50 μM. In order to increase the solubility of napthol AS-E, the chloride (Cl) was

replaced with a cyano (CN) functional group, yielding XX-650-23 with a molecular weight of 288.3 g (**Fig. 1.5**).

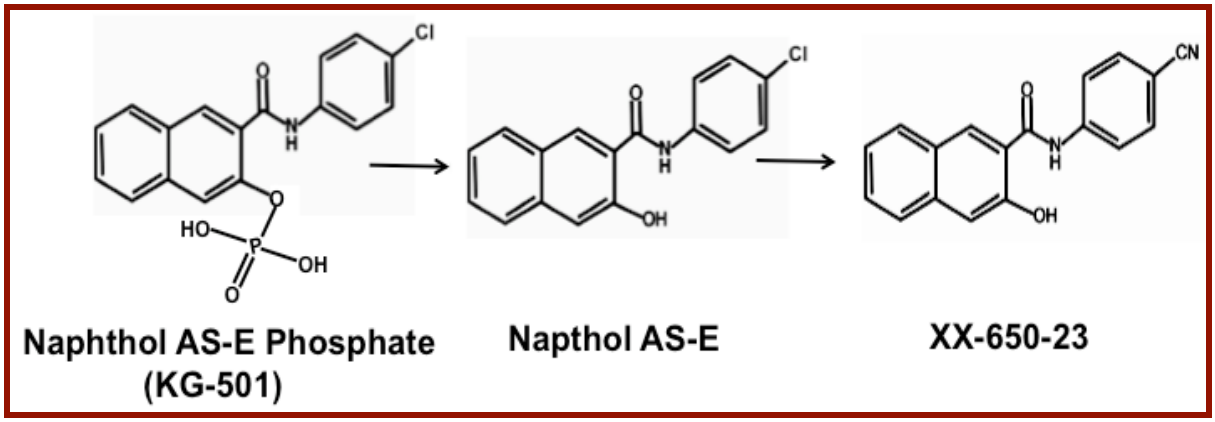

Figure 1.5. Molecular structures of KG-1, napthol AS-E, and XX-650-23. *In situ* dephosphorylation of KG-501 and replacement of the chloride group by a cyano group yields XX-650-23.

Our laboratory has tested the *in vivo* effects of XX-650-23 using xenograft NOD-SCID IL-2Rgamma null (NSG) mouse models (unpublished data). To assess toxicity, mice were treated with the drug at various concentrations, ranging from 10 to 20 mg/kg, by intraperitoneal (ip) injection once daily for 28 days. We did not observe any weight loss or hematologic, renal, hepatic, or cardiac toxicity in the mice. We also performed pharmacokinetic analysis to determine the half-life and stability of the drug. After one hour of treatment, the serum drug concentration was 33 nM. The estimated drug mean residence time was 7.5 hours. The plasma clearance divided by the ip injection absorption fraction was 9.6 L/minute/kg. We treated the mice daily with drug (17.5 mg/kg ip injection) or vehicle control once MV-4-11 cells reached a tumor size of 300 mm^3 or at the time cells were injected. Our results demonstrated significant inhibition of tumor growth when the drug treatment started on the day of injection of cells, compared to waiting until the tumor reached 300 mm^3. Together, these data suggest that a small-

molecule inhibitor targeting CREB and CBP interaction has potential as an avenue for drug development.

Hypothesis

XX-650-23 inhibits CREB:CBP interactions, resulting in the decreased survival and proliferation of AML cells.

Specific aims

Specific aim #1: To investigate whether XX-650-23 inhibits the growth and affects the survival of human AML cell lines and patient BM samples.

Specific aim #2: To determine whether combining XX-650-23 with other chemotherapy drugs produces synergistic, additive, or antagonistic effects in AML cells.

Specific aim #3: To ascertain whether XX-650-23 disrupts the pKID-CREB:KIX-CBP interactions in AML cells.

1-2 Overview of Experimental Design

Specific aim #1: To investigate whether XX-650-23 inhibits the growth and affects the survival of human AML cell lines and patient BM samples.

Previous work in our laboratory demonstrated the overexpression of CREB in the majority of BM samples with acute leukemia [10–12]. We also found that transduction of primary human stem cells or myeloid leukemia cells with lentiviral CREB shRNAs resulted in decreased proliferation [11]. KG-501 was identified as inhibiting the KID-KIX interaction, and this effect led to the reduced transcription of CREB target genes, such as the c-Fos oncogene [38]. The dephosphorylated form of KG-501 was further modified by replacing the chloride group with a cyano functional group, yielding a potent and more soluble compound, XX-650-23. RLuc complementation studies revealed an *in vitro* IC50 of 3.2 + 0.28 μM and an *in vivo* IC50 of 3.2 + 0.43 μM in HEK-293T cells (Xiao et al., unpublished data). XX-650-23 was also observed to have an effect on MCF7 and HeLa cells with lower IC50s (Xiao et al., unpublished data). We wanted to determine whether XX-650-23 would lead to cell growth inhibition in human AML cells.

Methods for aim #1

HL60 and KG-1 cells were treated with 0.1 percent DMSO or increasing concentrations of XX-650-23, ranging from 100 pM up to 10 μM, for 48 or 72 hours to determine the potential half maximal inhibitory concentration (IC50). Cell viability was calculated as the number of viable cells divided by the total number of cells. Trypan blue exclusion assay was performed to measure cell viability. Live cells possess intact cell membranes and

exclude the trypan blue dye. Those cells that take up trypan blue have compromised cell membranes and are considered nonviable — they turn blue. We used an automated cell counter, the Vi-CELL XR Cell Viability Analyzer from Beckman Coulter, to count the AML cell lines. Alternatively, we could have used the AlamarBlue assay, which incorporates a fluorometric/colorimetric oxidation-reduction (REDOX) indicator, to measure the metabolic activity of living cells. This assay reduces oxidized resazurin (nonfluorescent, blue) to resorufin (fluorescent, red). The fluorescence or change in color is proportional to the number of living cells.

Frozen BM samples from normal, AML, or relapsed AML patients were grown in methylcellulose and treated with XX-650-23. The colonies were scored on day 14 for granulocyte macrophage colony-forming units. Alternatively, frozen BM samples could have been grown in liquid media supplemented with cytokines, treated with XX-650-23, and counted after 48 or 72 hours. Cells were counted by trypan blue exclusion using the hemacytometer.

Expectations for aim #1:

We expected XX-650-23 to inhibit cell growth of AML cell lines, patient AML, and relapsed AML BM samples. We hoped to see a therapeutic index between normal BM and AML samples. Growth of AML cell lines in liquid media is a well-established standard procedure, so we did not expect to have a problem. AML BM samples may not form well-distinguished colonies in methylcellulose; therefore, AML BM samples were also grown in liquid media supplied with cytokines. Because XX-650-23 could have

proven not very soluble in methylcellulose, we also treated normal BM cells in liquid media.

Specific aim #2: To determine whether combining XX-650-23 with other chemotherapy drugs produces synergistic, additive, or antagonistic effects in AML cells.

Cytarabine is the backbone of AML therapy; however, since using a single agent in relapsed and refractory AML lacks efficiency, finding other agents to combine with it is of great interest. Currently, combining cytarabine with daunorubicin is considered the most effective induction chemotherapy treatment against AML. A course of three days of daunorubicin and seven days of cytarabine (3 + 7) is the standard accepted induction, yielding complete remission in 45 to 65 percent of older patients [1, 5]. However, most of those patients relapse, and only 20 percent will be cured of the disease [3]. We wanted to determine whether XX-650-23 would improve the effect of cytarabine or daunorubicin in AML cells.

Methods for Aim #2:

We determined the IC50 of XX-650-23, cytarabine, and daunorubicin in KG-1 and HL60 cells by treating the cells with escalating concentrations of XX-650-23. Once the IC50s were found, we planned to make an eightfold mixture of the IC50s of each drug and then to perform a series of dilution (8X, 4X, 2X, 1X, 0.5X, 0.25X and 0.125X). For the combination studies, XX-650-23 was combined with cytarabine or daunorubicin to make the eightfold mixture, followed by a series of dilutions. We plated the drug alone

or in combination and treated cells in parallel so that the number of cells and the drug concentrations were constant. After incubating for 48 or 72 hours, the cells were counted by trypan blue exclusion using the Vi-CELL automated cell counter. We then calculated the fraction affected and used those values to obtain the isobolograms and combination indices (CI) using the CalcuSyn software program (BIOSOFT). The CI provides a value that correlates with the effects of a combination treatment. The CI is defined as 1 if the drug is additive. A CI of less than 1 indicates synergy, and anything above 1 indicates antagonism between the two agents.

Expectations for Aim #2:

If XX-650-23 inhibited cell growth, it seemed possible that it behaves synergistically or additively with cytarabine or daunorubicin.

Specific Aim #3: To ascertain whether XX-650-23 disrupts the KIX-CBP:pKID-CREB interactions in AML cells.

We monitored the formation and potential XX-650-23-mediated disruption of the CREB:CBP complex in AML cells and determined whether this effect led to a decrease in transcriptional activity. KG-501 is a small-molecule compound that was found to inhibit the pKID-CREB:KIX-CBP *in vitro* and *in vivo* and to downregulate CREB target genes [38]. Replacing the chloride in the dephosphorylated form of KG-501 with a cyano group yielded XX-650-23. The more soluble XX-650-23 was also found to inhibit the pKID-CREB:KIX-CBP complex using a RLuc complementation assay in HEK-293T cell lysate extracts (Xiao et al., unpublished data). We perfomed RLuc activity assays

and immunoprecipitation (IP) studies to determine whether XX-650-23 disrupts the CREB:CBP complex.

Methods for Aim #3:

We planned to transfect or electroporate a plasmid containing a CRE site upstream from a TATA box promoter and a RLuc gene into AML cells. Electroporation uses short high-voltage pulses to produce temporary pores in the cell membrane through which foreign DNA can pass into the cells. We wanted to measure the RLuc activity and, if detected, to treat the electroporated cells with vehicle or XX-650-23. Alternatively, we could subclone a single CRE site upstream of a TATA box promoter and a RLuc reporter gene into a construct expressing mCherry under a CMV promoter. The CRE-RLuc construct would be transfected into HEK-293T cells along with a second generation lentiviral packaging system. The virus would then be used to transduce AML cells. We planned to treat transduced AML cells with 0.1 percent DMSO or with the IC50 of XX-650-23 and to perform the RLuc assay in order to measure CBP binding activity. Upon CBP recruitment, transcription of RLuc would be activated. RLuc protein catalyzes the oxidation of coelenterazine, producing light that is proportional to the transcriptional activity of CREB.

The expression of CREB and CBP in AML cells was investigated by Western blot (WB) analysis or qRT-PCR. Total AML cell extracts from previously treated and nontreated cells was used for IP studies to determine whether XX-650-23 disrupts the CREB:CBP complex. Alternatively, we could nucleofect AML cells with a CBP-expressing plasmid containing neomycin resistance. After sorting the neomycin-

resistant cells, we treated the cells with 0.1 percent DMSO or XX-650-23 and then performed an IP with total lysate. In order to concentrate the levels of CBP, we could also have performed an IP with the nuclear extraction lysate.

Expectations for Aim #3:

Using conventional methods in the transfection or electroporation of such suspension cells as HL60 or KG-1 AML has proven to be a difficult task. Although working with viruses is a lengthier and riskier method, we expected transduced AML cells to be functional for the RLuc studies. We expected XX-650-23 to decrease the RLuc activity, indicating that the CREB:CBP complex was disrupted.

Finding limited levels of CBP in AML cells might prevent using IP to identify the CREB:CBP complex. An alternative method would involve nucleofecting a CBP-expressing plasmid into AML cells, confirming the presence of CBP in cell lysates by WB, and determining binding of the complex by IP. Once having identified the complex, we would treat the cells with vehicle or XX-650-23 and perform IP studies.

1-3 Materials and Methods

Determination of XX-650-23, cytarabine, and daunorubicin IC50s in KG1 and HL60 cells

KG1 and HL60 cells were obtained from the American Type Culture Collection (ATCC; Manassas, VA) and maintained with Iscove's Modified Dulbecco's Medium (IMDM; Gibco, Carlsbad, CA) supplemented with 10 percent fetal bovine serum (FBS; Fisher Scientific, Fair Lawn, NJ) and 1X penicillin/streptomycin/glutamine (P/S/G; Gibco). Our experiments used cell passage numbers from 5 to 10. KG1 and HL60 cells were plated at 1 x 10^5 cells/mL and 3 x 10^5 cell/mL, respectively, into 24-well plates overnight at 37 °C in the presence of 5 percent CO_2. All experiments were performed in triplicate. The next day, the cells were treated with 0.1 percent DMSO (Sigma-Aldrich, St. Louis, MO) or with different concentrations of XX-650-23, cytarabine, or daunorubicin ranging from 100 pM to 20 μM. The final DMSO concentration was kept at 0.1 percent. The cells were incubated for 48 hours at 37 °C in the presence of CO_2. Cell count was performed by trypan blue exclusion using an automated cell counter, the Vi-CELL XR Cell Viability Analyzer (Beckman Coulter, Inc., Brea, CA). We analyzed the data with Microsoft Excel version 12.3.0 (Microsoft Corporation) and then with GraphPad Prism version 5.04 for windows (GraphPad Software, La Jolla, CA, USA), using a variable slope sigmoidal dose-response model to provide initial estimates of the the IC50s.

AML cell line drug combination studies

We performed experiments with drugs singly and in combination on the same day. AML cell lines were plated and maintained as before. Single drug serial dilutions were prepared to yield eight, four, two, one, 0.5, 0.25, and 0.125 times their IC50. We also prepared a mixture of two compounds (XX-650-23 with either cytarabine or daunorubicin), consisting of eight times the IC50s of each drug, followed by a series of dilutions (8X, 4X, 2X, 1X, 0.5X, 0.25X, 0.125X). After 48 hours, the cells were counted by trypan blue exclusion using the Vi-CELL XR Cell Viability Analyzer (Beckman Coulter). The observed fraction affected (fa) was calculated as 1 - fraction unaffected, the number of live cells with drug treatment/number of live cells with 0.1 percent DMSO). Each experimental run yielded three sets of fa values as a function of concentration (one for each drug alone and a third for the combination). The maximum possible biological effect was estimated by the common plateau the observed fa values approached as concentrations increased. This was done by a nonlinear regression procedure to fit simultaneously three separate variable slope sigmoidal dose-response models having a common asymptote to the combined fa data set. For subsequent analysis each observed fa value was divided by the asymptote to yield a normalized fa representing the fraction of the maximum possible biological effect. Combined index (CI) values were obtained with CalcuSyn version 2.1 software (Biosoft, Cambridge, UK), using the statistical assumption of mutually exclusive modes of action: $CI=[(D)_1/(D_x)_1] + [(D)_2/(D_x)_2]$, where $(Dx)_1$ and $(Dx)_2$ are the concentrations of each drug alone that yield normalized fraction affected x and $(D)_1$ and $(D)_2$ are the corresponding drug concentrations when present together as a combination that produce the same effect.

Specifically, CI<1, CI=1, and CI>1 indicate synergistic, additive, or antagonistic effects between two agents, respectively, and the CI values were typically estimated for x=0.50, 0.75 and 0.90 As an alternate approach to confirm the CalcuSyn results and provide appropriate asymptotic standard errors [40] the nonlinear regression procedure for normalizing the fa data was also used to estimate CI as a function of the sigmoidal model parameters. For graphical interpretation, isobolograms were computed with CalcuSyn under the assumption of mutually nonexclusive modes of action: $CI=[(D)_1/(D_x)_1] + [(D)_2/(D_x)_2] + [(D)_1(D)_2/((D_X)_1(D_X)_2)]$. These isobolograms are slightly conservative for detecting synergy because the iso-effect line or line of equivalency (the curve showing all combinations of two drugs interacting additively that have the same normalized fa) is based on assuming completely independent modes of drug action.

Effect of XX-65-23 in normal human BM plated in methylcellulose

Tubes containing methylcellulose-based media (Methocult; Stemcell Tech, Vancouver, BC, Canada) were treated with either 0.1 percent DMSO or escalating concentrations of XX-650-23, separately, and vortexed vigorously. Frozen normal BM sample was thawed and resuspended in media to yield a final concentration of 1.0×10^4 cells/mL in methylcellulose. Each methylcellulose tube was divided into two 1.2 mL aliquots and plated into BD Falcon tissue culture dishes. We performed the experiments in duplicate (using two methylcellulose tubes) and scored the colonies on day 14 for granulocyte macrophage colony-forming units.

Effect of XX-650-23 in patient AML BM, relapsed AML BM, and normal BM cells plated in liquid media

Human BM samples were collected following procedures approved by the IRBs at UCLA (98-09-036-24) and Stanford University (11062). Frozen BM samples were thawed at 37 °C and diluted with IMDM media containing 20 percent FBS and 1X P/S/G. The BM cells were resuspended with IMDM media containing 20 percent FBS, 1X P/S/G (Gibco), 50 ng/mL human stem cell factor (hSCF), 20 ng/mL human recombinant granulocyte macrophage colony-stimulating factor (hGM-CSF), 20 ng/mL human granulocyte-colony stimulating factor (hG-CSF), 20 ng/mL human interleukin 3 (hIL-3), and 10 ng/mL hIL-6 (growth factors and cytokines purchased from R&D Systems, Minneapolis, MN). The BM cells were plated at 2 to 3 x 10^6 cells/mL into a 24-well plate. After 48 hours of incubation at 37 °C in the presence of CO_2, the BM cells were plated at 1 x 10^5 cells/100 uL into a 96-well plate and treated with 0.1 percent DMSO (control) or different concentrations of XX-650-23 for 72 hours. We used Prism software to calculate the P values, where *=P<0.05, **=P<0.01, and ***=p<0.0001.

PHASE-CMV-mCherry-CRE-RLuc and PHASE-CMV-mCherry-RLuc constructs

Polymerase chain reaction (PCR) of CRE-RLuc and RLuc fragments were performed using the primers shown in Figure 1.13 for CRE-RLuc. The same reverse primer was used to amplify the RLuc sequence, along with the forward primer: 5'-ATTGGATCCCCATGGGCACTTCG-3'. Both PCR fragments and the PHASE-CMV-mCherry vector were double digested using BAMHI-HF and ClaI restriction enzymes

with buffer 4 (New England BioLabs, Inc., Ipswich, MA) for one hour at 37 °C, followed by restriction enzyme inactivation at 65 °C for 20 minutes. After digestion, the PHASE-CMV-mCherry vector was purified by gel extraction purification, using the PureLink Quick Gel Extraction Kit (Invitrogen, Carlsbad, CA). The purified vector was dephosphorylated using Antarctic Phosphatase (New England BioLabs). The digested PCR fragments were purified using the PureLink PCR Purification Kit (Invitrogen). Ligation (ratio of vector to insert used = 1:3) was performed using T4 DNA ligase (New England BioLabs) at 16 °C for 16 hours. Stbl3 chemically competent *E. coli* bacteria (Invitrogen) were transformed by ligation reaction. The ligation reaction was incubated on ice for 30 minutes, heat shocked at 42 °C for 30 seconds, and incubated on ice for two minutes. S.O.C. medium (Invitrogen) was added to the reaction and allowed to shake vigorously at 225 rpm for one hour at 37 °C. The transformation reaction was plated onto Luria broth agar plates supplemented with ampicillin (100 ug/mL) and incubated at 37 °C overnight. Colonies were picked, and miniprep was performed using the EZgene Plasmid DNA Purification System (Bioland Scientific LLC., Cerritos, CA). Constructs were analyzed on an 0.8 percent agarose gel and sequenced at the sequencing facility of Molecular Cloning Laboratories (MCLAB, San Francisco, CA). Purification of the correct constructs was performed using the Plasmid Maxiprep Kit (Bio-Rad, Hercules, CA).

Quantitative RT-PCR of CBP and CREB

KG-1 or HL60 cells (5 x 10^6 cells) were plated overnight at 37 °C in the presence of CO_2. Total RNA was isolated using TRIzol reagent (Invitrogen) according to the manufacturer's protocol. Reverse transcription was performed using the iScript cDNA Synthesis Kit for RT-PCR (Bio-Rad). Total RNA (1.5 ug) was reverse transcribed from each sample, and one-tenth of it was used as a template for quantitative (q)RT-PCR reaction using SYBR Green (Bio-Rad) and the following specific primers — human CBP primers: 5'-CCACGTCCCTTAGTAACCAG-3'and 5'-CCAAGTGTCCCTGATCTATG-3', obtained from Yu et al. [41], and human CREB primers: 5'-GTATATTGCCATTACCCAGGGAG-3' and 5'-CTGCTGCATTGGTCATGGT-3'. The data was analyzed using the standard curve method and normalized against β-actin.

Western blot for CREB expression

AML and HeLa cells (6 x 10^6 cells) were harvested at 1000 rpm for five minutes at room temperature, washed with PBS, and lysed in ice-cold radio-immunoprecipitation assay (RIPA; 50 mM Tris-HCl, pH 8.0, with 150 mM sodium chloride (Both chemicals were purchased from Fisher Scientific), 1.0 percent IGEPAL CA-630 (NP-40; Sigma, St. Louis, MO), 0.5 percent sodium deoxycholate, and 0.1 percent sodium dodecyl sulfate), containing Protease Inhibitor Cocktail and Phosphatase Inhibitor Cocktail 2 (All purchased from Sigma-Aldrich). Protein quantification was measured using the bicinchoninic acid assay (BCA) Protein Assay Kit (Thermo Scientific, Rockford, IL). HeLa (25 ug) and AML (200 ug) lysates were boiled in SDS-Laemmli buffer for five

minutes and separated on SDS-polyacrylamide gel (SDS-PAGE). Protein transfer was performed at 1.2 Amp overnight, at 4 °C. Nitrocellulose membrane (Whatman, Dassel, Germany) was blocked with 5 percent dry nonfat milk, resuspended in Tris-buffered saline containing 0.05 percent Tween-20 (Sigma-Aldrich) (TBS-T buffer) for one hour at room temperature, and immunoblotted with anti-CREB (1:1000; Millipore Corp., Billerica, MA) antibody in TBS-T with 5 percent BSA overnight at 4 °C. After washing the membrane three times with TBS-T, we incubated the membrane with goat anti-rabbit IgG (H&L) and horseradish peroxidase (HRP) conjugated (1:2000; Bio-Rad) in TBS-T containing 1 percent nonfat milk for 30 minutes. We washed the membranes as before and used Super Signal West Pico Chemiluminescent Substrate (Thermo Scentific) to identify proteins.

Western blot of HeLa and K562 nuclear extract

HeLa and K562 cells (6 x 10^6 cells; both cells were purchased from ATCC) were plated overnight at 37 °C in the presence of CO_2 and treated for two hours the next day with DMSO, XX-650-23, forskolin, or both XX-650-23 and forskolin. We lysed the cells using a nuclear extraction kit (Imgenex, San Diego, CA) and isolated cytoplasmic and nuclear extract according to the manufacture's protocol. The protein were quantified by BCA assay and boiled with Laemmli buffer for five minutes. Lysates (25 ug) were separated into an 8 percent SDS-PAGE gel. Transfer occurred over three hours at 0.20 Amp at 4 °C and immunoblotting was performed as before (See Western blot for CREB expression, above) with the respective primary antibodies, either rabbit anti-CREB

(1:1000; Millipore) or rabbit anti-CBP (1:1000; Cell Signaling Technology, Inc., Danvers, MA).

Immunoprecipitation of CREB:CBP complex

HeLa and K562 (6 x 10^6 cells) cells were harvested at 1000 rpm for five minutes and washed with 1X PBS. Cells were lysed with modified RIPA buffer (50 mM Tris-HCl pH 7.4; 150 mM sodium chloride; 1.0 percent NP-40) containing Protease Inhibitor Cocktail and Phosphatase Inhibitor Cocktail 2 and precleared with Protein A/G PLUS-Agarose (Santa Cruz Biotechnology, Inc., Santa Cruz, CA) for 30 minutes at 4 °C. Protein concentration was measured using BCA Protein Assay Kit (Thermo Scientific). Cell lysates (500 ug) were incubated with 5 ug primary antibody, either normal mouse (m) IgG or mouse anti-CREB-1 antibody (both antibodies purchased from Santa Cruz Biotechnology) overnight at 4 °C with gentle rocking on an orbital shaker. The lysate/antibody mixtures were transferred to 1.5 mL Eppendorf tubes containing protein A/G and incubated at 4 °C with gentle rocking for four hours. The agarose/sepharose beads were collected by pulse centrifugation at 3000 rpm for 1 minute at 4 °C. The beads were washed three times with cold 1X Dulbecco's phosphate-buffered saline (DPBS; Corning cellgro, Manassas, VA) resuspended with 2X Laemmi buffer, and boiled for five minutes at 98 °C. We then centrifuged the beads at 14,000 rpm for one minute and loaded the supernatant into an 8 percent SDS-PAGE along with 50 ug of cell lysates (Lys), separately. Protein transfer was performed at 0.2 Amp for three hours at 4 °C, and the nitrocellulose membrane was cut into two pieces and blocked with 5 percent nonfat milk in TBS-T for one hour at room temperature. The top part of the

membrane was incubated with rabbit anti-CBP (1:1000; Cell Signaling Technology) and the bottom part with rabbit anti-CREB (1:1000; Millipore) overnight at 4 °C. After washing the membrane three times with TBS-T, the membranes were incubated with goat anti-rabbit IgG (H & L)-HRP conjugated (1:2000; Bio-Rad). Membranes were washed as before, and enhanced chemiluminescence (ECL) was used to identify proteins.

Transfection and Western blot of HEK-293T

We plated 3 x 10^6 Hek293T cells in Dulbecco's modified Eagle's medium (DMEM; Gibco) containing 10 percent FBS and 1X P/S/G, into 10 cm dishes and incubated overnight at 37 °C in the presence of CO_2. Cells were transfected the next day with TransIT-293 Transfection Reagent (Mirus Bio LLC, Madison, WI) according to the manufacturer's protocol and incubated as before for 48 hours. The cells were dislodged with trypsin, washed with 1X DPBS (Corning cellgro), centrifuged at 1000 rpm for five minutes at room temperature, and frozen at -80 °C. Hek293T cells were thawed and lysed with TNN lysis buffer (50 mM Tris-HCl, pH 7.4; 150 mM NaCl; 5 mM EDTA (All three were purchased from Fisher Scientific), pH 8; 0.5 percent NP-40 (Sigma); and 10 percent glycerol (Aldrich, Gibbstown, NJ)). The cells were incubated on ice for 30 minutes and then centrifuged at 14,000 RMP for 30 minute at 4 °C. Protein quantification was performed as before. We also performed the SDS-Laemmli procedure as before and subjected 40 µg of lysates to SDS-PAGE. We ran 3–8% Tris-Acetate Mini gel (Invitrogen) at 150 V for one hour and performed the transfer at 0.2 A for three hours at 4 °C. The nitrocellulose membrane was blocked with 5 percent nonfat

milk in TBS-T for one hour at room temperature. The membrane was immunoblotted with rabbit anti-CBP (1:1000; Cell Signaling) in 1 percent BSA TBS-T buffer with 1 percent bovine serum albumin (BSA; Sigma) overnight at 4 °C. Washes were performed as before, and the membrane was incubated with anti-rabbit-HRP (1:2000; Bio-Rad) for one hour at room temperature. We detected HRP with SuperSignal West Pico Chemiluminescent Substrate (Thermo Scientific).

Nucleofection of KG-1 cells and G418 selection

KG-1 cells (2 x 10^6 cells) were plated into 12-well plates overnight at 37 °C in the presence of CO_2. The next day, the cells were nucleofected with 2 ug of either the pRc/RSV-CBP or pmaxGFP (positive control) constructs according to the manufacture's protocol (Lonza VCA-1001; Allendale, NJ) and incubated as before for 48 hours for Fluorescence-activated cell sorting (FACS) analysis or for G418 selection. Nucleofected KG-1 cells were plated at 1.0 x 10^3 cells/100 uL into 96-well plates and treated with 500 ng/mL G418 (Sigma-Aldrich). After three days, we changed the IMDM media containing 10 percent FBS (Fisher Scientific), 1X P/S/G (Gibco) and treated the cells with 500 ng/mL G418. We performed selection and expansion of nucleofected KG-1 cells for 40 days, and then stored the cells in liquid nitrogen. HL60 cells (6 x 10^6 cells) and nucleofected or non-nucleofected KG-1 (3 x 10^6 cells) cells were lysed with TNN lysis buffer and subjected to WB for CREB expression analysis.

KG-1 FACS analysis for pmaxGFP expression

After 48 hours of nucleofection, KG-1 cells were washed with 1X DPBS buffer (Corning cellgro) and centrifuged at 1000 rpm for five minutes at room temperature. The pellet was then resuspended in FACS buffer (1X DPBS containing 2 percent FBS (Fisher Scientific)) and filtered through a 5 mL polysterene round-bottom tube with a cell-strainer cap (BD Falcon; Becton, Dickinson and Company, Franklin Lakes, NJ). FACS was performed using the BD FACSCalibur flow cytometer (BD Biosciences, San Jose, CA).

Quantitative RT-PCR of CREB target genes

KG-1 and AML cell lines were plated at 1.5 x 10^5 cells/mL and 3 x 10^5 cells/mL, respectively, overnight at 37 °C in the presence of CO_2. The next day, the cells were treated either with 0.1 percent DMSO or with 1 μM or 5 μM XX-650-23 for six or twelve hours. The cells were centrifuged at 1000 rpm for five minutes at room temperature, washed with 1X DPBS (Corning cellgro), and centrifuged as before. RNA extraction of 2.5 x 10^6 cells was performed using a spin protocol procedure (Aurum Total RNA Mini Kit, Bio-Rad). Reverse transcription was performed using iScript cDNA synthesis kit for RT-PCR (Bio-Rad). Total RNA (200 ng) was reverse transcribed from each sample, and one-tenth of it was used as a template for qRT-PCR reaction using SYBR Green (Bio-Rad) and the respective specific human primers, which we designed using Primer-BLAST software (http://www.ncbi.nlm.nih.gov/tools/primer-blast) [42]. The following human primers were used — Beclin1: 5'-GCTCCCGAGGTGAAGAGCAT-3' and 5'-GCCTGGGCTGTGGTAAGTAA-3'; CCND1 (cyclin D1): 5'-

TGCTGCGAAGTGGAAACCATC-3' and 5'-CACTTCTGTTCCTCGCAGAC-3'; CCNA1 (cyclin A1): 5'-TCAGGACTGAGAACCTGGCTA-3' and 5'-CTCACTCAGGCAAGGCACAA-3'; FOS: 5'-TACTACCACTCACCCGCAGA-3' and 5'-CGTGGGAATGAAGTTGGCAC-3'. We analyzed the data using the standard curve method and normalized against β-actin.

FACS analysis of apoptosis in HL60 cells

HL60 cells (3 X 10^5 cells) were plated into 24-well plates overnight at 37 °C in the presence of 5 percent CO_2 and treated the next day with 0.1 percent DMSO or either 910 nM or 5 µM XX-650-23 for 24 hours or 48 hours. Cells were also treated with 68 µM etoposide (Sigma-Aldrich) used as a positive control. Experiments were performed in triplicate. We also used cells grown in 1X DPBS (Corning cellgro), instead of IMDM media with 10 percent FBS and 1X P/S/G, as a positive control. Cell pellets were stained with propidium iodide (PI), annexin V or both, following the Annexin V-APC Apoptosis Detection Kit protocol (eBioscience, Inc., San Diego, CA). FACS was performed using the BD FACSCalibur flow cytometer (BD Biosciences).

Cell cycle FACS analysis of HL60 cells

HL60 cells (9 x 10^5 cells) were plated into 6-well plates overnight and treated the next day with 0.1 percent DMSO or 1 µM XX-650-23 for 12, 24, or 48 hours at 37 °C in the presence of 5 percent CO_2. The cells were centrifuged at 1000 rpm for five minutes at room temperature, washed with 1X PBS, centrifuged as before, fixed with 70 percent ethanol, and stored at -20 °C. We centrifuged the HL60 cells as before and

resuspended the pellet with 300 µL DNA staining buffer (1X PBS containing 50 ug/mL RNase A, 0.1 percent sodium citrate, 10 ug/mL 7-aminoactinomycin D [7AAD; Calbiochem, San Diego, CA]). FACS was performed using the BD FACSCalibur flow cytometer (BD Biosciences).

Western blot analysis of PARP cleavage in HL60 and KG-1 cells

HL60 and KG-1 cells were plated at 3 x 10^5 cells/mL and 1.5 x 10^5 cells/mL, respectively, in a total volume of 20 mL. The next day, the cells were treated with either DMSO or XX-650-23 for 24 hours or 48 hours. HL60 and KG-1 cells were also treated with etoposide for five and ten hours, respectively. Cells were centrifuged at 1000 rpm at room temperature, washed with 1X DPBS (Corning cellgro), centrifuged as before, and stored at -80 °C. Cells were lysed with RIPA lysate buffer and quantitated by BCA assay (Thermo Scientific). HL60 and KG-1 cell lysates (50 µg and 100 µg, respectively) were boiled with Laemmli buffer for five minutes at 98 °C and subjected to SDS-PAGE analysis. Transfer was performed for two hours at 0.2 Amp at 4 °C. Nitrocellulose membrane was blocked with 5 percent nonfat milk in TBS-T buffer. Membranes were immunoblotted with rabbit anti-PARP (1:1000; Cell Signaling) or rabbit anti-β-tubulin (1:1000; Santa Cruz) overnight at 4 °C. Membranes were washed three times, five minutes each, with TBS-T at room temperature, immunoblotted with anti-rabbit-HRP (1:2000; Bio-Rad) for one hour at room temperature, and washed as before. Proteins were identified with using SuperSignal West Pico Chemiluminescent Substrate (Thermo Scientific).

1-4 Results

To examine the potential effect of XX-650-23 on the proliferation of AML cells, we treated KG-1 and HL60 cells with increasing concentrations of XX-650-23 for 48 hours (**Fig. 1.6**, top- and bottom-left panels). XX-650-23 decreased proliferation of both HL60 and KG-1 cells, with an IC50 ranging from 819 to 971 nM and 825 to 919 nM cells, respectively (**Fig. 1.6**, top- and bottom-right panels). An IC50 of approximately 910 nM was calculated from the sigmoidal curve of both AML cell lines using PRISM.

To assess the effect of XX-650-23 on normal BM cells, we grew the cells on methylcellulose and treated them with escalating concentrations of XX-650-23 for 14 days (**Fig. 1.7**). We treated the same number of colonies of normal BM cells with XX-650-23, at concentrations up to 10 μM, as those treated with DMSO. We also investigated the effect of XX-650-23 on normal BM and AML BM samples by growing the BM in liquid media supplemented with cytokines and treating the cells with 2 μM of XX-650-23 for 72 hours (**Fig. 1.8**). This concentration of XX-650-23 did not inhibit growth of normal BM cells (**Fig. 1.8A**). Three AML patient samples were treated under the same conditions, and we observed that XX-650-23 inhibited up to 40 percent of cell growth in two of the samples (**Fig. 1.8A**). The effect of XX-650-23 was also investigated in relapsed AML BM cells by treating these cells with 2 or 3 μM of XX-650-23. XX-650-23 inhibited the growth of relapsed AML BM cells in a dose-dependent manner, with 3 μM XX-650-23 inhibiting greater than 50 percent (**Fig. 1.8B**). In order to find a therapeutic index for XX-650-23, we placed normal BM cells in liquid media

supplemented with cytokines and treated them with increasing concentrations of the compound. XX-650-23 concentrations greater than 4 μM inhibited 50 percent of normal BM cell proliferation (**Fig. 1.8C**).

A)

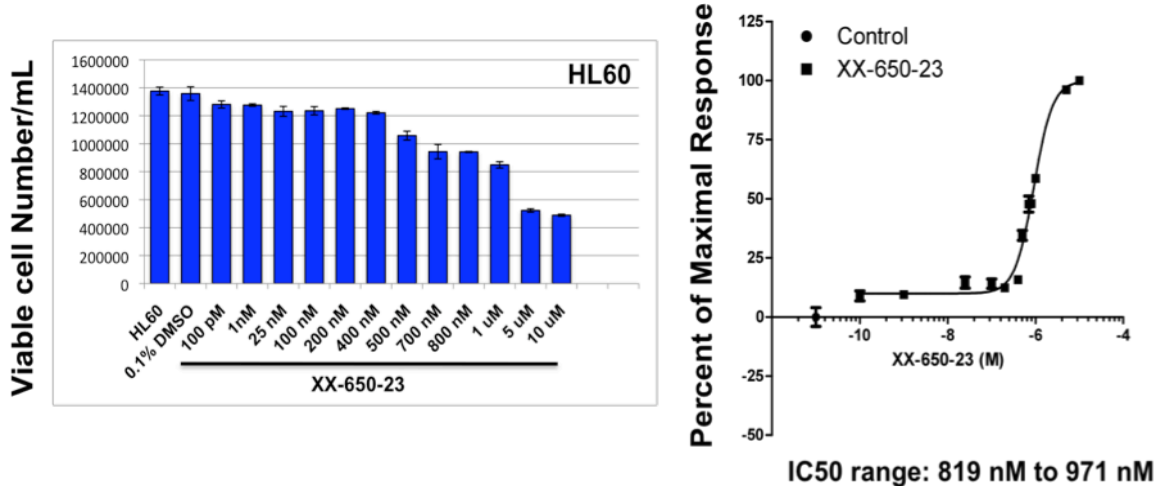

B)

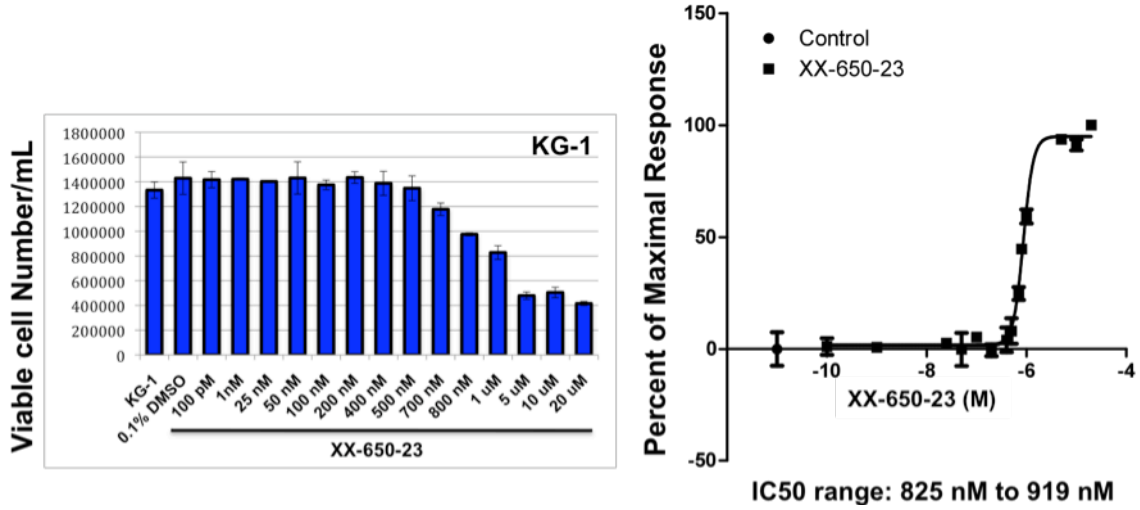

Figure 1.6. Determination of XX-650-23 IC50 in HL60 and KG-1 cells. A) HL60 (**top-left panel**) and **B)** KG-1 (**bottom-left panel**) cells were treated with 0.1% DMSO (control) or with increasing concentrations of XX-650-23 for 48 hours. Viable cells were identified using the trypan blue exclusion procedure. XX-650-23 IC50 in HL60 cells (**top-right panel**) ranged from 819 nM to 971 nM; in KG-1 cells **(bottom-right panel)**, the IC50 ranged from 825 nM to 919 nM.

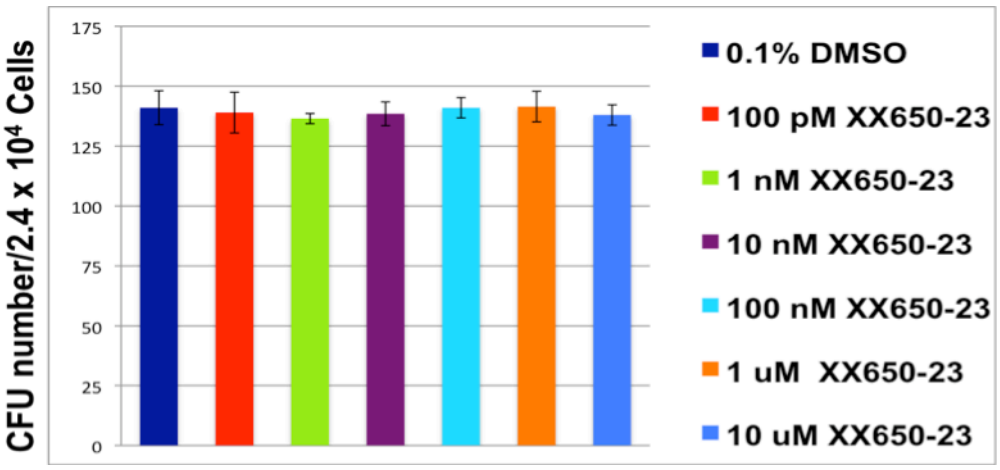

Figure 1.7. XX-650-23 is not toxic to normal BM cells grown in methylcellulose. Human BM cells from healthy donors were resuspended in media to a final concentration of 1.0 x 10^4 cells/mL and treated with escalating concentrations of XX-650-23. A methylcellulose tube containing the cells and DMSO or drug was divided into two 1.2 mL aliquots and plated into BD Falcon tissue culture dishes. Experiments were performed in duplicate, and the colonies were scored on day 14 for granulocyte macrophage colony-forming units.

A)

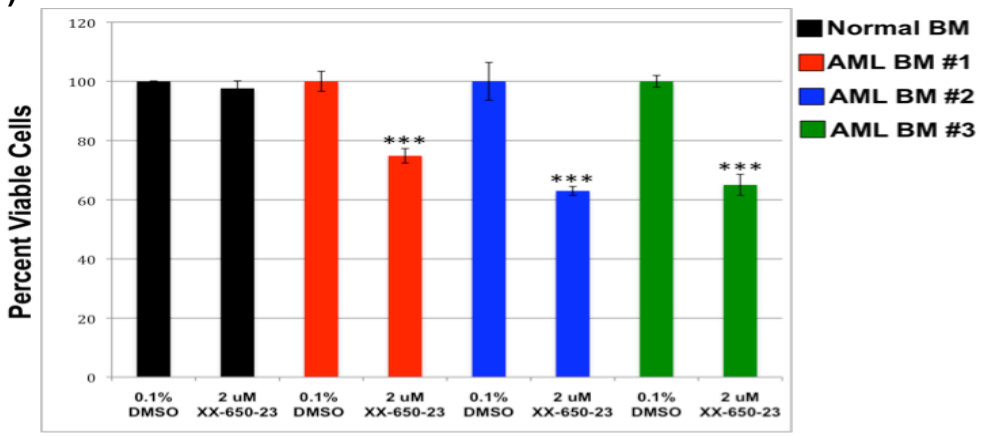

B)

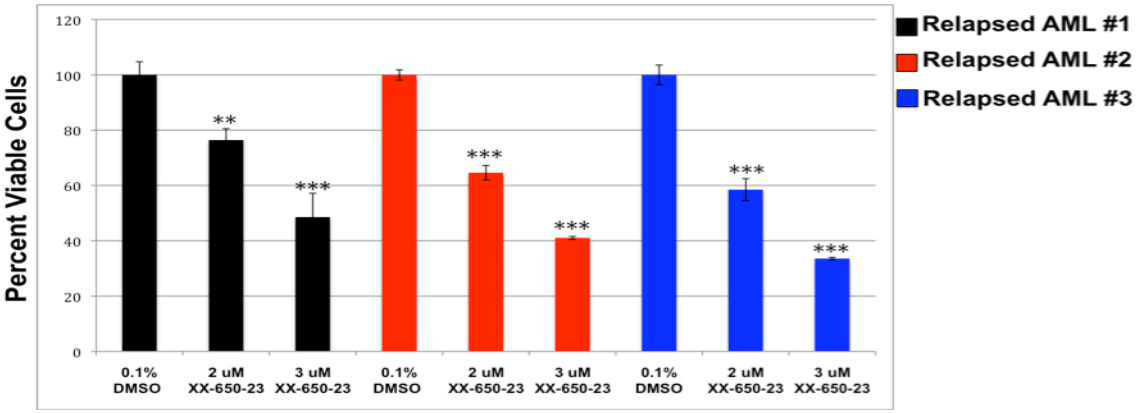

C)

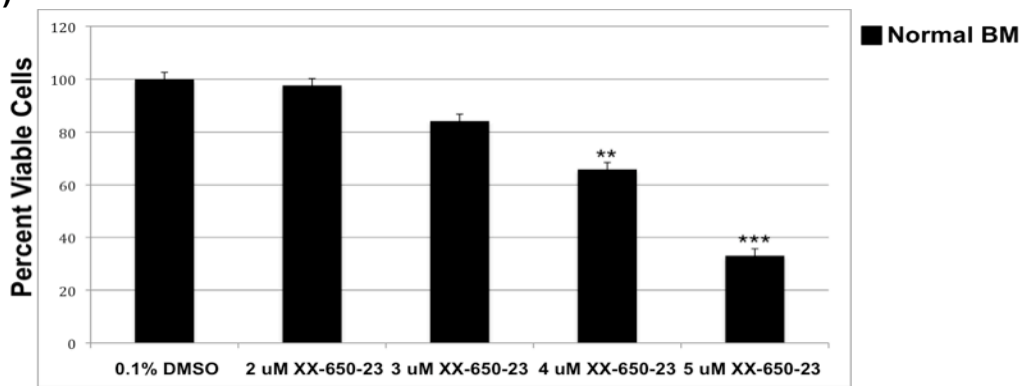

Figure 1.8. XX-650-23 exhibits greater specificity for AML and relapsed AML BM than for normal BM cells. A) Normal and AML BM cells were plated at 1 x 10^5 cells/well and treated with 0.1% DMSO (control) or 2 μM XX-650-23 for 72 h. **B)** Relapsed AML BM cells were plated and treated as in (A) and also with 3 μM XX-650-23. **C)** Normal BM cells were treated with different concentrations of XX-650-23 and incubated as in (A). *P<0.05, **P<0.01, ***p<0.0001.

To determine whether XX-650-23 has an additive, synergistic, or antagonistic effect when combined with two other chemotherapy drugs, daunorubicin or cytarabine, we started by determining the IC50 of each compound. We treated HL60 and KG-1 cells with increasing concentrations of XX-650-23 for 48 hours and performed the trypan blue exclusion assay to determine the number of live cells present after treatment. We estimated the IC50 for each drug using PRISM. In HL60 cells, we obtained IC50s of 910 nM, 21 nM, and 175 nM, corresponding to XX-650-23, daunorubicin, and cytarabine, respectively (**Fig. 1.9**). In KG-1 cells, we obtained IC50s of 910 nM, 11.5 nM, and 100 nM, corresponding to XX-650-23, daunorubicin, and cytarabine, respectively (**Fig. 1.10**). A serial dilution was prepared yielding 8, 4, 2, 1, 0.5, 0.25, and 0.125 times the IC50 of each compound, and we assessed the cell viability of HL60 (**Fig. 1.9**) or KG-1 cells (**Fig 1.10**) as before. For the combination study, we prepared a mixture of XX-650-23 with either cytarabine or daunorubicin and separately treated HL60 and KG-1 cells with each drug, alone or in combination, on the same day. The resulting isobolograms show points lying to the left of the line of equivalency, indicating that XX-650-23 acts synergistically with cytarabine in both HL60 and KG-1 cells (**Fig. 1.11**). **Table 1.1** shows the IC50, IC75, and IC90 CI values of XX-650-23 in combination with cytarabine. All values are less than 1 and were confirmed to be statistically significant by the alternate nonlinear regression approach, indicating a synergistic effect.

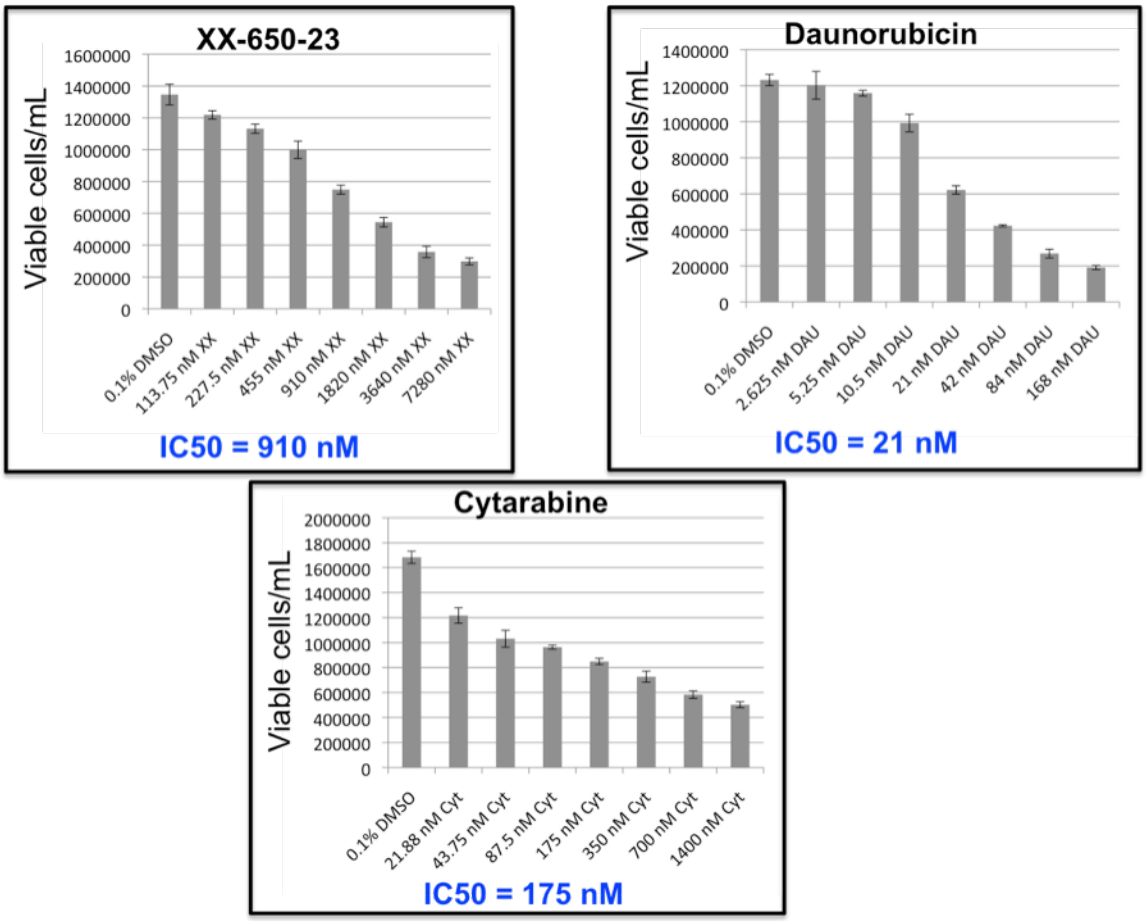

Figure 1.9. IC50s of XX-650-23, daunorubicin, and cytarabine in HL60 cells. We determined the IC50s of XX-650-23, daunorubicin, and cytarabine in HL60 cells and prepared eightfold solutions of the IC50s, followed by a series of dilutions (8X, 4X, 2X, 1X, 0.5X, 0.25X, 0.125X). The cells (3 x 10^5 cells/mL) were incubated for 48 hours and counted by trypan blue exclusion.

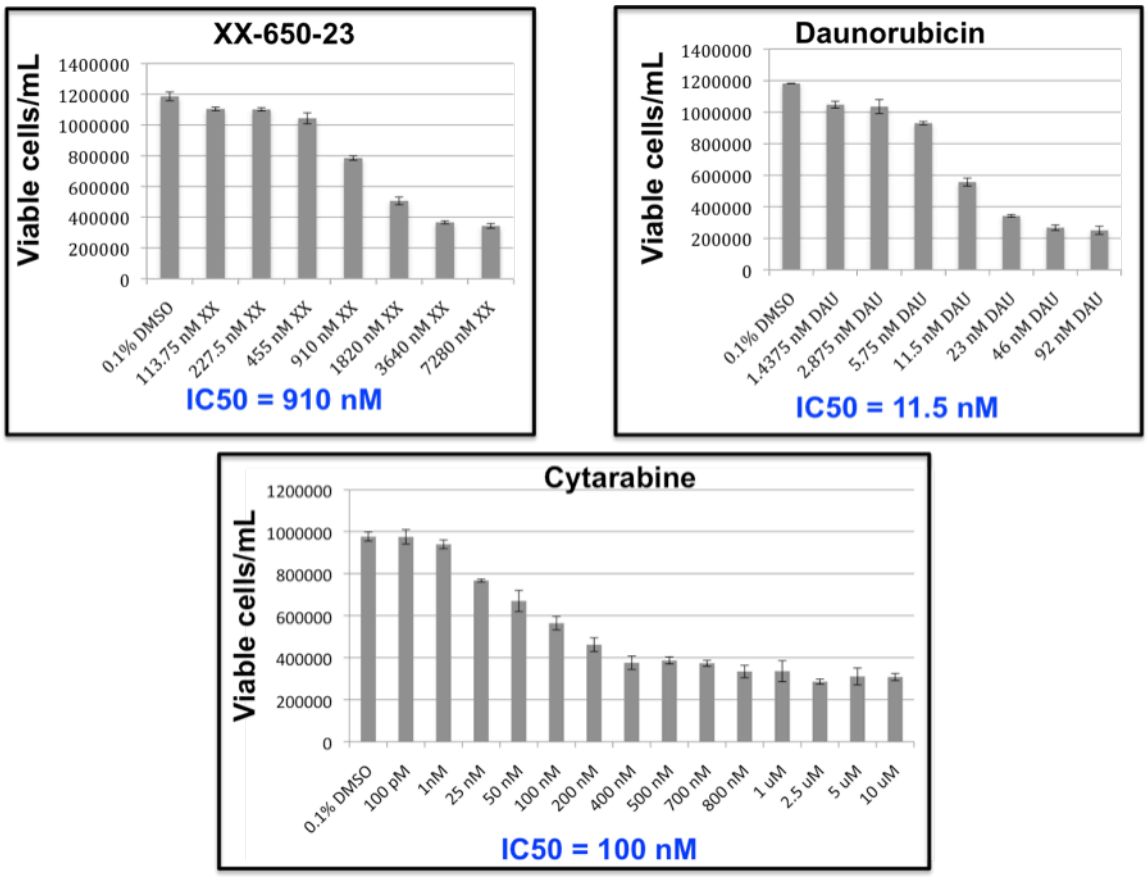

Figure 1.10. IC50s of XX-650-23, daunorubicin, and cytarabine in KG-1 cells. We determined the IC50s of XX-650-23, daunorubicin and cytarabine in KG-1 cells and prepared eightfold solutions of the IC50s, followed by a series of dilutions as in Fig. 1.9. The cells (1.5×10^6 cells/mL) were incubated for 48 hours and counted by trypan blue exclusion.

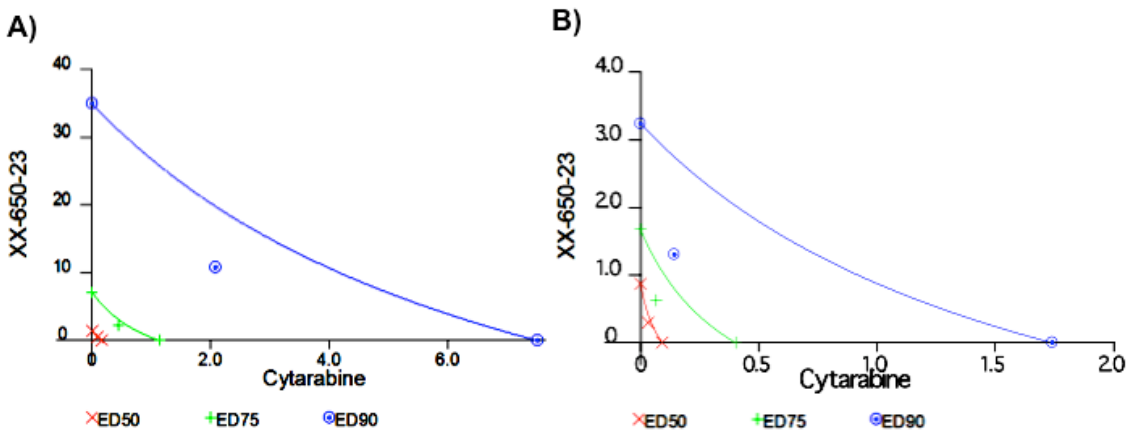

Figure 1.11. XX-650-23 is synergistic with cytarabine in HL60 and KG-1 cells. We determined the IC50s of XX-650-23 and cytarabine in HL60 **(A)** and KG-1 **(B)** cells and prepared an eightfold solution of the IC50s. We combined XX-650-23 with cytarabine to make an eightfold solution of each IC50 and then performed a series of dilutions (8X, 4X, 2X, 1X, 0.5X, 0.25X, 0.125X). The cells were treated alone or in combination with the compounds and then incubated for 48 hours. Cells were counted by trypan blue exclusion. Isobolograms were obtained using Calcusyn. Points lying to the left of the line of equivalency indicate a synergistic effect.

Table 1.1. CI values for the effects of XX-650-23 and cytarabine on HL60 and KG-1 cells.

Cell line: HL60

Drug	CI Values at ED50	ED75	ED90	Dm	m
XX-650-23 (Not a combination)	N/A	N/A	N/A	0.98870	0.76752
Cytarabine (Not a combination)	N/A	N/A	N/A	0.11253	0.68049
XX-650-23 Cytarabine (5.2:1)	0.97439	0.63057	0.41140	0.35819	0.99222

Cell line: KG-1

Drug	CI Values at ED50	ED75	ED90	Dm	m
XX-650-23 (Not a combination)	N/A	N/A	N/A	0.86906	1.66882
Cytarabine (Not a combination)	N/A	N/A	N/A	0.09332	0.75077
XX-650-23 Cytarabine (9.1:1)	0.69792	0.54353	0.48562	0.29977	1.49207

CI values equal to 1 indicate an additive effect; less than 1, a synergistic effect; and significantly greater than 1, an antagonistic effect of the two compounds. ED50 = the dose required to inhibit proliferation of cells to 50% of untreated controls. D_m = the median-effect dose or potency m = sigmoidicity of the dose effect curve.

We also combined XX-650-23 with daunorubicin and analyzed its effect using the same procedures as in the cytarabine combination study. Isobolograms show points lying to the right of the line of equivalency, indicating that XX-650-23 acts slightly as an antagonist to daunorubicin in HL60 (**Fig. 1.12A**). In KG-1 cells, the points fall very close to the line, indicating an additive effect (**Fig. 1.12B**). The CI values obtained at ED50, ED75, and ED90 are greater than 1 in HL60 cells and very close to 1 in KG-1 cells, indicating a slightly antagonistic and an additive effect, respectively (**Table 1.2**).

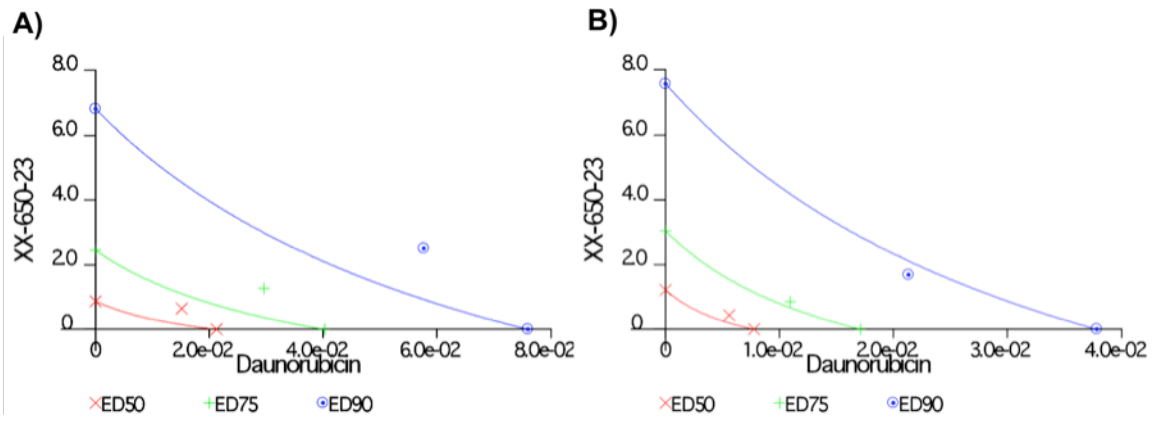

Figure 1.12. XX-650-23 is slightly antagonistic with daunorubicin in HL60 and additive in KG-1 cells. We determined the IC50s of XX-650-23 and cytarabine in HL60 **(A)** and KG-1 **(B)** cells and prepared an eightfold solution of the IC50s. XX-650-23 was combined with daunorubicin to make an eightfold solution of each IC50, and then a series of dilutions was performed as in Fig. 1.11. The cells were treated alone or in combination with the compounds, incubated for 48 hours, and analyzed as in Fig 1.11. Points lying to the right of the line of equivalency indicate an antagonistic effect, points on the line of equivalency indicate an additive effect, and those points to the left indicate a synergistic effect.

Table 1.2. CI values for the effects of XX-650-23 and daunorubicin on HL60 and KG-1 cells.

Cell line: HL60

Drug	CI Values at ED50	ED75	ED90	Dm	m
XX-650-23 (Not a combination)	N/A	N/A	N/A	0.88063	1.07433
Daunorubicin (Not a combination)	N/A	N/A	N/A	0.02131	1.72773
XX-650-23 Daunorubicin (43.33:1)	1.45973	1.25928	1.12632	0.65802	1.64588

Cell line: KG-1

Drug	CI Values at ED50	ED75	ED90	Dm	m
XX-650-23 (Not a combination)	N/A	N/A	N/A	1.22524	1.20539
Daunorubicin (Not a combination)	N/A	N/A	N/A	0.00776	1.38674
XX-650-23 Daunorubicin (79.13:1)	1.08916	0.92361	0.78560	0.44565	1.65055

CI values equal to 1 indicate an additive effect; less than 1, a synergistic effect; and values significantly greater than 1, an antagonistic effect of the two compounds.

In order to measure the CREB transcriptional activity induced by CREB:CBP binding, we formed a reported lentiviral construct that expressed mCherry and contained the CRE element followed by the TATA box and the RLuc gene (**Fig. 1.13**). Primers flanking the CRE and RLuc regions (**Fig. 1.13**) or only the RLuc region (experimental methods) were designed. The PHAGE-mCherry vector was double digested using BAMHI-HF and ClaI, and the top band at about 7000 kbp, lanes 2 and 3 (**Fig. 1.14**) was gel purified. We amplified the RLuc and CRE-RLuc fragments with their respective primers and analyzed their molecular weight on an agarose gel (**Fig. 1.15**). The agarose gel shows bands below and above the 1000 kbp marker band,

corresponding to RLuc, lanes 2 to 5, and the CRE-RLuc amplified fragments, lanes 7 to 10.

After ligation, colonies were picked, purified, and analyzed on an agarose gel to determine those that had the correct PCR inserts. Agarose gel analysis of the double digested constructs with BamHI-HF and ClaI (**Fig. 1.16**) showed that lanes 4 to 14 and 15 to 17 potentially contained the RLuc and CRE-RLuc fragments, respectively.

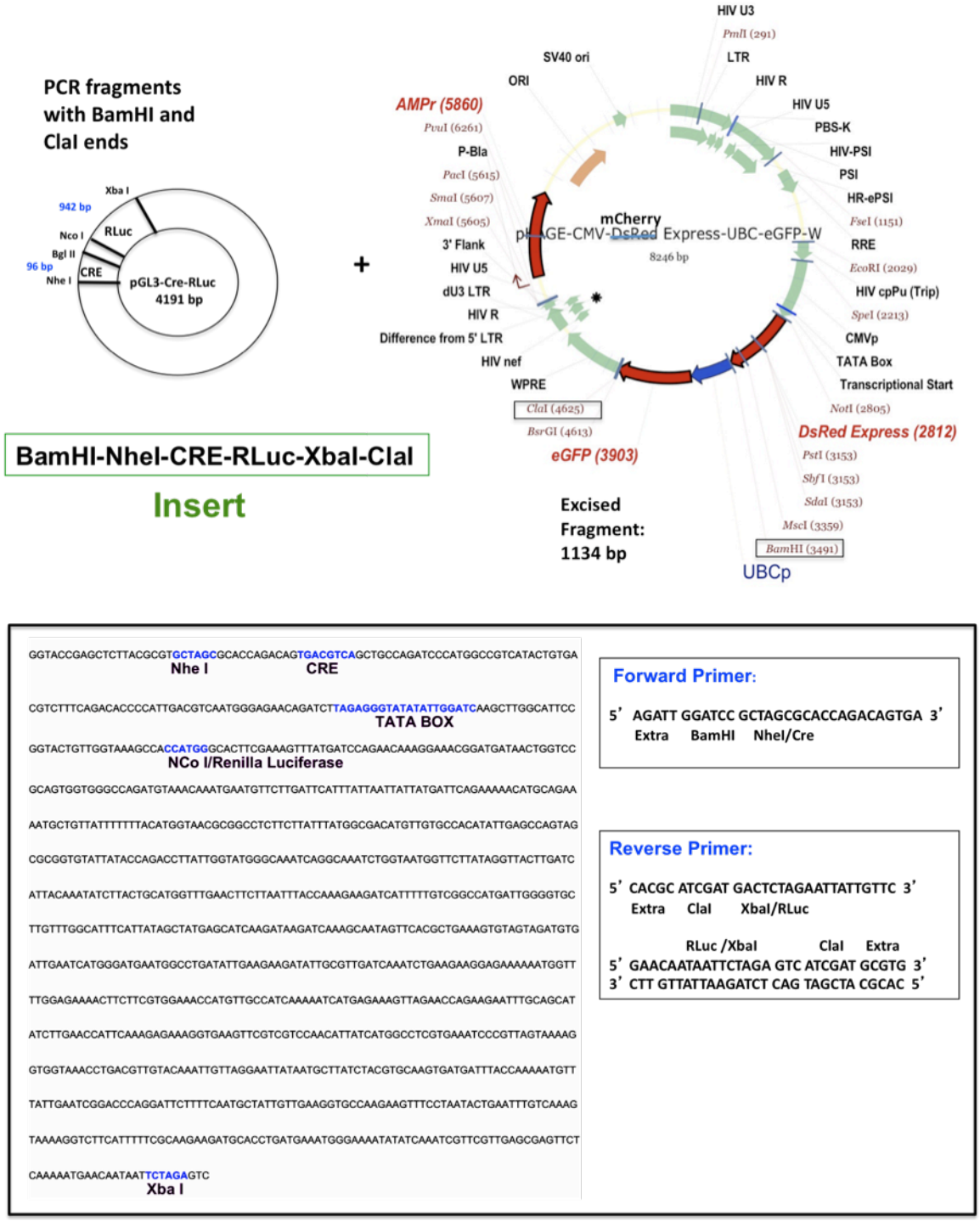

Figure 1.13. Formation of mCherry-CRE-*Renilla* luciferase construct. We analyzed the sequence of CRE-RLuc to design primers that flank the CRE-RLuc region. The insert was subcloned into the mCherry lentiviral vector. The original DsRed sequence was previously replaced by the mCherry sequence.

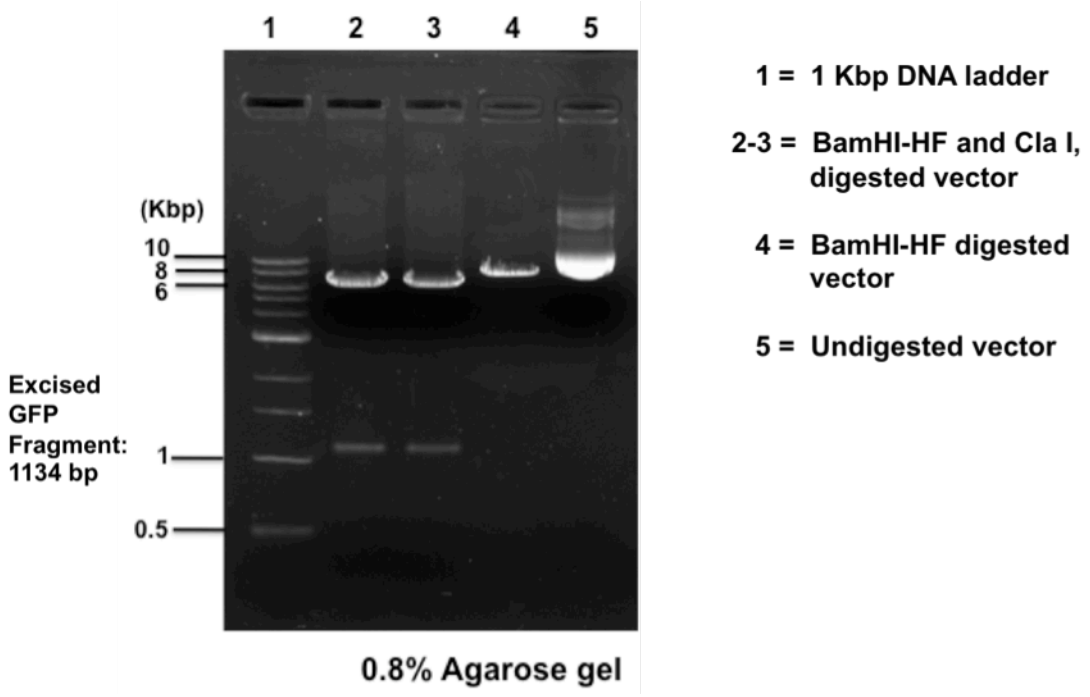

Figure 1.14. Restriction digest of PHAGE-CMV-mCherry vector. Double digested PHASE-CMV vector (top band at ~7 Kbp) was purified by gel extraction using a quick gel extraction kit (Invitrogen).

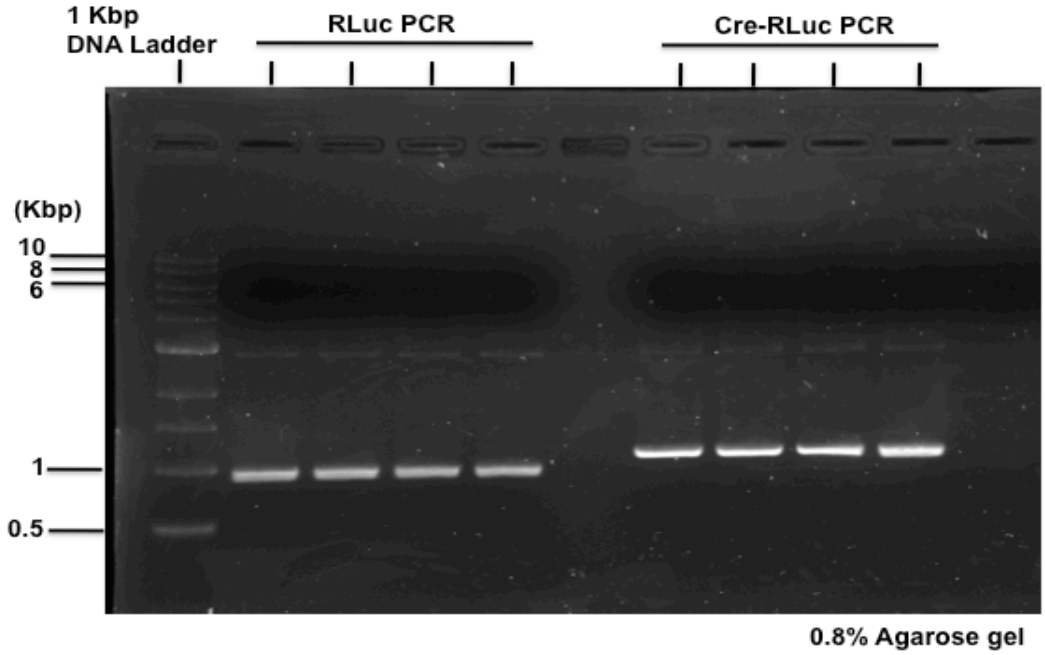

Figure 1.15. RLuc and CRE-RLuc PCR products. The molecular size of RLuc or CRE-RLuc PCR products were analyzed on an 0.8% agarose gel. RLuc expected fragment <1000 kbp, and CRE-RLuc expected fragment >1000 kbp.

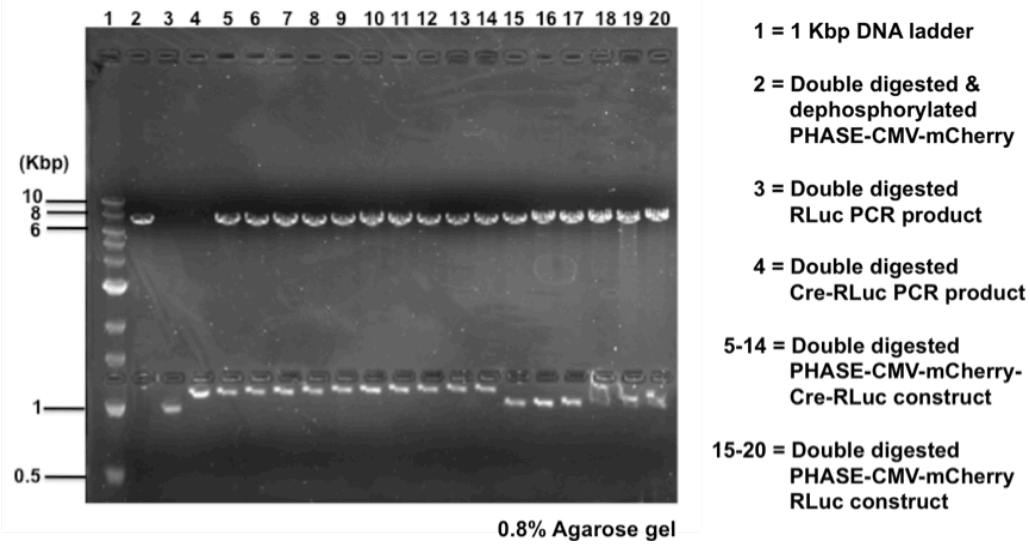

Figure 1.16. Restriction digest of purified PHASE-CMV-mCherry CRE-RLuc and PHASE-CMV-mCherry RLuc constructs. Purified and double digested constructs, using BamHI-HF and ClaI restriction enzymes, were analyzed on an 0.8% agarose gel.

CREB:CBP-binding studies can also be performed by IP. We first measured the relative mRNA expression of CREB and CBP in different AML cell lines (**Fig. 1.17**). K562 cells and chronic myelogenous leukemia (CML) were used as a positive control. KG-1 and HL60 cells express the highest levels of CBP and CREB. Expression of CREB and CBP protein was also examined by the WB procedure. The same amount of protein from AML cells was subjected to SDS-PAGE (**Fig. 1.18**). HeLa cells were used as a positive control for CBP expression. We observed the expression of CREB in all cell lines; however, CBP was only identified in HeLa cells, even after two minutes of exposure. The anti-CREB antibody recognizes both the unphosphorylated and phosphorylated serine, showing two bands.

The CREB:CBP IP assay was performed in HeLa and K562 control cell lysates. The results showed that CREB was immunoprecipitated in both cells, but CBP was only identified in the HeLa cell lysate (**Fig. 1.19**). To concentrate the CBP protein, we

performed nuclear extractions in HeLa and K562 cells; however, CBP was still found only in HeLa cells (**Fig. 1.20**). We observed no change in expression of CBP or CREB with forskolin treatment, either by itself or in combination with XX-650-23.

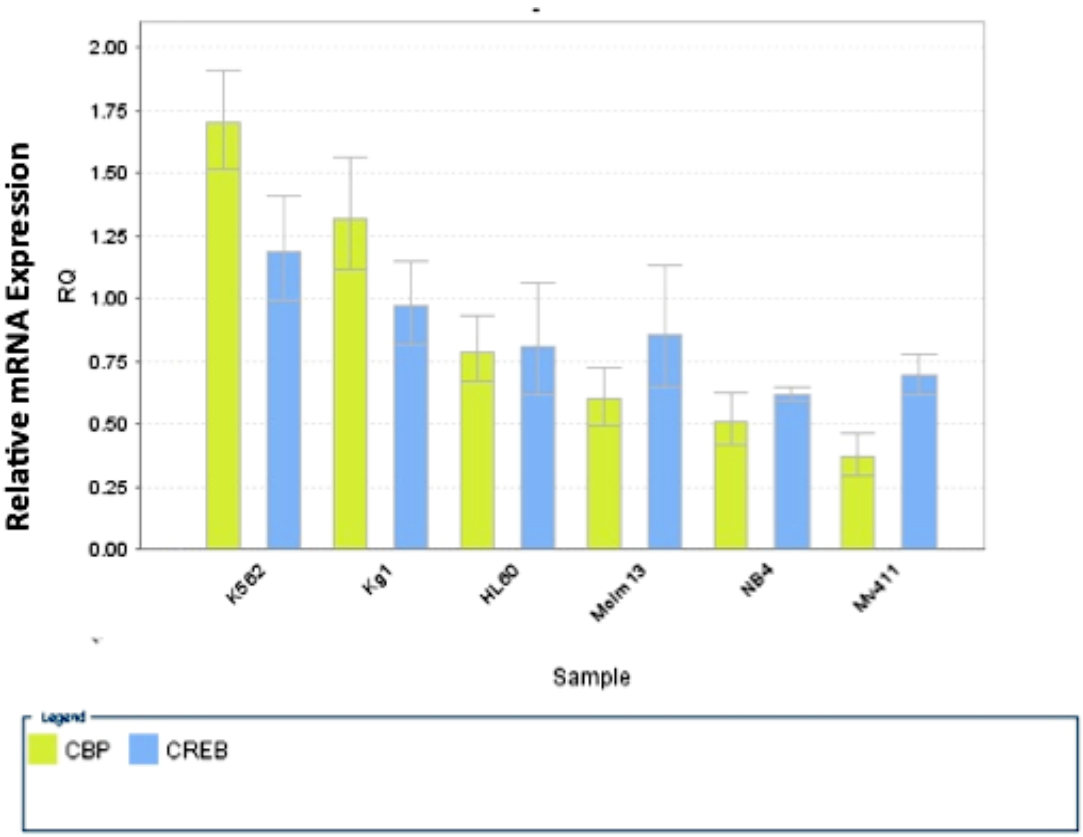

Figure 1.17. Relative mRNA expression of CBP and CREB in different AML cell lines. Total RNA was extracted using TRIzol reagent. RT-PCR and qRT-PCR were performed using iScript cDNA synthesis and SyberGreen (Bio-Rad), respectively. We used CBP- and CREB-specific primers and normalized expression to the housekeeping gene β-actin.

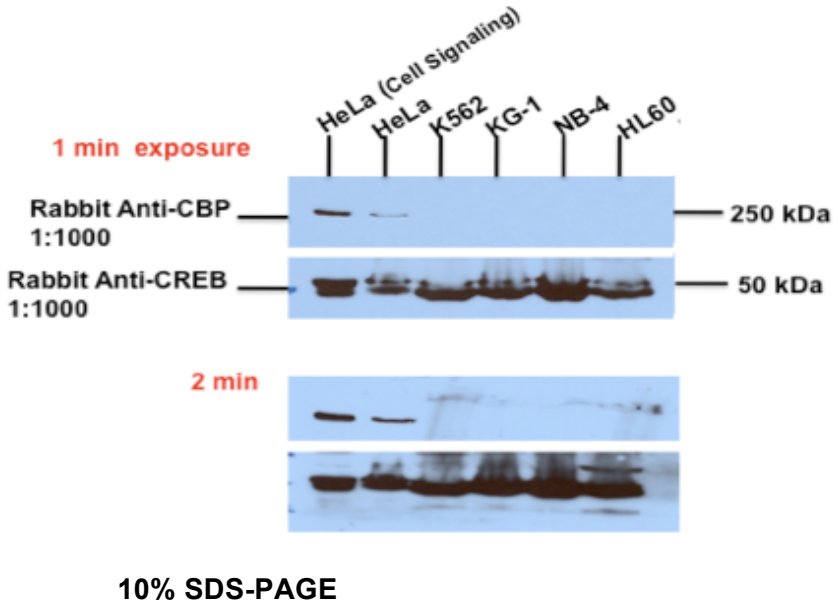

Figure 1.18. Protein expression of CBP and CREB in different AML cell lines. AML cell lines were lysed with RIPA buffer, and protein quantification was performed by BCA assay. HeLa (25 ug) and AML protein lysates (200 ug) were subjected to SDS-Laemmli buffer and SDS-PAGE. The top membrane was immunoblotted with anti-CBP; the bottom membrane, with anti-CREB. Two different exposures were performed to detect levels of CBP. HeLa cell lysates were loaded as a positive control for CBP expression.

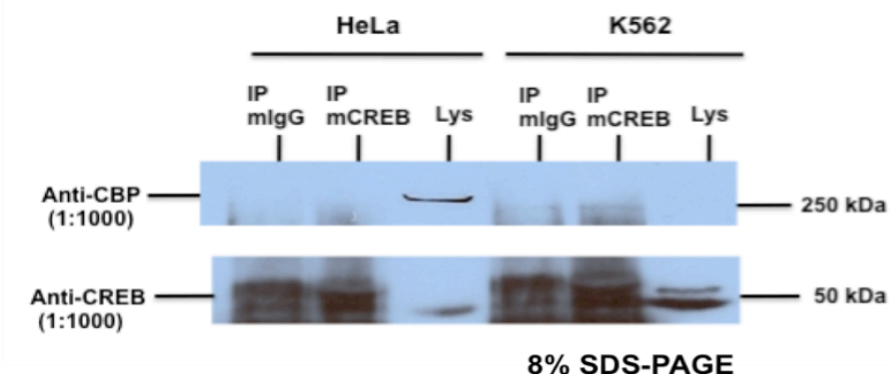

Figure 1.19. Immunoprecipitation of CREB:CBP complex. HeLa or K562 cells were lysed in modified RIPA buffer. Total protein lysate was immunoprecipitated with mouse anti-IgG or mouse anti-CREB antibody and subjected to SDS-PAGE. The membranes were cut in two (top and bottom panels) and immunoblotted with rabbit anti-IgG, rabbit anti-CREB, or rabbit anti-CBP.

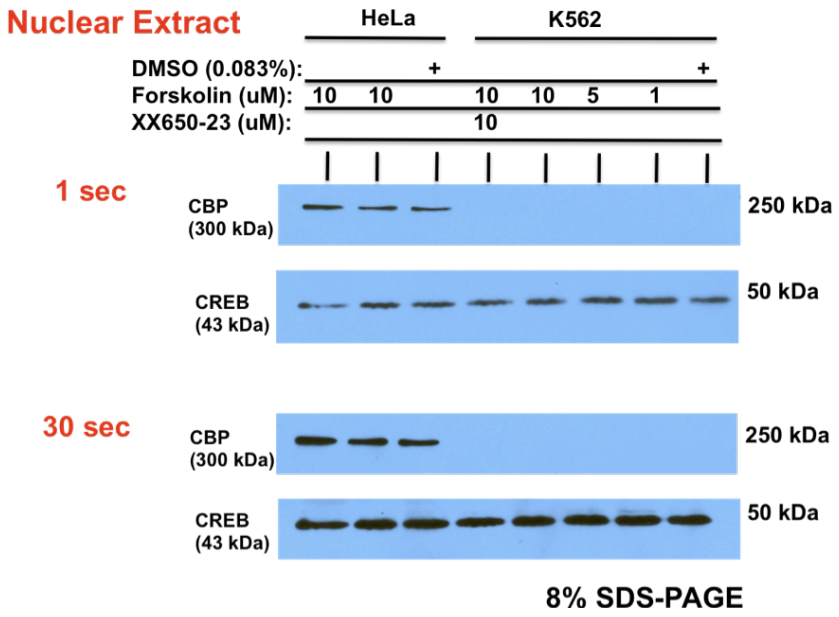

Figure 1.20. Expression of CREB and CBP in HeLa and K562 cells. HeLa or K562 cells were treated with DMSO, forskolin, or both forskolin and XX650-23 for 2 hours. The cells were lysed using a nuclear extraction kit (Imgenex), and cytoplasmic and nuclear extracts were quantified, boiled with Laemmi buffer, and loaded into an 8% SDS-PAGE gel. ECL was used to identify the respective proteins.

In order to increase the levels of CBP in AML cells and perform IP studies, we first transfected a CBP-expressing plasmid under the RSV promoter (**Fig. 1.21**) into HEK293T cells and examined its expression by WB (**Fig. 1.22**). The same amount of total protein lysates was loaded on the WB, and the results show that the nucleofected Hek293T cells express CBP protein levels similar to those found in HeLa cells. We could not transfect KG-1 or HL60 cells; however, the alternative nucleofection method yielded GFP-expressing cells (**Fig. 1.23D**). CBP protein expression, in non-nucleofected and nucleofected AML cells, was analyzed by WB (**Fig. 1.24**). The results show the expression of CBP in transfected Hek-293T, positive control, and nucleofected KG-1 cells.

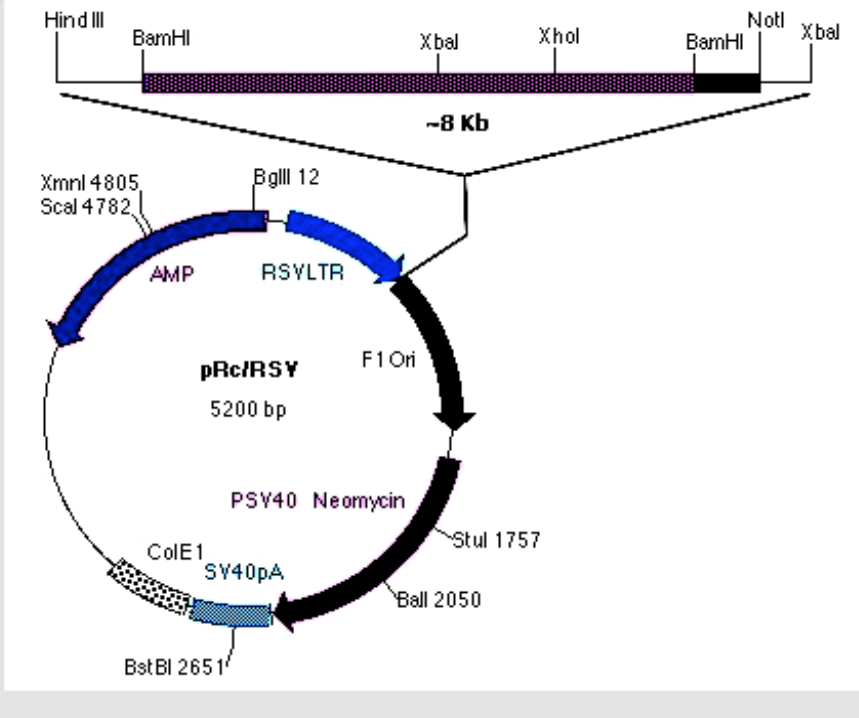

Figure 1.21. Map of Rc/RSV-CBP vector. The RSV promoter drives the expression of CBP. The plasmid contains the ampicillin (AMP) and and neomycin resistance genes.

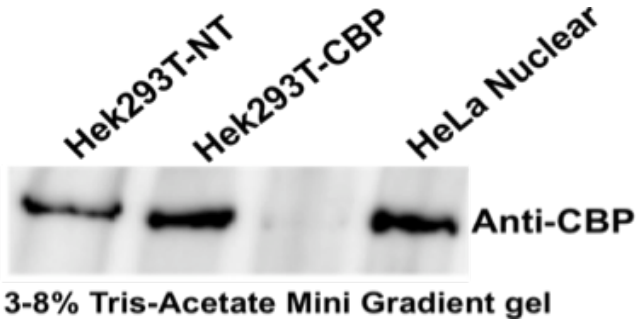

Figure 1.22. Expression of CBP in transfected or nontransfected Hek293T cells. Hek293T cells were transfected with Rc/RSV-CBP plasmid using TransIT-293 reagent. After 48 hours, the cells were lysed with TNN lysis buffer, quantitated by BCA assay, and analyzed by WB. HeLa nuclear extract was used as a positive control for CBP expression.

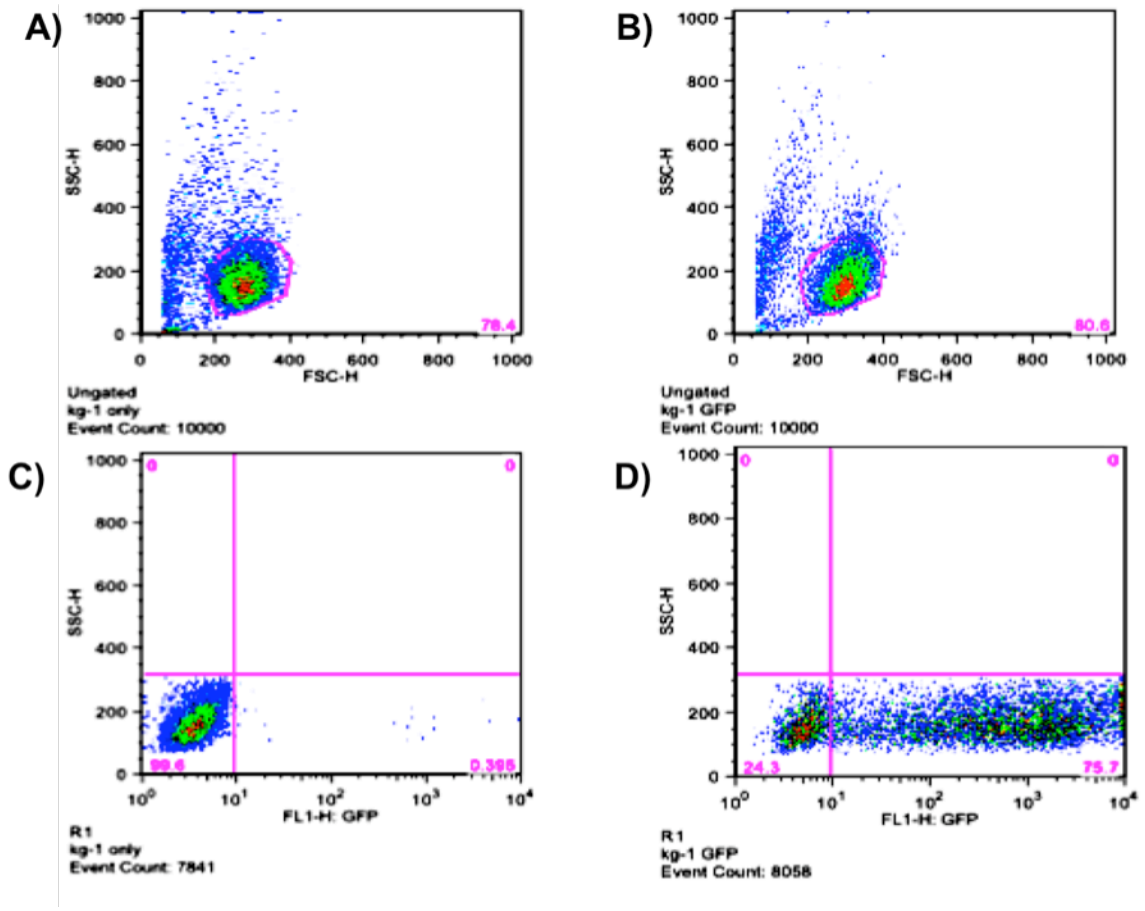

Figure 1.23. FACS analysis of GFP expression in nucleofected KG-1 cells. KG-1 cells were nucleofected with pmaxGFP as a positive control for 48 hours. The top two plots show the percentage of viable non-nucleofected **(A)** and GFP-nucleofected KG1 cells **(B).** Bottom panels show the percent of GFP expression in non-nucleofected (**C)** and GFP-nucleofected KG1 cells **(D)**. FACS was analyzed using DB FACSCalibur flow cytometry.

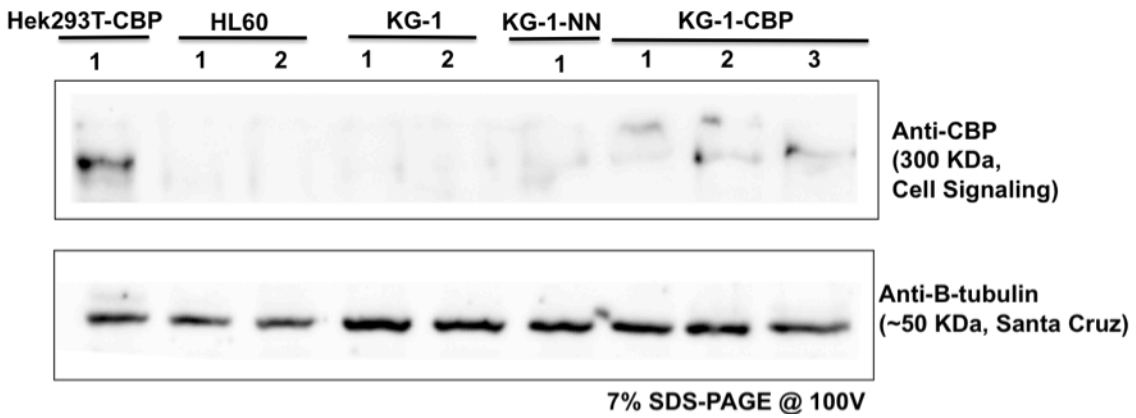

Figure 1.24. Expression of CBP in non-nucleofected and nucleofected AML cells. HL60, KG-1, and CBP-nucleofected KG-1 cells were lysed with TNN lysis buffer and quantitated by BCA assay procedure. Total lysate (40 ug) was separated by SDS-PAGE, and nitrocellulose membrane was blotted with the respective antibodies.

To examine whether apoptosis induced XX-650-23-mediated inhibition of AML cell proliferation, we treated HL60 cells with XX-650-23 for 24 and 48 hours. A small sample of cells was separated to determine its cell viability by trypan blue exclusion (**Table 1.3**), and another portion of cells were stained with PI, annexin V, or both to separate necrotic and apoptotic cell populations (**Fig. 1.25**). **Table 1.3** shows that the cell viability for HL60 cells treated with 0.1 percent DMSO or 910 nM of XX-650-23 for 24 hours remained almost the same, yielding only 0.69 percent change in cell viability. After 48 hours of treatment, the difference in cell viability only reached about 4 percent. We observed a 10 percent reduction in the viability of cells treated with 5 μM XX-650-23; after 48 hours, the difference was about 45 percent. The number of cells in the samples, including the controls and the cells treated with etoposide or 1X PBS, reduced dramatically after 24 hours. The number of cells treated with 910 nM and 5 μM XX-650-23 was reduced by 22.6 and 46.13 percent, respectively, after 24 hours, and those values approximately doubled after 48 hours.

HL60 cells were examined for evidence of apoptosis. **Figs. 1.25a–d** show control samples corresponding to unstained, PI, annexin V, and both PI and annexin V positive controls, respectively. The results indicate that treatment with 910 nM of XX-650-23, after 24 hours (**Fig. 1.25f**) or 48 hours (**Fig. 1.25j**), did not significantly contribute to apoptosis. Treatment with 910 nM of XX-650-23 left 92.7 and 86.4 percent of cells viable after 24 hours (**Fig. 1.25f)** or 48 hours (**Fig. 125j**), respectively. After 48 hours, about 5 percent were positive for necrosis and 7 percent for both necrosis and apoptosis (**Fig. 5i**). At higher concentrations (5 μM) of XX-650-23, 70 and 25 percent of cells remained viable after 24 hours (**Fig. 1.25g**) or 48 hours of treatment (**Fig. 1.25j**), respectively. After 48 hours, 5.51 percent of cells were apoptotic, 32.2 percent were necrotic, and 37.3 percent were positive for both necrosis and apoptosis (**Fig. 1.25j**).

Table 1.3. Effect of XX-650-23 on HL60 cell viability.

	Percent Cell Viability 24 hours	Viable Cells x 10^5/mL 24 hours	Percent Cell Viability 48 hours	Viable Cells X 10^5/mL 48 hours	Possible XX-650-23 Effect
0.1 % DMSO	95.7	10.88			
68 uM Etoposide	42.1	2.42			
68 uM Etoposide	44.0	2.34			
1X PBS	8	0.320			
0.1 % DMSO	95.1 95.8 95.7 Average: 95.53	11.39 10.95 11.75 Average: 11.36	94.7 95.3 94.8 Average: 94.93	20.60 19.30 19.79 Average: 19.90	
910 nM XX-650-23	93.6 95.2 95.8 Average: 94.87 (Affected Cells = 0.69%)	8.91 8.49 8.98 Average: 8.79 (Affected Cells = 22.62%)	89.8 92.4 90.1 Average: 90.77 (Affected Cells = 4.38%)	11.97 12.46 11.58 Average: 12.00 (Affected Cells = 39.70%)	Cell cycle arrest?
5 uM XX-650-23	85.8 88.2 84.3 Average: 86.1 (Affected Cells = 9.87%)	6.07 6.11 6.18 Average: 6.12 (Affected Cells = 46.13%)	50.1 51.9 52.0 Average: 51.33 (Affected Cells = 45.93%)	3.61 4.03 3.84 Average: 3.83 (Affected Cells = 80.75%)	Necrosis or apoptosis?

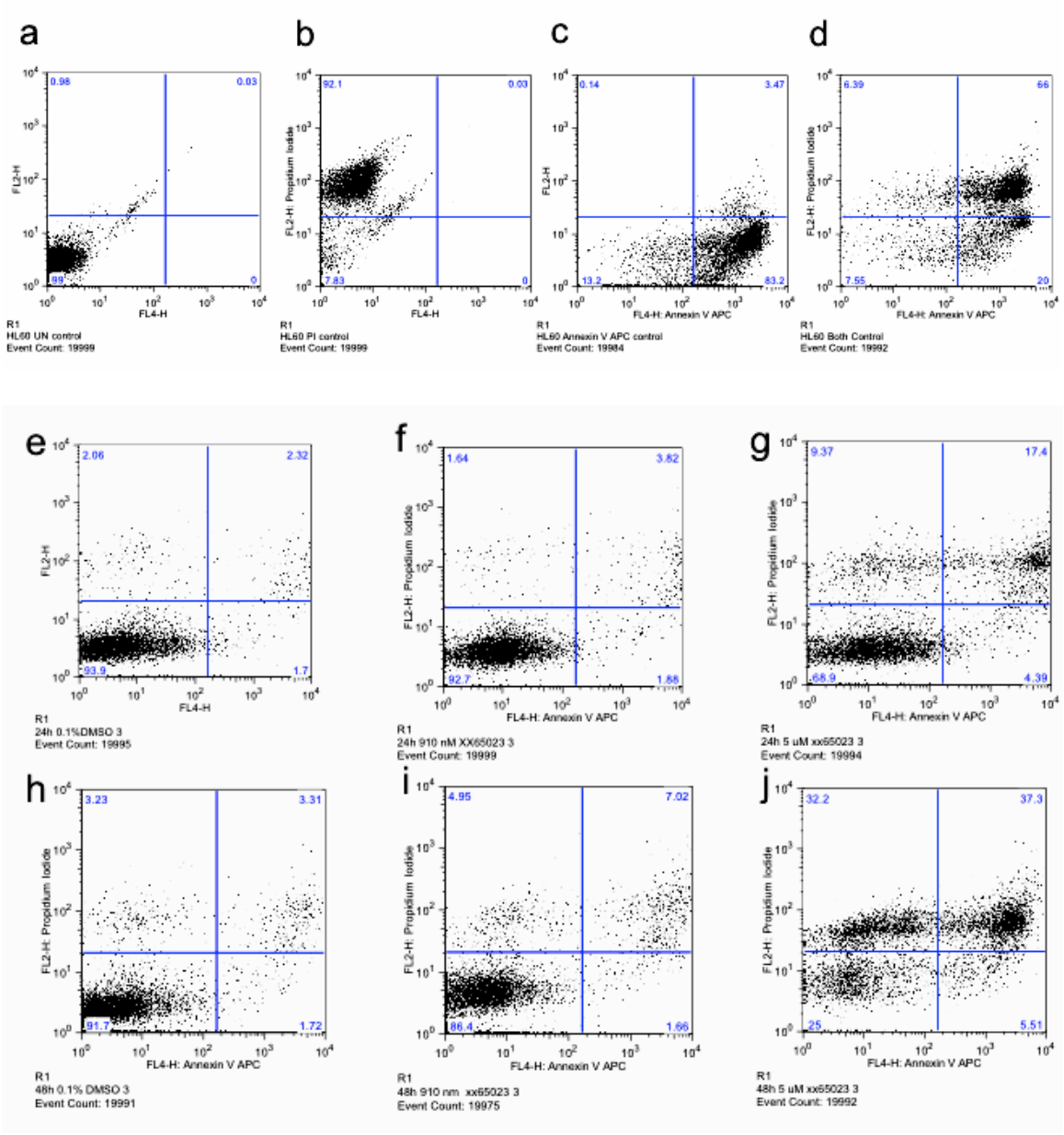

Figure 1.25. FACS analysis of apoptosis in HL60 cells treated with XX-650-23. Controls for HL60 cells included cells that were treated but unstained (**a**), HL60 cells grown in 1X PBS instead of media and stained with PI (**b**), and HL60 cells treated with etoposide and stained with both PI and annexin V (**c**). HL60 cells were treated with either 0.1% DMSO (**e, h**), 910 nM XX-650-23 (**f, i**) or 5 μM XX-650-23 (**g, j**) for 24 and 48 hours, respectively.

The potential XX-650-23-mediated apoptotic effect was also analyzed by identifying poly(ADP-ribose) polymerase (PARP) cleavage after treatment of HL60 or

KG-1 cells with 910 nM or 5 μM XX-650-23 (**Fig. 1.26**). Cells were also treated with etoposide as a positive control for apoptosis. A very intense band, corresponding to cleaved PARP, can be seen in the HL60 sample treated with etoposide (first panel). After 24 hours of 5 μM XX-650-23 treatment, a faint cleaved PARP band can be observed. After 48 hours of treatment, a band is present in both HL60 samples that were treated with either 910 nM or 5 μM XX-650-23. KG-1 cells treated with etoposide or 5 μM XX-650-23 show a very faint band, corresponding to cleaved PARP (third panel).

The potential effect of XX-650-23 on the cell cycle of HL60 cells was also analyzed (**Fig. 1.27**). We found that XX-650-23 increased the number of cells present in the G1/S phase and decreased the number of cells entering the S and S/G2M phases of the cell cycle during a 48 hour period.

To determine whether XX-650-23 affects CREB target genes involved in the cell cycle, differentiation, or apoptosis, we treated HL60 and KG-1 cells with 910 nM XX-650-23 for various times and assessed their relative mRNA expression by qRT-PCR **(Fig. 1.28**). The results showed that in HL60 cells, XX-650-23 downregulates Beclin1 and FOS1 by 20 and 40 percent, respectively, after twelve hours. In KG-1 cells, we observed the downregulation of cyclin A1 by 60 percent after six hours. In HL60 cells, cyclin D1 was also downregulated by 60 percent after 48 hours.

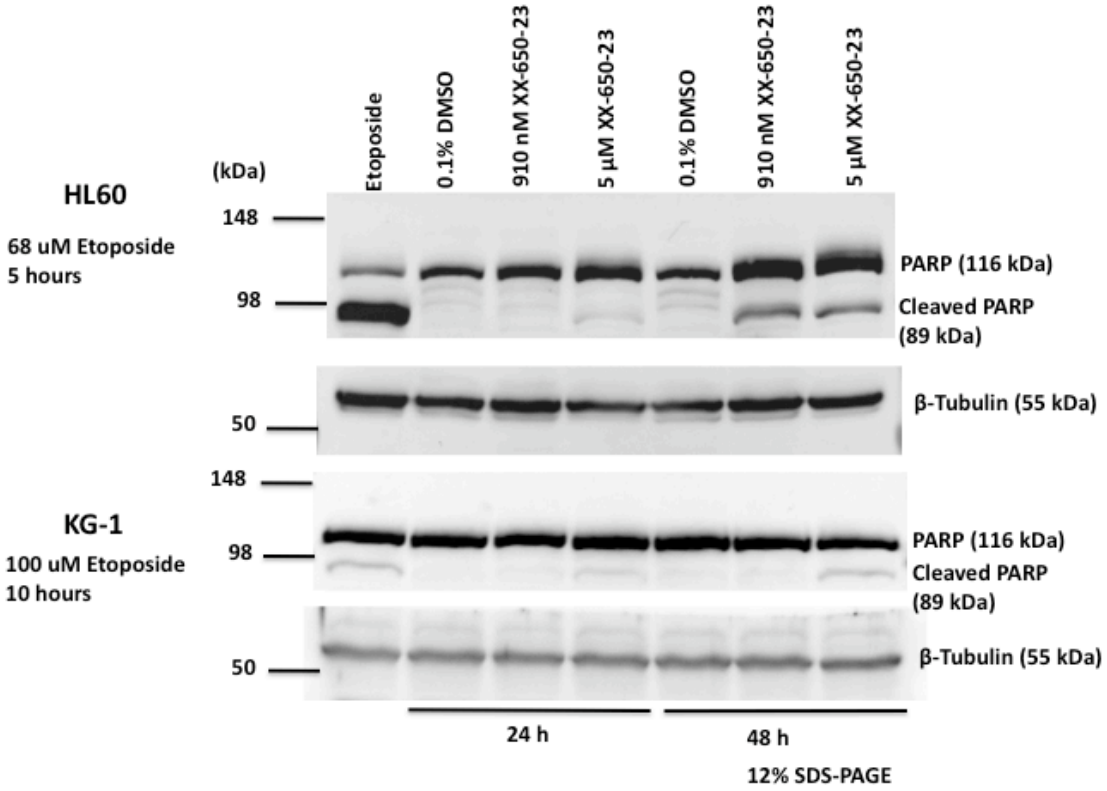

Figure 1.26. XX-650-23 induces apoptosis in HL60 cells but not in KG-1 cells. HL60 and KG-1 were treated with 0.1% DMSO or either 910 nM or 5 µM of XX-650-23 for 24 or 48 hours. Etoposide was used as a positive control. Cell lysates were subjected to SDS-PAGE. Nitrocellulose membranes were blotted with anti-PARP (Cell Signaling) or β-tubulin (Santa Cruz). We used ECL to identify the bands.

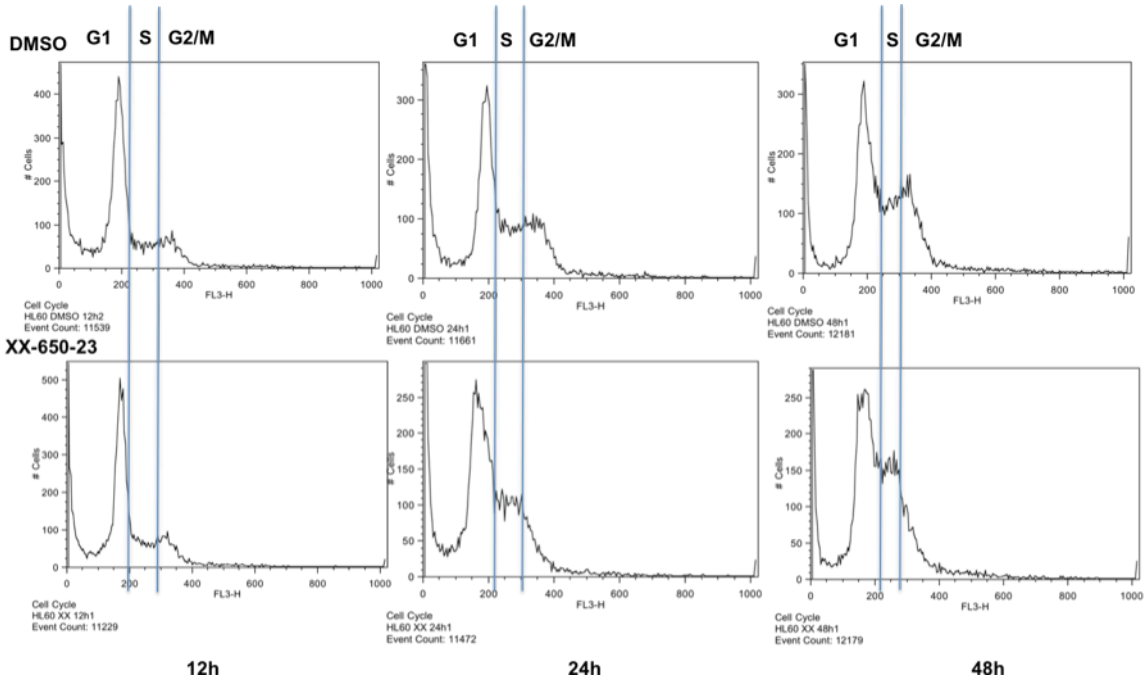

Figure 1.27. XX-650-23 delays cell cycle in the G1/S phase. HL60 cells were treated with either 0.1% DMSO **(top panels)** or with 1 μM XX-650-23 **(bottom panels)** for 12, 24, or 48 hours. Cells were fixed with 70% ethanol and, prior to FACS analysis, the cell pellet was resuspended with cell cycle buffer containing 7ADD.

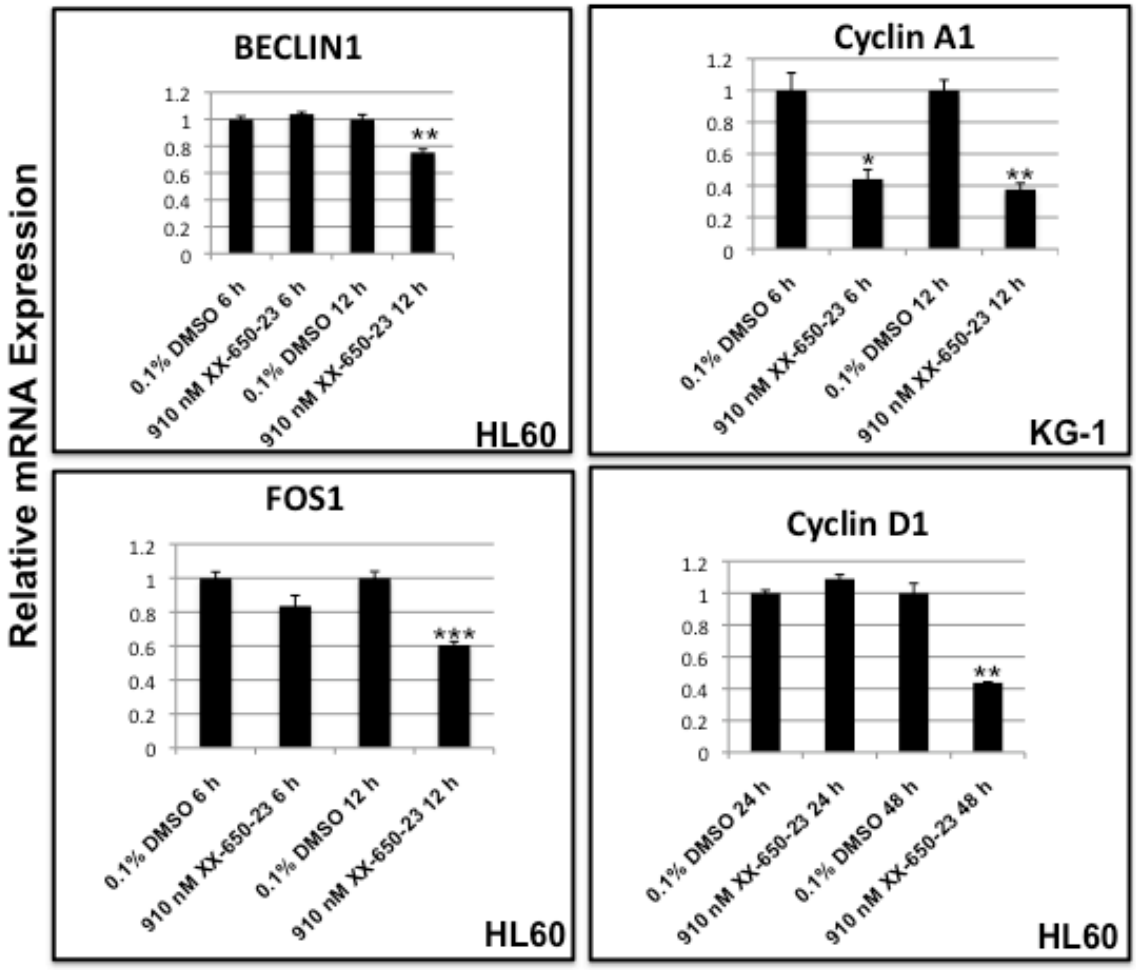

Figure 1.28. Relative mRNA expression of CREB target genes in the presence of XX-650-23. HL60 and KG-1 cells were treated with 0.1% DMSO or 910 nM XX-650-23 at different times. Total RNA was extracted using the Aurum Total RNA Mini Kit (Bio-Rad). RT-PCR and qRT-PCR were performed using iScript cDNA synthesis and SyberGreen (Bio-Rad), respectively. We used CREB-specific primers and normalized expression to the housekeeping gene β-actin. *p<0.05, **p<0.01, ***p<0.001.

1-5 Discussion

AML is the most common type of leukemia in adults. Despite chemotherapy, most patients relapse and die of their disease. Therefore, new targets and therapeutic agents need to be developed. Our lab found CREB overexpressed in the majority of BM samples with AML [10, 12]. XX-650-23 is a small molecule that can disrupt the CREB:CPB complex and potentially inhibit the expression of genes involved in cell proliferation, differentiation, and survival. Our study showed that XX-650-23 affected AML, HL-60, and KG-1 cells, with an IC50 of approximately 910 nM (**Fig. 1.6**). More interesting, the methylcellulose assay showed that XX-650-23 does not affect normal BM cells at XX-650-23 concentrations up to 10 μM (**Fig. 1.7**). We tried performing the same experiment with AML BM cells but did not succeed in colony formation — instead, we observed small clusters or smears. Therefore, we decided: (a) to grow normal BM and AML BM cells in liquid media supplemented with cytokines; (b) to treat the BM samples with different concentrations of XX-650-23; and (c) to determine cell viability using the trypan blue dye exclusion method (**Fig. 1.8**). We found that 2 μM XX-650-23 had no effect on normal BM cells but sufficed to inhibit up to 40 percent of cell proliferation of AML and relapsed AML BM samples (**Fig 1.8**).

In order to determine the XX-650-23 therapeutic index, we treated AML BM, relapsed AML BM, and normal BM cells under the same liquid media conditions. We found that it took over 4 μM to inhibit 50 percent of normal BM cell proliferation, yielding a therapeutic window of more than fourfold for AML cell lines (KG-1 and HL-60 cells)

and approximately twofold for both AML BM and relapsed AML BM samples. The discrepancy in the effect of XX-650-23 on normal BM cells may be due to the lack of solubility in methylcellulose or to drug instability after 14 days. In order to test its stability after 14 days at 37 °C, the drug can be incubated in liquid media under those conditions and then used to treat AML cell lines for 48 hours. A dramatic reduction of the effect of XX-650-23 would indicate its instability under those conditions.

Cytarabine in combination with daunorubicin is widely known to be the standard therapy against AML. However, this combination is very toxic, and the relapse rate remains high. We examined whether XX-650-23 could be used in combination with either drug. We hoped that XX-650-23 would behave synergistically with both cytarabine and daunorubicin. We found XX-650-23 to be synergistic with cytarabine in HL-60 and KG-1 cells (**Fig. 1.11** and **Table 1.1**) and slightly antagonistic with daunorubicin in HL60 (**Fig. 1.12** and **Table 1.2**). CalcuSyn could not take into account the statistical properties in the normalization step that we had to take in order to estimate the signal corresponding to the theoretical maximum biological effect. In general, the confidence intervals are tightest in the middle (near ED50) and wider at the extremes. Therefore, CalcuSyn tended to underestimate the uncertainties at the extremes. We used a nonlinear regression approach to verify the CalcuSyn's results and found them to be in general agreement. For the KG-1 cells treated with XX-650-23 combined with daunorubicin, CalcuSyn estimated CI values was slightly larger than 1 at ED50 and sightly smaller than 1 at ED75 and ED90. Our nonlinear regression estimates for CI ± asymptotic standard errors at ED50, ED75 and ED90 were 1.252±0.146, 1.193 ±0.195 and 1.140 ±0.294, respectively. These uncertainties are large enough that we

could not statistically distinguish any of CI estimates from 1.00. Our results indicate that XX-650-23 combined with cytarabine yields a synergistic effect in both cell types, but the effect of XX-650-23 along with daunorubicin depends on the cell type, yielding a slightly antagonistic effect in HL60 and consistent with an additive effect in KG-1 cells. This finding suggests that XX-650-23 combined with cytarabine may overcome resistance to cytarabine in AML or AML relapsed patients known to have developed that phenotype; therefore, AML BM cells from such patients should be treated with the same combination of compounds to determine whether their AML BM cells respond.

To examine whether XX-650-23 disrupts the CREB:CBP complex in AML cells, we measured the CREB transcriptional activity using a reporter gene, RLuc. To accomplish this study, we formed a CRE-RLuc lentiviral construct and verified that the insert sequence was correct (**Fig 1.13**). We transfected Hek293T cells with the CRE-RLuc lentiviral construct and treated them with 1 μM XX-650-23. We observed a reduction in RLuc transcriptional activity, with an IC50 of approximately 1 μM (data not shown). This result suggests that XX-650-23 binds to CBP and disrupts the CREB:CBP complex. Future studies will transfect the CRE-RLuc construct into Hek293T cells to produce a virus that can be used to transduce HL60 or KG-1 cells.

To further test whether XX-650-23 disrupts the CREB:CBP complex in AML cells, HeLa cells and K562 cells were used as positive controls to optimize the IP assay. CREB:CBP IP assays were not successful, since the levels of CBP protein were found to be limited in K562 and AML cells (**Figs. 1.18** to **1.20**). For the IP assay, we used two different strains of anti-CREB antibodies in order to avoid identifying the IgG, which

migrates almost the same as the CREB band (**Fig. 1.19**). The washes were performed with 1X PBS; in the future, the washes should be performed with either modified RIPA or TNN lysis buffer to get rid of the background. Nuclear extraction yielded concentrated levels of CBP protein in HeLa cells; however, the levels of CBP in K562 cells could not be increased. This finding suggested that the nuclear extraction procedure could not concentrate the levels of CBP in KG-1 or HL60 cells. We decided to change strategy and transfect or, alternatively, nucleofect KG1 cells with a CBP-expressing plasmid**-** **(Fig. 1.21**). Hek293T cells were easily transfected with the CBP-expressing plasmid (**Fig. 1.22**). However, the transfection of suspension cells proved difficult. An alternative method of nucleofecting KG-1 cells with the CBP plasmid yielded an increase in CBP expression (**Fig. 1.24**). The nucleofected samples were selected and expanded with G418 for about 40 days and stored in liquid nitrogen. In future studies, the cells should be treated with 500 ng/mL G418 for about two weeks prior to performing an experiment to make sure that only the cells that have the CBP construct are used. For protein expression, more than 100 µg of protein lysate should be loaded in the SDS-PAGE, since 40 µg of nucleofected KG-1 protein lysate yielded very small amounts of identifiable CBP. An immunoprecipitation assay to identify potential proteins that bind to CBP is necessary to determine compound specificity. We cannot disregard the possibility that XX-650-23 affects other proteins that bind to the KIX-CBP domain. Proteins observed to bind to the KIX-CBP domain include ATF-1, ATF-4, SREBP, YY1, Tax, c-myb, c-Jun, p45/NF-E2, BRCA1, HPV E2, Cubitus interruptus, and Gli3 [43].

Having observed that XX-650-23 decreased cell proliferation, we investigated whether the compound would induce this effect through apoptosis, cell cycle, or both.

We treated HL60 cells with 910 nM or 5 μM XX-650-23 for 24 and 48 hours and determined the percent viability and concentration by the trypan blue dye exclusion method (**Table 1.3**). The percent viability of the HL60 cells treated with 910 nM of XX-650-23 remained almost the same; however, the cell concentration decreased by approximately 40 percent after 48 hours. This result suggests that only a very small number of cells are dying either by necrosis or apoptosis, opening the possibility that XX-650-23 may induce cell cycle arrest. At higher concentrations (5 μM) of XX-650-23, cell viability and concentrations decreased by approximately 45 and 80 percent, respectively, suggesting that necrosis or apoptosis may also contribute to the reduction of both cell viability and concentration.

To test our hypothesis, we used FACS and PARP cleavage to analyze apoptosis (**Figs. 1.25** and **1.26**), respectively. The results indicate that XX-650-23 contributed to apoptosis in a time- and dose-dependent manner, but apoptosis was not the predominant pathway by which cell proliferation was reduced. KG-1 cells were more resistant to apoptosis when treated longer and with higher concentrations of etoposide than those used for HL60 cells (**Fig. 1.26**). The same resistance effect was observed with 5 μM of XX-650-23. Possibly, XX-650-23 inhibits the cell cycle, causing stress in the cells and resulting in a small percentage of cells undergoing apoptosis.

We performed cell cycle analysis, and the results showed that XX-650-23 delays the cell cycle in the G1/S phase, reducing the cell number in the S and G2/M phases of the cell cycle (**Fig. 1.27**). The XX-650-23-mediated cell cycle delay effect needs further investigation, including studying the cell cycle in smaller intervals. Our present result

agrees with a previous report that CREB downregulation in TF-1 and K562 cells decreased the number of cell in the S phase [11]. The ability of this compound to delay the cell cycle at the G1/S transition may improve the effect of cytarabine and other chemotherapeutic agents that work best during the S phase of the cell cycle.

To determine whether XX-650-23 affected CREB target genes involved in the cell cycle, cyclin A1, and cyclin D1 [11], or whether it affected those genes involved in cell proliferation, differentiation, and apoptosis, such as FOS1 [38] and Beclin1 [44], we performed qRT-PCR. The results suggest that XX-650-23 affects CREB target genes (**Fig. 1.28**). XX-650-23 downregulated cyclins A1 and D1, suggesting that it may affect the cell cycle. A decrease in cell proliferation and apoptosis can also be attributed to the XX-650-23-mediated downregulation of Beclin1 and FOS1. In order to further analyze the effect of XX-650-23 on CREB target genes, we treated HL60 cells with 1 μM XX-650-23 for six and twelve hours and performed RNA extraction for microarray analysis. Future studies will validate the microarray data by qRT-PCR.

Together, these results indicate that XX-650-23 disrupts the CREB:CBP complex, leading to a decrease in cell proliferation and apoptosis by downregulating cyclins A1 and D1, FOS1, and Beclin1. XX-650-23 decreases cell proliferation, predominantly by delaying the cell cycle at the G1/S phase. The delay in the cell cycle creates stress that leads to a small percent of apoptosis. Treatment of AML cells with high concentrations of XX-650-23 (5 μM) induced cell death. XX-650-23 combined synergistically with cytarabine, suggesting the potential of XX-650-23 as a candidate to target AML.

1-6 References

1. Burnett, A., Wetzler, M., Löwenberg, B. Therapeutic advances in acute myeloid leukemia. J. Clin. Oncol. 2011; 29(5):487–94.

2. American Cancer Society. Cancer Facts & Figures 2012. Atlanta: American Cancer Society; 2012.

3. Pui, C. H., Carrol, W.L., Meshinchi, S., Arceci, R. J. Biology, risk stratification, and therapy of pediatric acute leukemias: an update. J. Clin. Oncol. 2011; 29(5):551–565.

4. Gale, P.R., Advances in the treatment of acute myelogenous leukemia. NEJM 2010; 300(21):1189–1199.

5. Chabner, B. A., Myers, C. E., Coleman, N., Johns, D. G. The clinical pharmacology of antineoplastic agents (Second of two parts). N. Engl. J. Med. 2010; 292(22):1159–1168.

6. Minotti, G., Menna, P., Salvatorelli, E., Cairo, G., Gianni, L. Anthracyclines: molecular advances and pharmacologic developments in antitumor activity and cardiotoxicity. Pharmacol. Rev. 2004; 56(2):185–229.

7. Look, A. T. Oncogenic transcription factors in the human acute leukemia. Science 1997; 278:1059–1064.

8. Marcucci, G., Haferlach, T,. Dohner, H. Molecular genetics of adult acute myeloid leukemia: prognostic and therapeutic implications. J. Clin. Oncol. 2011; 29(5):475–86.

9. Zucman, J., Delattre, O., Desmaze, C., Epstein, A. L., Stenman, G. Speleman, F. Fletchers, C. D., Aurias, A., Thomas, G. EWS and ATF1 gene fusion induced by t(12;22) translocation in malignant melanoma of soft parts. Nature genet. 1993; 4:341–5.

10. Crans-Vargas, H. N., Landaw, E. M., Bhatia, S., Sandusky, G., Moore, T. B., Sakamoto, K. M. Expression of cyclic adenosine monophosphate response-element binding protein in acute leukemia. Blood 2002; 99(7): 2617–2619.

11. Shankar, D. B., Cheng, J. C., Kinjo, K., Federman, N., Moore, T. B., Gill, A., Rao N. P., Landaw, E. M., Sakamoto, K. M. The role of CREB as a proto-oncogene in hematopoiesis and in acute myeloid leukemia. Cancer Cell 2005; 7(4):351–62.

12. Kinjo, K., Sandoval, S., Sakamoto, K. M., Shankar, D. B. The role of CREB as a proto-oncogene in hematopoiesis. Cell Cycle 2005; 4:1134–1135.

13. Desdouets, C., Matestic, G., Molina, C. A., Foulkes, N. S., Sassone-Corsi, P., Brechot, C., Sobczak-Thepot, J. Cell cycle regulation of cyclin A gene expression by the cyclic AMP-responsive transcription factors CREB and CREM. Mol. Cell. Biol. 1995; 15:3301–9.

14. Lee, R. J., Albanese, C., Stenger, R. J., Watanabe, G., Inghirami, G., Haines, G. K. 3rd, Webster, M., Muller, W. J., Brugge, J. S., Davis, R. J., Pestell, R. G. pp60(v-src) induction of cyclin D1 requires collaborative interactions between the extracellular signal-regulated kinase, p38, and Jun kinase pathways. A role for cAMP response element-binding protein and activating transcription factor-2 in pp60(v-src) signaling in breast cancer cell. J. Biol. Chem. 1999; 274:7341–7350.

15. Cheng, J.C., Kinji, K., Judelson, D. R., Chang, J., Wu, W. S., Schmid, I., Shankar, D. B., Kasahara, N., Stripecke, R., Bhatia, R., Landaw, E. M., Sakamoto, K. M. CREB is a critical regulator of normal hematopoiesis and leukemogenesis. Blood 2008; 111(3):1182–1192.

16. Shaywitz, A. J., Greenberg, M. E. CREB: a stimulus-induced transcription factor activated by a diverse array of extracellular signals. Annu. Rev. Biochem. 1999; 68:821–861.

17. Sakamoto, L. M., Frank, D. A. Creb in the pathophysiology of cancer: Implications for targeting transcription factors for cancer therapy. Clin. Cancer Res. 2009; 15(8):2583–2587.

18. Cho, E.-C., Mitton, B., Sakamoto, K. M. Creb and Leukemogenesis. Crit. Rev. Oncog. 2011; 16(1–2):37–46.

19. Mayr, B., Montminy, M. Transcriptional regulation by the phosphorylation-dependent factor CREB. Nat. Rev. Mol. Cell Biol. 2001; 2(8):599–609.

20. Montminy, M. R., Sevarino, K. A., Wagner, J. A., Mandel, G., Goodman, R. H. Identification of cyclic-AMP responsive element within the rat somatostatin gene. Proc. Natl Acad. Sci. USA 1986; 83:6682–6686.

21. Short, J. M., Wynshaw-Boris, A., Short, H. P., Hanson, R. W. Characterization of the phosphoenolpyruvate carboxykinase (GTP) promoter-regulatory region. II. Identification of cAMP and glucocorticoid regulatory domains. J. Biol. Chem. 1986; 261:9721–9726.

22. Comb. M., Birnberg N. C., Seasholtz, A., Herbert, E., Goodman, H. M. A cyclic AMP- and phorbol ester-inducible DNA element. Nature 1986; 323:353–356.

23. Zhang, X., Odom, D.T., Koo, S.–H., Conkright, M. D., Canettieri, G., Best, J., Chen, H., Jenner, R., Herbolsheimer, E., Jacobsen, E., Kadam, S., Ecker, J. S., Emerson, B., Hogeneshch, J. B., Unterman, T., Young, R. A., Montminy, M. Genome-wide

analysis of cAMP-response element binding protein occupancy, phosphorylation, and target gene activation in human tissues. PNAS 2005; 102: 4459–4464.

24. Quinn, P.G., Distinct activation domains within cAMP response element-binding protein (CEB) mediate basal and cAMP-stimulated transcription. J. Biol. Chem. 1993; 268:16999–17009.

25. Xing, L., Quinn, P.G. Three distinct regions within the constitutive activation domain of cAMP regulatory element-binding protein (CREB) are required for transcription activation. J. Biol. Chem. 1994; 269:28732–28736.

26. Bannister, A. J., Kouzarides, T. The CBP co-activator is a histone acetyltransferase. Nature 1996; 384:641–643.

27. Kee, B., Arias, J., Montminy, M. Adaptor-mediated recruitment of RNA polymerase II to a signal dependent activator. J. Biol. Chem 1996; 271:2373–2375.

28. Radhakrishnan, I., Perez-Alvarado, G. C., Parker, D., Dyson, H. J., Montminy, M. R., Wright, P. E. Solution structure of the KIX domain of CBP bound to the transactivation domain of CREB: A model for activator:coactivator interactions. Cell 1997; 91:741–752.

29. Chrivia, J. C., Kwok R. P., Lamb, N., Hagiwara, M., Montminy, M. R., Goodman R. H. Nature 1993; 365:855–859.

30. Parker, D., Ferreri, K., Nakajima, T., LaMorte, V. J., Evans, R., Koerber, S. C., Hoeger, C., Montminy, M. R. Phosphorylation of CREB at Ser-133 Induces complex formation with CREB-binding protein via a direct mechanism. Mol. Cell Biol. 1996; 16(2):694–703.

31. Brindle, P., S. Linke, and M. Motminy. Protein-kinase-A-dependent activator in transcription factor CREB reveals new role for CREM repressors. Nature 1993; 364:821–824.

32. Bohm, M., Moellmann, G., Cheng, E., Alvarez-Franco, M., Wagner, S., Sassone-Corsi, P., Halaban, R. Identification of p90RSK as the probable CREB-Ser133 kinase in human melanocytes. Cell Growth Differ. 1995; 6(3):291–302.

33. Wong, A., Sakamoto, K. M. Granulocyte-macrophage colony-stimulating factor induces the transcriptional activation of 3gr-1 through a protein kinase A-independent signaling pathway. J. Biol. Chem. 1995; 270(51):30271–30273.

34. Kwon, E. M., Raines, M. A., Blenis, J., Sakamoto, K. M. Granulocyte-macrophage colony-stimulating factor stimulation results in phosphorylation of cAMP response element-binding protein through activation of pp90RSK. Blood 2000; 95(8):2552–2558.

35. Yeung-Tung, S., Dong-Yan, J. CREB – a real culprit in oncogenesis. FEBS J. 2007; 274:3224–3232.

36. Altarejos, J. Y., Montminy, M. CREB and the CRTC co-activators: sensors for hormonal and metabolic signals. Nat Rev Mol Cell Biol. 2011; 12(3):141–151.

37. Xu, W., Chen, H., Du, K., Asahara, H., Tini, M., Emerson, B. M., Montminy, Evans, R. M. A transcriptional switch mediated by cofactor methylation. Science 2001; 294:2507–2511.

38. Best, J. L., Amezcua, C. A., Mayr, B., Flechner, L., Murawsky, C. M., Emerson, B., Zor, T., Gardner, K. H., Montminy, M. Identification of small-molecule antagonists that inhibit an activator:coactivator interaction. PNAS 2004; 101(51):17622–17627.

39. Li, B., X., Xiao, X. Discovery of a small-molecule inhibitor of the KIX-KID interaction. ChemBioChem. 2009; 10:2721–2724.

40. Zhao, L., Wientjes, M.G., Au, J.L. Evaluation of combination chemotherapy: integration of nonlinear regression, curve shift, isobologram, and combination index analyses. Clin. Cancer Res. 2004; 10(23):7994–8004.

41. Yu, J., Belle, L.D., Liang, H., Adamson, E., D. Coactivating factors p300 and CBP are transcriptionally cross regulated by Egr1 in prostate cells, leading to divergent response. Mol. Cell 2004; 15:83–94.

42. Ye, J., Coulouris, G., Zaretskaya, I., Cutcutache, I., Rozen, S., Madden, T. Primer-BLAST: A tool to design target-specific primers for polymerase chain reaction. BMC Bioinformatics 2012; 13:134.

43. Vo, Ngan, Goodman, R. H. CREB-binding protein and p300 in transcriptional regulation. J. Biol. Chem 2001; 276(17):13505-13508.

44. Wang, J. Beclin 1 bridges autophagy, apoptosis and differentiation. Autophagy 2008; 4(7):947–948.

CHAPTER 2

Tubacin Suppresses Proliferation and Induces Apoptosis of Acute Lymphoblastic Leukemia Cells

---

2-1 Introduction

Histone acetylase inhibition and cancer

The inhibition of histone acetylation has been a common subject of clinical research in cancer [1–5]. Histone deacetylases (HDACs) and histone acetylase transferases (HATs) are two classes of enzymes that modulate the degree of acetylation of histones, thereby regulating access of the transcriptional machinery to DNA [6]. HDACs are associated with repression of gene transcription due to the removal of charge-neutralizing acetyl groups from the histone lysine tails, which can lead to a more compact chromatin structure [6]. HDACS are classified into three groups based on their primary homology to three *Saccharomyces cerevisiae* HDACs [7–9].

Class I HDACs, which include HDACs 1, 2, 3, and 8, share similarity with the yeast transcriptional regulatory protein γRPD3; class II HDACs, which include HDACs 4, 5, 6, 7, 9, and 10, are more similar to γHDA1. HDAC11 has not been classified, but it is more closely related to class I HDACs. Class III HDACs are similar to the NAD^+-dependent γSIR2. Most HDACs are located in the nucleus; however, class II HDACs can translocate to the cytoplasm [7]. Although the primary function of HDAC proteins is to deacetylate histones [6–9], some HDACs, such as HDAC6, can also affect cytoplasmic nonhistone proteins. Surprisingly, HDAC6 was found to deacetylase histones only *in vitro* [9].

HDAC6 has been reported to play a role in cancer. HDAC6 was found to be required for Ras-induced oncogenic cell transformation by providing anchorage-independent proliferation. This effect allows the cells to escape a type of cell death known as anoikis, which is characterized by insufficient adhesion of cells to the surrounding basement membrane and extracellular matrix [10]. Expression of HDAC6 was found to increase cell motility, a key event in tumor metastasis, and its inhibition led to hyperacetylated cortactin and impaired cell motility [5]. HDAC6 is also involved in heat-shock-protein (Hsp)-90-mediated proteosomal degradation of vascular endothelial growth factor receptors (VEGFRs) 1 and 2 [11]. VEGFRs play major roles in tumor growth and angiogenesis, the formation of new blood vessels [11]. HDAC6 was also identified as a novel estrogen-regulated gene with prognostic significance in estrogen-receptor α-positive breast cancer cells [3]. The estrogen receptor is the most reliable marker for selecting antiestrogen treatment in breast cancer [3]. Another group of researchers reported that combining the farnesyltransferase inhibitor lonafarnib with

paclitaxel (taxol) enhances HDAC6-dependent tubulin deacetylation in breast and small-cell lung carcinoma cells [2].

The finding that HDC6 could not deacetylase histone *in vivo* led to the search for an HDAC inhibitor that mediates acetylation of proteins other than histones. Tubacin (*tub*ulin *ac*etylation *in*ducer) (**Fig. 2.1**) was discovered by Stuart Schreiber's laboratory after a multidimensional chemical genetic screen of 7,392 small molecules that selected for acetylation activity [12]. Tubacin was found to inhibit HDAC6-mediated α-tubulin deacetylation [13] in multiple myeloma cells (MM) and not in normal peripheral blood mononuclear cells [14]. Tubulin, the main component of microtubules (MTs), forms a heterodimer comprising α and ß subunits [15]. Deacetylation occurs at the conserved lysine 40 (Lys40) ε-amino group near the N-terminus of α-tubulin [16, 17]. The effect of tubacin in combination with bortezomib, a proteasome inhibitor, was investigated in MM cells [14]. Tubacin was found to increase the bortezomib-induced apoptotic effect in myeloma cells by activating c-Jun NH2-terminal kinase/caspase. Hence, tubacin was considered a good candidate for multiple myeloma therapeutic application [14]. Unlike other histone deacetylase inhibitors, tubacin does not induce histone acetylation, cell cycle arrest, gene expression, or spindle morphology [13]. Specific inhibitors of HDAC6 have not been previously studied with ALL cells.

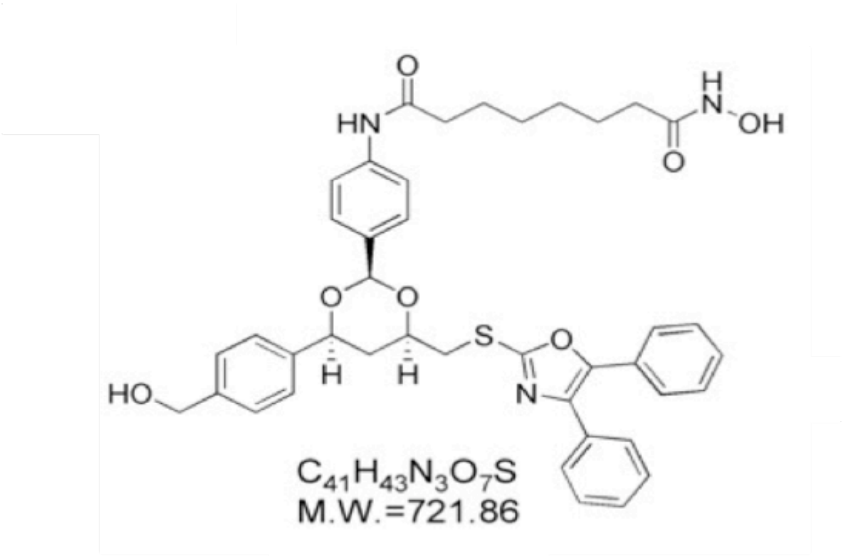

Figure 2.1. Tubacin molecular structure. The carboxylic end that attaches to a linker element serves as a metal chelator (adapted from [14]).
*Reprinted by permission from National Academy of Sciences of the USA: [National Academy of Sciences], **(102)**, copyright (2005).*

Characteristics of HDAC6

HDAC6 is the largest protein yet identified in humans, with 1,216 amino acids [9]; its two homologous catalytic domains make it a unique HDAC protein [9, 18] (**Fig. 2.2**). These domains have been reported to contribute independently to the protein's overall tubulin deacetylase (TDAC) activity. One study showed that both HDAC6 domains target tubulin [19, 20], but other studies found that only the second domain exhibited TDAC activity [13, 17, 21]. HDAC6 also contains a ubiquitin-binding zinc finger domain (ZnF-UBP domain) in its C-terminal region, and a dynein-binding domain (DBD) that play a key role in protein degradation through the aggresome (**Fig. 2.2**) [5, 22]. HDAC6 predominates in the cytoplasm, due to the NES and SE14 motifs (**Fig. 2.2**) [7, 23], but it

is also found on the perinuclear and leading-edge subcellular regions, which are associated with $p150^{glued}$-containing motor complex [16].

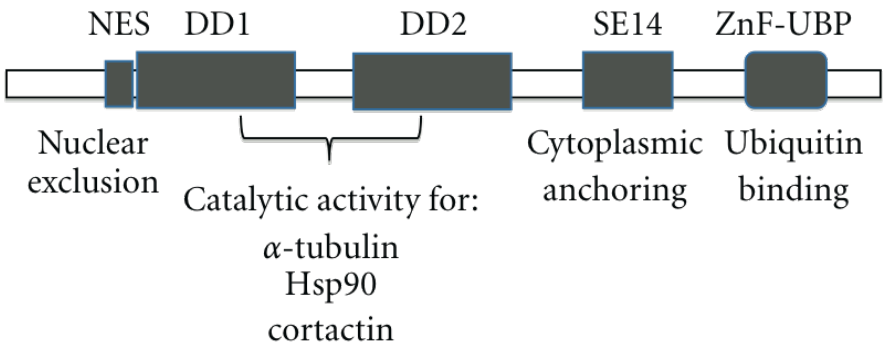

Figure 2.2. The functional domains of HDAC6. HDAC6 is the only HDAC that contains two tandem catalytic domains. Deacetylase domains (DDs 1 and 2) have been reported to interact with α-tubulin, Hsp90, and cortactin. HDAC6 contains a nuclear export signal (NES) and a Ser-Glu-containing tetrapeptide (SE14) that are responsible for the export of the protein from the nucleus and its anchorage in the cytoplasm, respectively. The linker between both DDs binds dynein. HDAC6 also contains a high-affinity ubiquitin-binding zinc finger domain (ZnF-UBP) [5].

HDAC6 and tubacin interaction

Crystal structure investigations of a homologue histone deacetylase-like protein (HDLP), from the bacterium *Aquifex aeolicus*, in complex with the deacetylases trichostatin A (TSA) and suberoylanilide hydroxamic acid (SAHA), respectively revealed the histone acetylase catalytic core and provided a general mechanism for HDAC inhibition [24]. HDLP shares 35.2 percent identity with human HDAC1 [24]. TSA and SAHA are HDAC inhibitors that have been reported to suppress cell growth and induce terminal differentiation [24]. The catalytic domain of HDAC forms a tube-like pocket with a wider bottom. A “charge-relay system” — comprising two adjacent histidine residues, two aspartic residues, and one tyrosine residue at the bottom of the pocket — allows the removal of an acetyl group from a substrate. A zinc ion (Zn^{2+}) that binds near the

bottom of the pocket is coordinated by two additional aspartates, one histidine, and a water molecule (**Fig. 2.3**). HDAC inhibitors chelate the Zn^{2+} ion in the catalytic pocket of HDACs, making the charge-relay system dysfunctional [24].

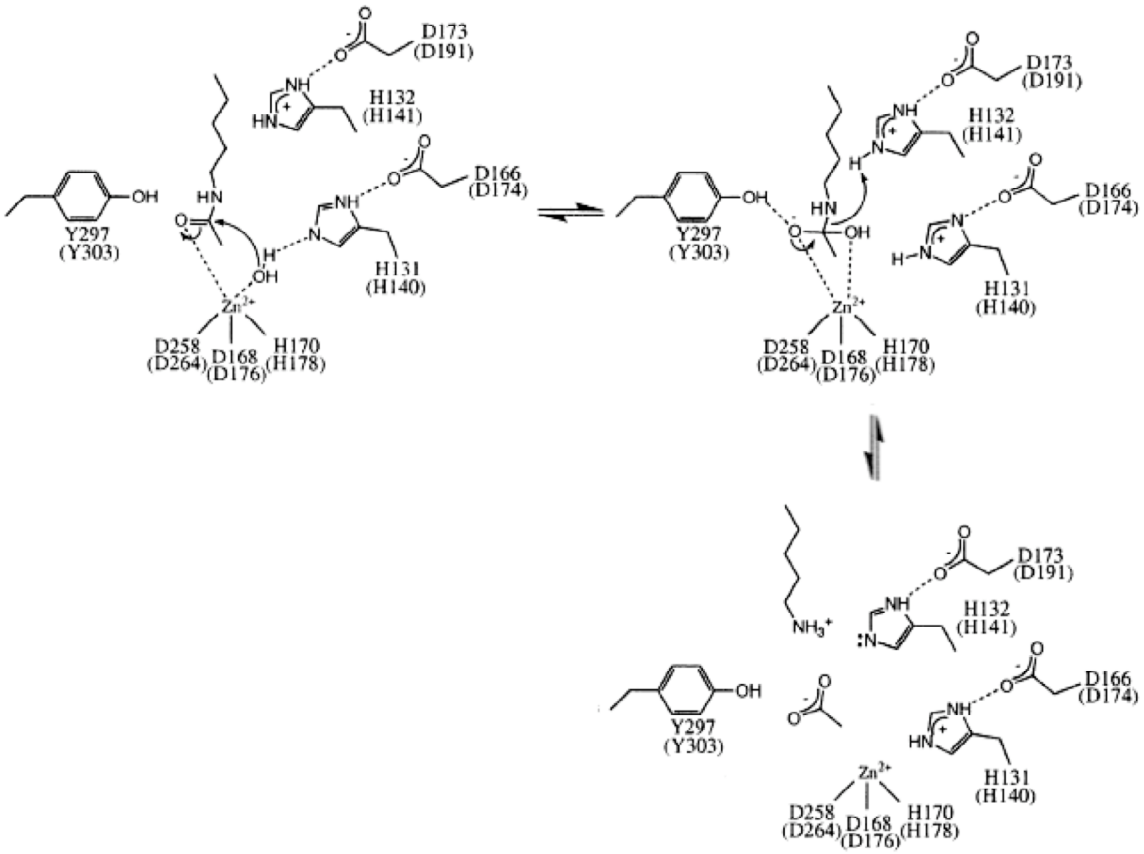

Figure 2.3. The proposed deacetylation mechanism of lysine 40 of α-tubulin by HDLP and HDAC1. The active-site residues of HDLP and the proposed HDAC1 (Amino acids in parenthesis). The carbonyl group of the N-acetyl amide bond binds zinc, making the carbon group a better electrophile. Zinc also binds two aspartates (Asp258 and Asp168), a histidine (His170), and a water molecule. The water molecule is oriented by zinc and becomes more nucleophilic by the negative charge of the Asp166-His131 "charge-relay system". The more nucleophilic water molecule attacks the carbonyl carbon, forming a tetrahedral intermediate that is stabilized by a hydrogen bond from the Tyr297 hydroxyl group. The carbon-nitrogen bond intermediate breaks, accepting a proton from Asp173-His132 "charge relay," generating acetate and lysine. Y=Tyrosine, D=Aspartate, H=Histidine (adapted from [24]).

Tubacin-mediated apoptotic effect

Targeting the proteasome or the aggresome to induce apoptosis is one method to target cancer cells [14, 22]. Cells use the proteasome and the aggresome pathways, are two separate mechanisms, to dispose misfolded proteins for survival [22, 25, 26]. The proteasome is a multiprotein proteolytic complex that recognizes and binds short-lived ubiquitin-marked misfolded proteins [26]. The aggresome, an alternative pathway, activates when the proteasome becomes inhibited [5, 22]. The ubiquitinated-misfolded proteins form aggregates that HDAC6 recognizes, facilitating their clearance by autophagy [5, 22]. Transformed cells accumulate more misfolded proteins than nonmalignant cells. Therefore, they depend more on proteasome and aggresome activity [22]. Apoptosis, or programmed cell death, is an important process for cells during cell development and cellular homeostasis, and its inhibition can lead to cancer [27, 28]. The rate of cell accumulation in cancer can arise from either an increase in the rate of cell proliferation or a decrease in cell death [29]. Cell death occurs in essentially all tissues capable of self-renewal in order to offset the rate of cell production by the rate of old cell death [29].

HDAC6 plays a major role in the aggresome pathway because it can bind both polyubiquitinated proteins and dynein. Dynein is a motor protein that transports cellular cargo along MTs to the major microtubule organizing center (MTOC), where the aggresome is generated [5, 22, 30]. The aggresome consists of ubiquitinated-misfolded proteins that form particulate (about 200 nm) miniaggregates that are surrounded by intermediate filament cytoskeleton. The dynamic aggresome recruits chaperones,

ubiquitination enzymes, and proteasome subunits that eventually activate autophagic clearance [5, 22, 30]. Tubacin was found to disrupt molecular complexes of HDAC6 with intracellular proteins, including tubulin or dynein [13, 14]. Tubacin synergistically increased the apoptotic effect of bortezomib by disrupting the molecular complexes of HDAC6 with dynein [14] in multiple myeloma cells (**Fig. 2.4**).

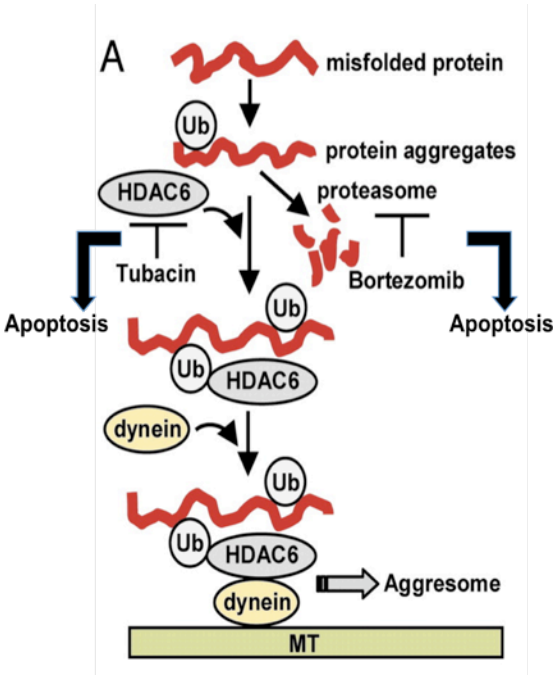

Figure 2.4. Tubacin inhibits binding of HDAC6 with dynein and synergistically induces apoptosis. Misfolded proteins are ubiquitinated (Ub) and degraded by the proteasome and/or the aggresome. Bortezomib inhibits the proteasome, and accumulation of unfolded proteins leads to apoptosis. Tubacin inhibits the binding of HDAC6 with dynein, preventing the transportation of misfolded proteins to the aggresome along MTs. This effect leads to a synergistic increase in apoptosis (adapted from[14]).

*Reprinted by permission from National Academy of Sciences of the USA: [National Academy of Sciences], **(102)**, copyright (2005).*

The increase in acetylated tubulin is also known to inhibit Na^+/K^+-ATPase activity, leading to apoptosis [31] (**Fig. 2.5**). Na^+/K^+-ATPase, an integral membrane protein found in the cells of all higher eukaryotes, uses the hydrolysis of adenosine triphosphate (ATP) to drive the transfer of three sodium ions (Na^+) to the extracellular membrane and two potassium ions (K^+) into the intracellular membrane [32]. This ion exchange helps maintain ion homeostasis, keeping the required cell volume for the cell to function properly [32, 33]. Various kinases — including cyclic adenosine monophosphate

(cAMP)-dependent protein kinase (PKA), cyclic guanosine monophosphate (cGMP)-dependent protein kinase (PKG), and protein kinase C, as well as serum, hormones [33], and L-glutamate and its association with acetylated tubulin — can regulate Na^+/K^+-ATPase activity [15, 33–36]. The association of tubulin with the α subunit of Na^+/K^+-ATPase was found to require acetylation of α-tubulin at Lys40 [31, 35], and this tubulin acetylation consequently inhibits Na^+/K^+-ATPase activity [31]. The inhibition of Na^+/K^+-ATPase by cardiac glycosides, such as oleandrin and ouabain, increase the acetylation of tubulin, leading to an increase in Na^+ and a decrease in K^+. This ion imbalance generates the release of calcium ions (Ca^{2+}), which activates caspases involved in apoptosis [37–39].

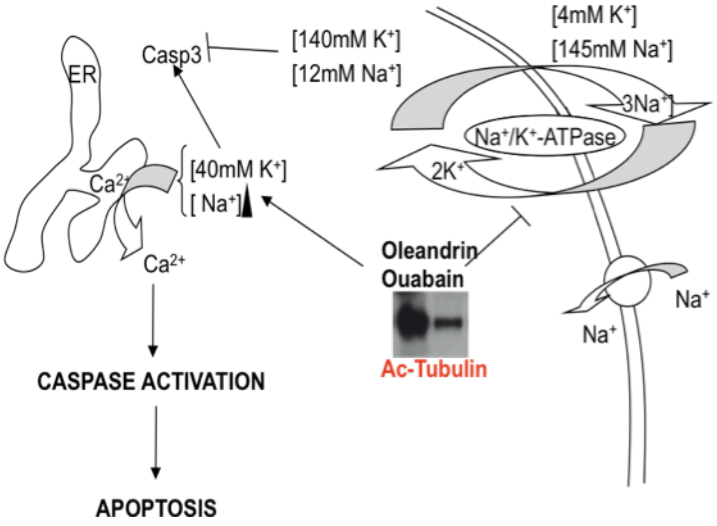

Figure 2.5. Inhibition of Na^+/K^+-ATPase protein leads to apoptosis. The normal intracellular and extracellular concentrations of K^+ and Na^+ inhibit caspase (Casp) 3 activation. Increased acetylation of tubulin (WB) inhibits Na^+/K^+-ATPase. Inhibition of Na^+/K^+-ATPase by oleandrin or ouabain induces ion imbalance (an intracellular decrease in K^+ and an increase in Na^+), release of Ca^{2+}, caspase activation, and apoptosis [37–39].

Work by other scientists involving the inhibition of HDACs, accumulation of acetylated tubulin, and apoptosis (as discussed in this paper) led us to consider the aggresome and the Na^+/K^+-ATPase pathways as two potential targets that could be used to inhibit growth of ALL cells. In our laboratory, 3-(4,5-dimethylthiazol-e-yl)-2,5-diphenyl tetrazolium bromide (MTT) assays showed that tubacin induced an inhibition of

ALL cell growth at a half maximal inhibitory concentration (IC50) of 1.2 to 2 μM [40]. We also found that normal lymphocyte proliferation was inhibited at much higher concentrations (IC50 of 16 μM), indicating the existence of a therapeutic window. The difference in sensitivity may be due to the levels of HDAC6 present. HDAC6 was overexpressed in ALL cell lines and ALL patients, compared to normal proliferating lymphocytes [40]. Together, these results suggest that tubacin affects ALL cells. Therefore, we studied the effect of tubacin in ALL cells further.

Hypothesis

Tubacin-mediated acetylation of tubulin in ALL cells may lead to inhibition of Na^+/K^+-ATPase, ion imbalance, and apoptosis.

Specific aims

Specific aim #1: To verify that tubacin suppresses proliferation of Jurkat cells.

Specific aim #2: To examine whether cell growth inhibition in Jurkat cells is due to tubacin-mediated apoptosis.

Specific aim #3: To examine whether tubacin induces α-tubulin acetylation in ALL cells, leading to ion imbalance and subsequently contributing to apoptosis.

2-2 Overview of Experimental Design

Specific aim #1: To verify that tubacin suppresses proliferation of Jurkat cells

Previous MTT data from our laboratory showed that tubacin inhibits proliferation of various ALL cells at IC50s concentrations ranging from 1.2 to 2 μM [40]. We wanted to verify the tubacin IC50 in Jurkat cells using a different method.

Methods for aim #1:

To confirm that tubacin inhibits cell growth proliferation, we performed AlamarBlue assays. The AlamarBlue assay incorporates a fluorometric/colorimetric oxidation-reduction (REDOX) indicator that is used to measure the metabolic activity of living cells. Oxidized resazurin (nonfluorescent, blue) is reduced to resorufin (fluorescent, red). The fluorescence or change in color is proportional to the number of living cells.

Expectation for Aim #1:

We expected tubacin to inhibit the proliferation of Jurkat cells at an IC50 of approximately 2 μM.

Specific aim #2: To examine whether cell growth inhibition in Jurkat cells is due to tubacin-mediated apoptosis

Previous work has demonstrated that the inhibition of the growth of myeloma cells occurred in combination with bortezomib, a proteasome inhibitor. We wanted to determine whether tubacin, as a single agent, would suffice to induce apoptosis.

Methods for aim #2:

We planned to treat Jurkat cells separately with DMSO or tubacin for four, six and twelve hours and to identify the potential presence of cleaved PARP by WB procedure. Full length PARP is 116 kDa, and cleaved PARP is 89 kDa and 24 kDa. ALL cells would be treated with etoposide as a positive control.

Expectation for aim #2

We expected apoptosis to be one of the pathways by which tubacin inhibits cell growth. The presence of cleaved PARP would indicate that apoptosis occurred.

Specific aim #3: To examine whether tubacin induces α-tubulin acetylation in ALL cells, leading to ion imbalance and subsequently contributing to apoptosis

Previous work has demonstrated that accumulation of α-tubulin acetylation leads to the inhibition of the Na^+/K^+-ATPase pump, ion imbalance, and activation of caspases involved in apoptosis [31, 37–39, 41]. Our lab planned to examine whether tubacin-mediated inhibition of the Na^+/K^+-ATPase pump and ion imbalance would lead to calcium release and activation of caspases.

Methods for aim #3

We planned to treat Jurkat and Nalm6 Cells separately with DMSO or tubacin for six and twelve hours and the presence and to determine levels of α-tubulin by WB procedure. We would perform Na^+/K^+-ATPase K^+ transport using a FluxOR Thallium Detection Kit (Invitrogen). We would treat ALL cells with DMSO or tubacin for six hours, and then incubate the cells with the FluxOR dye. Because K^+ channels are permeable to thallium (Tl^+), as the K^+ goes down, its concentration gradient the fluorescence will increase. We planned to measure the fluorescent signal using a flow cytometer at an excitation wavelength of 495 nm.

The direct *ex-vivo* $Na^{+/}K^+$-ATPase enzymatic activity (adapted from [42, 43]) would be performed in ALL cells, followed by a Malachite Green Phosphate Assay Kit (BioAssay Systems, Hayward, CA). Jurkat cells would be harvested by centrifugation and lysed. The cell lysates would then be incubated with ATPase assay buffer and treated with DMSO, tubacin, or ouabain for 15 minutes at 37 °C. After treatment, we would incubate the cells with malachite green reagent. This assay is based on the quantification of the green complex formed among malachite green, molybdate, and free orthophosphate. We planned to measure absorbance at 620 nM on a spectrophotometer (Multiskan MCC type 341 plate reader; Titertek, Huntsville, AL).

We planned to measure cytoplasmic Ca^{2+} as in Kulikov et al. [44], using a fluorescence assay that includes the calcium-specific dye FLUO 3/AM (Calbiochem). The FLUO 3/AM is nonfluorescent until hydrolyzed in the cell by cytosolic esterases, trapping the indicator in the cell. FLUO 3/AM is almost nonfluorescent at resting calcium

levels, but fluorescence levels increase upon calcium binding. We planned to measure the fluorescent signal using a flow cytometer at an excitation wavelength of 495 nm.

Expectation for aim #3:

We expected tubacin to increase the levels of acetylated α-tubulin in ALL cells. If this occurred, then the ATPase pump activity could be inhibited; therefore, in the cytosol, the levels of K^+ would decrease, Ca^{2+} would increase, and caspases would be activated.

2-3 Materials and Methods

Cell lines

We obtained Jurkat T-ALL cells from ATCC and Nalm-6 pre-B ALL cells from the German Collection of Microorganisms and Cell Cultures (DSMZ; Deutsche Sammlung von Mikroorganismen und Zellkulturen; Brunswick, Germany). ALL cell lines were cultured in RPMI medium 1640 containing L-glutamine (Invitrogen), 10 percent FBS (Omega Scientific, Tarzana, CA), 100 U/mL penicillin, and 100 ug/mL streptomycin (Invitrogen).

Reagents

We synthesized tubacin in-house and obtained ouabain octahydrate from Sigma.

Growth inhibition assay

The inhibitory effect of tubacin on Jurkat cells was examined by AlamarBlue assay (Invitrogen). Jurkat cells were plated at 3 x 10^5 cells/mL at 37 °C in the presence of 5 percent CO_2. The next day, the cells were treated with tubacin or DMSO and incubated as before for 24 hours, after which we incubated the cells with AlamarBlue for four hours. All experiments were performed in triplicate. Absorbance was monitored at 570 nM excitation wavelength and 600 nM emission wavelength on a spectrophotometer (Multiskan MCC Type 341).

Immunoblotting

Cells cultured with DMSO or tubacin were harvested at 1000 rpm for five minutes at room temperature, washed with 1X DPBS, and lysed with RIPA buffer. Protein quantification was performed by BCA protein assay procedure (Thermo Scientific). We used the boiled SDS-Laemmli method for all WB analysis. Whole cell lysates were subjected to SDS/PAGE, transferred to nitrocellulose membrane (Whatman) and immunoblotted with specific antibodies: anti-acetylated α-tubulin (Sigma), goat anti-mouse IgG-HRP (1:1000; Santa Cruz Biotechnology), monoclonal anti-β-tubulin (1:1000; Santa Cruz Biotechnology), anti-PARP antibody (1:1000; Cell Signaling) and goat-anti-rabbit IgG (H+L)-HRP conjugated (1:2000; Bio-Rad).

Na^+/K^+-ATPase K^+ transport assay

Jurkat cells (3 X 10^5 cells/mL) were incubated for six hours with DMSO or tubacin; then the Na^+/K^+-ATPase K^+ transport was measured using a FluOR Thallium Detection Kit (Invitrogen). Initially, we incubated cells with FluxOR dye. K^+ channels were permeable to thallium (Tl^+); when potassium channels were opened by a stimulus and K^+ went down its concentration gradient, the fluorescence increased. Fluorescence was measured at an excitation wavelength of 485 nm and an emission wavelength of 535 nm, using a plate reader (DTX880; Beckman Coulter).

Na^+/K^+-ATPase enzymatic activity assay

The enzymatic activity of the Na^+/K^+-ATPase pump was determined by direct *ex vivo* enzymatic assay (adapted from [42, 43]) and a Malachite Green Phosphate Assay

Kit (BioAssay Systems). Jurkat cells were harvested by centrifugation at 500 x g for five minutes at 4 °C. The pellet was washed with 1 mL 280 mM HEPES buffer (4-(2-hydroxyethyl)-1-piperazineethanesulfonic acid [Fischer Scientific]), centrifuged as before, resuspended with 280 mM HEPES buffer (5.0 x 10^7 cells/mL), and stored at -80 °C. The cells were lysed by the freeze-thaw method in 280 mM HEPES buffer containing 0.1 mM SDS (2.5 x 10^7 cells/mL) for ten minutes at room temperature. The cell lysates were then incubated with ATPase assay buffer (127 mM NaCl (Fischer Scientific); 20 mM KCl; 5 mM $MgCl_2$ (Fischer Scientific); 3 mM Na_2-ATP (Sigma-Aldrich); 30 mM histidine (Sigma-Aldrich), pH 7.4; 1 mM ethylene glycol tetraacetic acid (EGTA; Sigma-Alrich) and treated with tubacin, ouabain, or DMSO for 15 minutes at 37 °C, followed by a 30 minute incubation with malachite green reagent, also at 37 °C. The absorbance was measured at 620 nM on a spectrophotometer (Multiskan MCC type 341).

Cytosolic Ca^{2+} assay

In order to investigate whether tubacin-mediated Ca^{2+} release occurs, we measured the release of Ca^{2+} as in Kulikov et al. [44], using a fluorescence assay that included the calcium-specific dye FLUO 3/AM (Calbiochem-Millipore; Billerica, MA). The fluorescent signal was measured using a flow cytometer at an excitation wavelength of 495 nm.

2-4 Results

To verify the effect and IC50 of tubacin on Jurkat AML cells, an AlamarBlue assay was performed. The result shows that tubacin inhibits the proliferation of Jurkat cells, with an IC50 of about 2 μM (**Fig. 2.6**). To investigate the mechanism by which tubacin inhibits cell proliferation in ALL cells, we tested whether tubacin is involved in apoptosis. Jurkat cells were treated for six and twelve hours, separately, with DMSO or tubacin, and WB analyses were performed to examine PARP cleavage. A band at 89 kDa was observed after twelve hours of tubacin treatment, suggesting that tubacin induces apoptosis in Jurkat cells (**Fig. 2.7**).

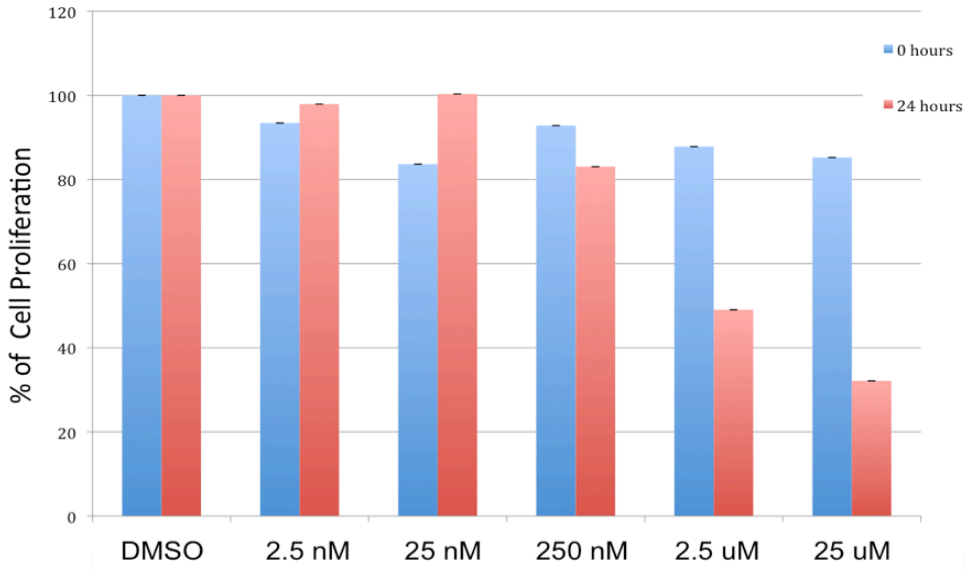

Figure 2.6. Tubacin suppresses proliferation of Jurkat cells. Jurkat cells (3 x 10^5 cells/mL) were treated with 0.1% DMSO or increasing concentrations of tubacin for 0 and 24 hours. The AlamarBlue assay yielded a tubacin IC50 of about 20 uM.

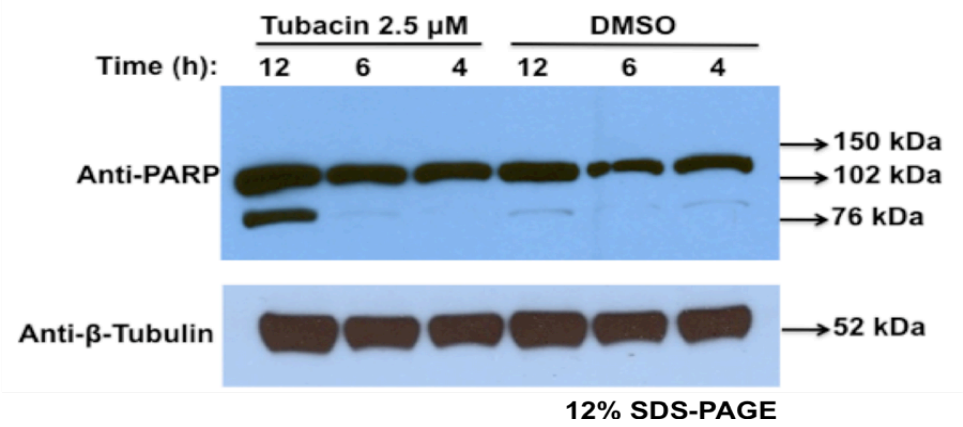

Figure 2.7. Tubacin induces apoptosis in Jurkat cells. Jurkat cells (6 x 10^6 cells) were treated with tubacin or 0.1% DMSO for various times. Cell lysates (40 ug) were subjected to SDS-PAGE. Nitrocellulose membranes were blotted with the respective antibodies, anti-PARP, or anti-β-tubulin (loading control). Full length PARP=116 kDa and cleaved PARP=89 kDa.

Previous studies had demonstrated that tubacin increases acetylation of α-tubulin through inhibition of HDAC6 [5, 14]. To examine whether tubacin increases α-tubulin acetylation in ALL cells, we treated Jurkat and Nalm-6 cells with tubacin for six and twelve hours, separately. WB was performed, and the results show an increase in acetylated α-tubulin in both ALL cell lines (**Fig. 2.8**).

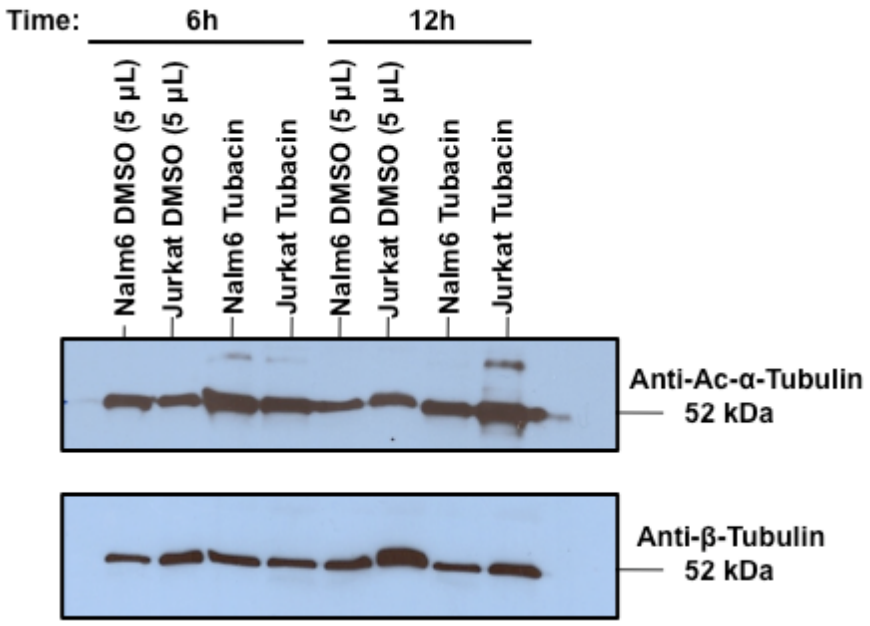

Figure 2.8. Tubacin induces acetylation of α-tubulin in ALL cells. We treated cells with 0.1% DMSO or 2.5 µM tubacin for 6 and 12 hours, separately. Cell lysates were subjected to SDS-PAGE analysis. Nitrocellulose membrane was blotted with anti-Ac-α-tubulin antibody and anti-rabbit IgG (H+L)-HRP-conjugated antibody. The membrane was stripped using Blot Restore Membrane Rejuvenation Kit (Millipore) and reblotted with anti-β-tubulin and anti-mouse IgG-HRP-conjugated antibody.

Acetylation of α-tubulin was previously reported to inhibit the Na^+/K^+-ATPase pump [34, 45, 46]. To determine whether the tubacin-mediated increase in acetylation in AML cells leads to the inhibition of Na^+/K^+-ATPase, we treated Jurkat cells with tubacin or ouabain and measured the transport of K^+. Our result demonstrated that both tubacin and ouabain inhibit intracellular K^+ transport by the Na^+/K^+-ATPase in a similar manner (**Fig. 9**).

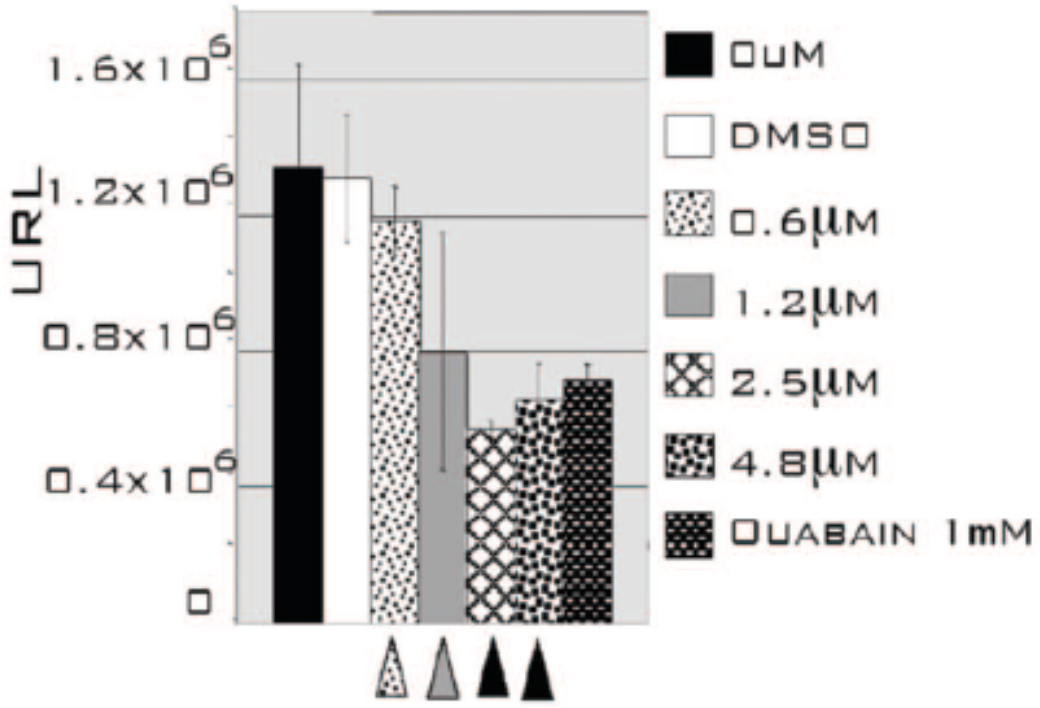

Figure 2.9. Transport of K^+ by the Na^+/K^+-ATPase. Jurkat cells were incubated with DMSO or tubacin for 6 hours, and then Na^+/K^+-ATPase K^+ transport was measured using a FluOR Thallium Detection Kit. The amount of fluorescence correlates with the amount of K^+ present in the cytosol.

*Reprinted by permission from Informa Healthcare: [Leukemia & Lymphoma], **(52)**, copyright (2011).*

The Na^+/K^+-ATPase activity in the presence of tubacin was also measured by direct *ex vivo* enzymatic assay, where the absorption values were directly proportional to the concentration of inorganic phosphate (P_i). Our results suggest that ouabain directly inhibits the Na^+/K^+-ATPase activity but that tubacin-mediated inhibition of the Na^+/K^+-ATPase pump is nonenzymatic (**Fig. 2.10**).

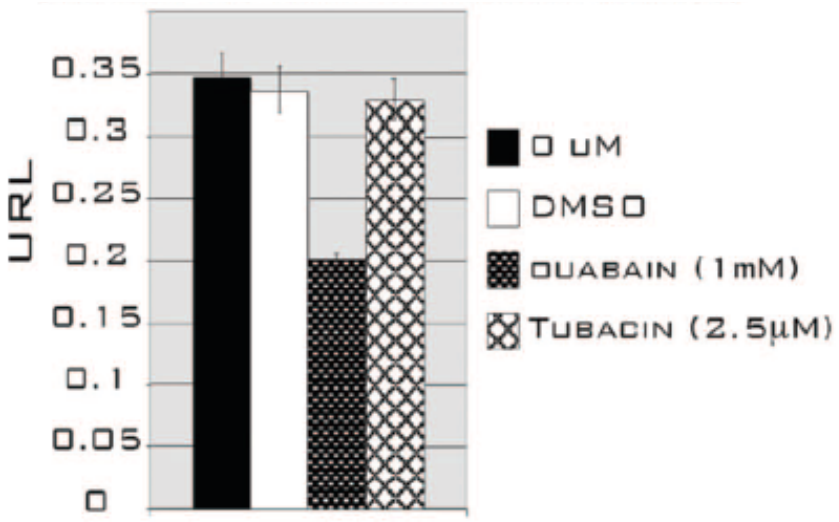

Figure. 2.10. Na^+/K^+-ATPase direct *ex vivo* enzymatic assay. Jurkat cell lysates incubated with ATPase buffer and treated with tubacin, ouabain, or 0.1% DMSO, followed by incubation with malachite green reagent. The green complex formed between malachite green, molybdate, and free orthophosphate was measured at 640 nM on a spectrophotometer.

*Reprinted by permission from Informa Healthcare: [Leukemia & Lymphoma], **(52)**, copyright (2011).*

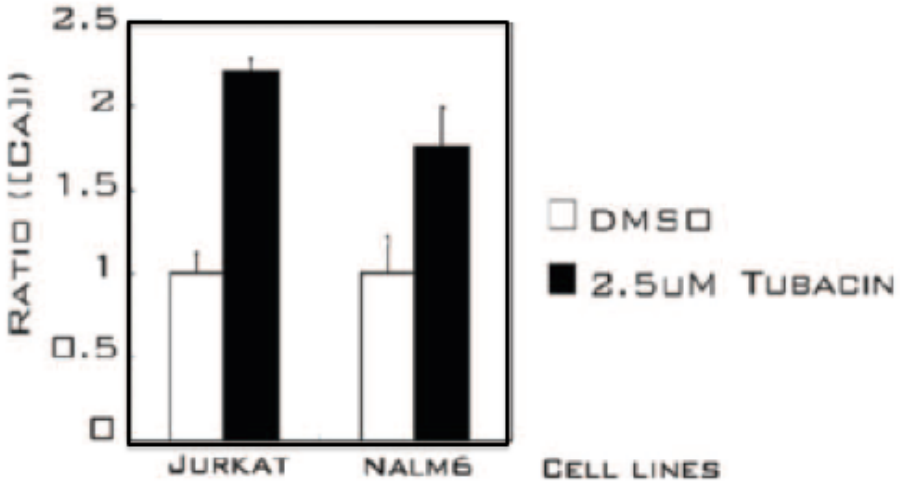

Figure 2.11. Tubacin mediates calcium influx. Cells were treated for 12 hours with 0.1% DMSO or tubacin. Ca+ release from the ER to the cytosol was measured by correlating the levels of fluorescence produced by hydrolyzed FLUO 3/AM in the presence of Ca^2+.

*Reprinted by permission from Informa Healthcare: [Leukemia & Lymphoma], **(52)**, copyright (2011).*

The increase in acetylation, which occurs as early as 30 minutes [40], and inhibition of the Na^+/K^+-ATPase correlated with PARP cleavage twelve hours after tubacin treatment. Finally, we observed increased calcium levels in Jurkat and Nalm-6 cells treated with tubacin for twelve hours (**Fig. 2.11**). Therefore, treatment of ALL cells with tubacin significantly alters the ion homeostasis, including K^+ and Ca^{2+}; however, this is due to an indirect inhibition of the Na^+/K^+-ATPase pump.

2-5 Discussion

Tubacin inhibits Jurkat cell proliferation, with an IC50 of approximately 2 μM. This result agrees with the previous IC50 found in our laboratory using the MTT colorimetric assay [40]. We had also found that tubacin displayed a greater effect against ALL cells than normal T-lymphocytes or BM progenitor cells, yielding a tenfold therapeutic index [40]. These results suggest that HDAC6 should be considered as a potential target for ALL therapy.

To investigate its mechanism of action, we focused on the effects of tubacin on apoptosis, signaling pathways, and metabolism. Previous studies reported that tubacin inhibits HDAC6, resulting in an increase of tubulin acetylation in multiple myeloma cells [14]. Our investigation revealed that tubacin inhibits proliferation of ALL cells due to an increase in acetylation of α-tubulin (**Fig. 2.6**), which leads to a sufficient increase in polyubiquitinated proteins [40] to induce apoptosis, as shown by PARP cleavage (**Fig. 2.7**). These findings indicate that tubacin also inhibits the aggresome pathway in ALL cells similarly to MM cells [14]; however, the tubacin-mediated apoptosis in ALL cells was found to occur through a SAPK/JNK-independent signaling pathway [40].

An increase in α-tubulin acetylation was previously reported to inhibit the Na^+/K^+-ATPase pump [31, 34, 45–46]; hence, we tested whether tubacin could mediate this inhibition in ALL cells. We found that a tubacin-mediated increase in α-tubulin acetylation correlated with inhibition of the Na^+/K^+-ATPase K^+ transport, as expected. However, this inhibition was not direct. Tubacin may possibly induce an alteration in

membrane fluidity that leads to inactivation of Na^+/K^+-ATPase. In fact, evidence suggests that HDAC6 and the aggresome pathway play a role in the integrity of the cytoskeleton and migration of lymphocytes [5, 23]. The reduction of intracellular K^+ concentration was able to induce the endoplasmic reticulum (ER) to release greater levels of Ca^{2+} into the cytosol (**Fig. 2.11**) and activate downstream caspases, as shown by PARP cleavage (**Fig. 2.7**), contributing to apoptosis.

A recent report observed that tubacin-mediated HDAC6 inhibition significantly and selectively increased the cell death effect of the topoisomerase II inhibitors etoposide and doxorubicin and the HDAC inhibitor SAHA in transformed cells, such as LNCaP and MCF-7 cells [47]. Our laboratory also investigated whether combining tubacin with other chemotherapy drugs could increase their effect in ALL cells. Low concentrations of tubacin (0.6 μM) increased the effect of standard chemotherapy drugs, such as vincristine or Velcade *in vitro* [40]. Furthermore, tubacin combined with vincristine, dexamethasone, and L-asparaginase increased the survival of NOD/SCID mice that were previously injected with primary leukemia cells from a relapsed ALL patient [40]. These results make tubacin an attractive agent for use in combination with standard chemotherapy treatment in order to improve the survival prognosis of ALL patients.

In summary, our findings indicate that tubacin treatment induces an accumulation of acetylated α-tubulin, which could lead to altered membrane stiffness. The effects on the membranes could reduce the activity of Na^+/K^+-ATPase, resulting in an increase of intracellular Na^+ and osmotic stress. This osmotic stress could induce intracellular

calcium release that could subsequently trigger apoptosis (**Fig. 2.5**). Taken together, the cumulative damage done to cells by inhibiting HDAC6 and the aggresome leads to apoptosis of ALL cells, thereby providing a rationale to target this pathway for therapy.

2-6 References

1. Marks, P.A., Miller, T., Richon, V. M. Histone deacetylases. Curr. Opin. Pharmacol. 2003; 3:344–351.

2. Marcus, A. I., Zhou, J., O'Brate, A., Hamel, E., Wong, J., Nivens, M., El-Naggar, A., Yao, T. P., Khuri, F. R., Giannakakou, P. The synergistic combination of the farnesyl transferase inhibitor lonafarnib and paclitaxel enhances tubulin acetylation and requires a functional tubulin deacetylase. Cancer Res. 2005; 65:3883–3893.

3. Saji, S., Kawakami, M., Hayashi, S., Yoshida, N., Hirose, M., Horiguchi, S., Itoh, A., Funata, N., Schreiber, S. L., Yoshida, M. Significance of HDAC6 regulation via estrogen signaling for cell motility and prognosis in estrogen receptor-positive breast cancer. Oncogene 2005; 24:4531–4539.

4. Carew, J. S., Giles, F. J., Nawrocki, S. T. Histone deacetylase inhibitors: Mechanisms of cell death and promise in combination cancer therapy. Cancer Lett. 2008; 269:7–17.

5. Aldana-Masangkay, G. I., Sakamoto, K. M. The Role of HDAC6 in Cancer. J. Biomed. and Biotech. 2011; 2011:875824.

6. Marks, P. A., Rifkind, R. A., Richon, V. M., Breslow, R., Miller, T., Kelly, W. K. Histone deacetylases and cancer: causes and therapies. Nature Rev. Cancer 2001; 1:194–202.

7. De Ruijter, A. J. M., Van Gennip, A. H., Caron, H. N., Kemp, S., Van Kuilenburg, A. B. P. Histone deacetylates (HDACs): characteriztion of the classical HDAC family. Biochem. J. 2003; 370:737–749.

8. Verdin, E., Dequiedt, F., Kasler, H. G. Class II histone deacetylases: versatile regulators. Trends Genet. 2003; 19:286–293.

9. Grozinger, C. M., Hassig, C. A., Schreiber, S. L. Three proteins define a class of human histone deacetylases related to yeast Hda1p. Proc. Natl. Acad. Sci. USA 1999; 96:4868–4873.

10. Lee, Y.-S., Lim, K.-H., Guo, X., Kawaguchi, Y., Gao, Y., Barrientos, T., Ordentlich, P., Wang, X. F., Counter, C. M., Yao, T. P. The cytoplasmic deacetylase HDAC6 is required for efficient oncogenic tumorigenesis. Cancer Res. 2008; 68:7561–7569.

11. Park, J.-H., Kim, S.-H., Choi, M.-C., Lee, J., Oh, D.-Y., Im, S.-A., Bang, Y.-Y., Kim, T.-Y. Class II histone deacetylases play pivotal roles in heat shock protein 90-mediated proteosomal degradation of vascular endothelial growth factor receptors. Biochem. Biophys. Res. Commun. 2008; 368:318–322.

12. Haggarty S. J., Koeller, K. M., Wong, J. C., Butcher, R. A., Schreiber, S. L. Multidimensional chemical genetic analysis of diversity-oriented synthesis-derived deacetylase inhibitors using cell-based assays. Chem. Biol. 2003; 10(5):383–396.

13. Haggarty, S. J., Koeller, K. M., Wong, J. C., Grozinger, C. M., Scheiber, S. L. Domain-selective small-molecule inhibitor of histone deacetylase 6 (HDAC6)-mediated tubulin deacetylation. PNAS 2003; 100:389–4394.

14. Hideshima, T., Bradner, J. E., Wong, J., Chauhan, D., Richardson, P., Schreiber, S. T., Anderson, K. C. Small-molecule inhibition of proteasome and aggresome function induces synergistic antitumor activity in multiple myeloma. PNAS 2005; 102:8567–8572.

15. Arce, C. A., Casale, C. H., Barra, H. S. Submembraneous microtubule cytoskeleton: regulation of ATPases by interaction with acetylated tubulin. FEBS 2008; 275:4664–4674.

16. Hubbert, C., Guardiola, A., Shao, R., Kawaguchi, Y., Ito, A., Nixon, A., Yoshida, M., Wang, X. F. and Yao, T. P. HDAC6 is a microtubule-associated deacetylase. Nature 2002; 417:455–458.

17. Matsuyama, A., Shimazu, T., Sumida, Y., Saito, A., Yoshimatsu, Y., Seigneurin-Berny, D., Osada, H., Komatsy, Y., Nishino, N., Knochbin, S., Horinouchi, S., Yoshida, M. In vivo destabilization of dynamic microtubules by HDAC6-mediated deacetylation. EMBO J. 2002; 21:6820–6831.

18. Verdel, A., Khochbin, S. Identification of a new family of higher eukararyotic histone deacetylases: coordinate expression of differentiation-dependent chromatin modifiers. J. Biol. Chem. 1999; 274:2440–2445.

19. Zhan, Y., Li, N., Caron, C. Matthias, G., Hess, D., Khochbin, S., Matthias, P. HDAC-6 interacts with and deacetylates tubulin and microtubules in vivo. EMBO J. 2003; 1168–1179.

20. Zhang, Y., Gilquin, B., Khochbin, S., Matthias, P. Two catalytic domains are required for protein deacetylation. J. Biol. Chem. 2006; 281:2401–2404

21. Zou, Y., Navre, M., Sang, B. –C. Characterization of the two catalytic domains in histone deacetylase 6. Biochem. Biophys. Res. Commun. 2006; 341:45–50

22. Rodriguez-Gonzalez, A., Lin, T., Ikeda, A. L., Simms-Waldrip, T., Fu, C., Sakamoto, K. M. Role of the aggresome pathway in cancer: targeting histone deacetylase 6-dependent protein degradation. Cancer Res. 2008; 68:2557–2560.

23. Boyault, C., Sadoul, K., Pabion, M., Khochbin, S. HDAC6 at the crossroads between cytoskeleton and cell signaling by acetylation and ubiquitination. Oncogene 2007; 26:5468–5476.

24. Finnin, M. S., Donigian, J. R., Cohen, A., Richon, V. M., Rifkind, R. A., Marks, P. A., Breslow, R., Pavletich, N. P. Structures of a histone deacetylase homologue bound to the TSA and SAHA inhibitor. Nature 1999; 401:188–193.

25. Miller, C. P., Ban, K., Dujka, M. E., McConkey, D. J., Munsell, M., Palladino, M., Chandra, J. NPI-0052, a novel proteasome inhibitor, induces caspase-8 and ROS-dependent apoptosis alone and in combination with HDAC inhibitors in leukemia cells. Blood 2007; 110:267–277.

26. Hershko, A. Ciechanover, A. The ubiquitin system. Annu. Rev. Biochem. 1998; 67:425–479.

27. Vaux, D. L., Cory, S., Adams, J. M. Bcl-2 gene promotes haemopoietic cell survival and cooperates with c-myc to immortalize pre-B cells. Nature 1988; 335:440–442.

28. Kaufann, S. H., Hengartner, M. O. Programmed cell death: alive and well in the new millennium. Trends Cell Biol. 2001; 11:526–534.

29. Reed, J. C. Bcl-2 and the regulation of programmed cell death. J. Cell Biol. 1994; 124:1–6.

30. Kawaguchi, Y., Kovacs, J. J., McLaurin, A., Vance, J. M., Ito, A., Yao, T. P. The deacetylase HDAC6 regulates aggresome formation and cell viability in response to misfolded protein stress. Cell 2003; 115(6):727–738.

31. Santander, V. S., Bisig, C. G., Purro, S. A., Casale, C. H., Arce, C. A., Barra, H. S. Tubulin must be acetylated in order to form a complex with membrane Na^+, K^+ - ATPase and to inhibit its enzyme activity. Mol. Cell Biochem. 2006; 291(1-2):167–174.

32. Lingrel, J. B., Kuntzweiler, T. Na+,K+-ATPase. J. Biol. Chem. 1994; 269:19659–19662.

33. Koksoy, A. A., Na^+,K^+-ATPase: a review. J. Ankara Med. Sch. 2002; 24:73–82.

34. Casale C. H., Previtali, G., Barra, H. S. Involvement of acetylated tubulin in the regulation of Na^+,K^+-ATPase activity in cultured astrocytes. FEBS J. 2003; 534:115–118.

35. Fujiki, Y., Hubbard, A. L., Fowler, S., Lazarow, P. B. Isolation of intracellular membranes by means of sodium carbonate treatment: application to endoplasmic reticulum. J. Cell Biol. 1892; 93:97–102.

36. Alonso, A del C., Nunez-Fernandez, M., Beltramo, D. M., Casale, C. H., Barra, H. S., Na^+,K^+-ATPase was found to be the membrane component responsible for the hydrophobic behaviour of the brain membrane tubulin. Biochem. Biophys. Res. Commun. 1998; 253:924–927.

37. Hughes, F. M., Bortner, C. D., Purdy, G. D., Cidlowski, J. A. Intracellular K^+ suppresses the activation of apoptosis in lymphocytes. Biol. Chem. 1997; 272:30567–30576.

38. Bortner, C. D., Gomez-Angelats, M., Cidlowski, J. A. Plasma Membrane depolarization without repolarization is an early molecular event in anti-Fas-induced apoptosis. Biol. Chem. 2001; 276:4304–4314.

39. Raghavendra, P. B., Sreenivasan, Y., Ramesh, G. T., Manna, S. K. Cardiac glycoside induces cell death via FasL by activating calcineurin and NF-AT, but apoptosis initially proceeds through activation of caspases. Apoptosis 2007; 12:307–318.

40. Aldana-Masangkay, G. I., Rodriguez-Gonzalez, A., Lin, T., Ikeda, A. K., Hsieh, Y-T., Kim, Y.-M., Lomenick, B., Okemoto, K., Landaw, E. M., Wang, D., Mazitschek, R., Bradner, J. E., Sakamoto, K. M. Tubacin suppresses proliferation and induces apoptosis of acute lymphoblastic leukemia cells. Leuk. Lymphoma 2011; 52:1544–1555.

41. Wang, X. Q., Xiao, A. Y., Sheline, C., Krzystztof , H., Yang, A., Golberg, M. P. Choi, D. W., Yu, S. P. Apoptotic insults impair Na^+, K^+-ATPase activity as a mechanism of neuronal death mediated by concurrent ATP deficiency and oxidant stress. J. Cell Sci. 2003; 116:2099–2110.

42. Nobel, C. S., Aronson, J. K., van den Dobbelsteen, D. J., Slater, A. F. G. Inhibition of Na^+-K^+-ATPase may be one mechanism contributing to potassium efflux and cell shrinkage in CD95-induced apoptosis. Apoptosis 2000; 5:153–163.

43. Esmann, M. ATPase and phosphatase activity of Na^+,K^+-ATPase: molar and specific activity, protein determination. Meth. Enzymol. 1979; 156:105–115.

44. Kulikov, A., Eva, A., Kick, U., Boldyrev, A., Scheiner-Bobis, G. Oubain activates signaling pathways associated with cell death in human neuroblastoma. BBA 2007; 1768:1691–1702.

45. James, P. F., Grupp, I. L., Grupp, G., Woo, A. L., Askew, G. R., Croyle, M. L., Walsh, R. A., Lingrel, J. B. Identification of a specific role for the Na,K-ATPase alpha 2 isoform as a regulator of calcium in the heart. Mol. Cell 1999; 3:555–563.

46. Grupp, I., Im, W. B., Lee, C. O., Lee, S. W. Pecker, M. S., Schwartz, A. Relation of sodium pump inhibition to positive inotropy at low concentrations or ouabain in rat heart muscle. J. Physiol. 1985; 360:149–160.

47. Namdar, M. Perez, G., Ngo, L. Marks, P. A. Selective inhibition of histone deacetylase 6 (HDAC6) induces DNA damage and sensitizes transformed cells to anticancer agents. Proc. Natl. Acad. Sci. USA 2001; 107:20003–20008.

CHAPTER 3

Summation

3.1 Conclusions and Future Work

This project has sought to target the survival pathways of AML and ALL with, respectively, such small molecules as XX-650-23 and tubacin and to understand their mechanisms of action. Contemporary chemotherapy treatments against AML and ALL have resulted in five-year event-free survival of 60 percent for childhood AML, 20 percent for adult AML, and 80 percent for pediatric ALL [1]. In order to improve the selective killing of transformed cells, we targeted CREB in AML cells with XX-650-23 and the aggresome pathway and ATPase pump in ALL cells with tubacin.

Chapter 1 introduced CREB as a transcription factor that plays a critical role in regulating normal hematopoiesis and leukemogenesis. Previous reports from our laboratory found the overexpression of CREB in myeloid leukemic blasts and in leukemia stem cells from patients with myeloid leukemia [2, 3]. Our lab found that CREB contributed to — but could not, by itself, cause — leukemogenesis in CREB transgenic mice [3]. These results suggested that the inhibition of CREB could lead to a decrease of AML survival.

For this reason, our project sought to target CREB to establish whether this transcription factor may be an important therapeutic target. We reported that XX-650-23 is a small, cell-permeable molecule that inhibits the formation of the CREB:CBP complex and works to decrease the expression of CREB-dependent genes. Our study found that XX-650-23 inhibited proliferation of HL60 and KG-1 cells, with an IC50 of less than 1 μM. XX-650-23 (2 μM) had a similar growth-inhibiting effect on AML BM and relapsed AML BM cells but, at the same concentration, did not affect normal BM cells. This study reported approximately twofold and fourfold therapeutic indices in AML BM samples and AML cell lines, respectively.

To examine the mechanism of XX-650-23, we attempted to perform coimmunoprecipitation experiments with CBP and CREB to demonstrate disruption of the complex following XX-650-23 treatment. Our attempts to perform binding studies using immunoprecipitation assays proved technically infeasible, since AML cells have limited levels of CBP. However, our laboratory observed the suppression of luciferase activity in HEK-293T cells transiently transfected with a CRE-RLuc plasmid in the presence of XX-650-23 at an IC50 of less than 1 μM. Future investigations will measure CREB transcriptional activity using AML cells that have been transduced with a CRE-RLuc plasmid in the presence of XX-650-23 to investigate the efficacy of this compound in AML cells.

To investigate whether apoptosis contributes to the observed inhibition of AML cell growth is due to apoptosis, we treated both HL60 and KG-1 cells with XX-650-23 and found that although apoptosis occurs, it is not the predominant pathway, as

indicated by the low levels of cleaved PARP at the studied dose. FACS analysis showed that XX-650-23 does induce cell death in a time- and dose-dependent manner. The observation that HL60 cells were more sensitive than KG-1 cells to apoptosis suggests the need to investigate the potential apoptotic effect mediated by XX-650-23 in more AML cell lines.

We found that at a dose of approximately 1 micromolar XX-650-23 delays the cell cycle in the G1/S phase, and this is likely the predominant mechanism by which CREB inhibition reduces AML cell growth. This is mediated through downregulation of CREB target genes, such as cyclin A1, cyclin D1, FOS1 and Beclin1. The delayed cell cycle could stress the cells, producing a secondary apoptotic effect that contributes to the inhibition of AML cell survival and proliferation. We plan to perform a cell cycle analysis of KG-1 cells in the presence and absence of XX-650-23 at four-hour intervals to verify our result. A microarray analysis of AML cells treated with 1 μM XX-650-23 will help determine the genes directly affected by the compound in order to further analyze its mechanism of action.

Combination chemotherapy is the standard of care for patients with AML, and establishing drug synergy is an important goal for new chemotherapeutics. XX-650-23 is unique, in that because it delays the cell cycle at the G1/S transition, chemotherapeutics that work best when cells are in this phase would be more efficacious. In order to test the hypothesis that CREB inhibition would improve the efficacy of already established chemotherapeutics, we combined XX-650-23 with cytarabine or daunorubicin and found that XX-650-23 acts synergistically with cytarabine in both KG-1 and HL60 cell lines.

The effect of combining XX-650-23 with daunorubicin depended on the cell type, yielding a slightly antagonistic effect in HL60 and an additive effect in KG-1 cells. Our results indicate that XX-650-23 increases the effect of cytarabine in both AML cells; therefore, future experiments in our laboratory should include *in vivo* drug combination studies in which we subcutaneously inject AML cells into SCID IL-2Rgamma Null (NSG) to induce them to develop tumors. Our finding also suggests that XX-650-23 may induce a response in AML patients that exhibit resistance to cytarabine. To validate this hypothesis, AML cells could be treated with cytarabine for 72 hours and the cells that survive could then be treated with XX-650-23 for 72 hours to examine whether those cells respond to this treatment.

CREB and CBP are both known to regulate critical cellular processes such as the cell cycle and apoptosis; however the KIX domain of CBP can also bind other proteins. It will be of interest to determine if XX-650-23 disrupts the binding of other molecules to the KIX domain of CBP, thus having a dual effect on inhibiting other key pathways important for leukemia cell growth and survival. This would establish increased versatility of this compound, as it is possible that it may not only disrupt the CREB:CBP complex. In the future, KG-1 cells that were nucleofected with CBP can be used to perform coimmunoprecipitation studies with the already known proteins that bind to the KIX-CBP domain. Another alternative is to perform a protein pull down assay, by incubating purified Tag-KIX-CBP domain with AML or shRNA CREB AML cell extracts. The eluted bound proteins can be examined by western blot and the identified bands can be analyzed by mass spectrometry.

Although, it is known that CREB is capable of altering the transcription of a multitude of genes, it is unclear which ones are key for the abnormal proliferation and survival of leukemia cells. Our microarray experiment will offer clues as to the changes mediated by XX-650-23, by determining which CREB genes stand as the primary determinant of cell function. From our microarray data, one could select targets more likely to influence specific cell processes such as apoptosis or cell cycle, and manipulate the levels of these genes to examine their importance in AML cell function. .

In conclusion, XX-650-23 stands as a novel CREB inhibitor; it is efficacious, nontoxic, and synergizes with cytarabine, a chemotherapeutic drug already in clinical use against AML.

Chapter 2 described tubacin as a small molecule specific for the tubulin deacetylase activity of HDAC6. Inhibition of HDAC6 has been reported to induce acetylation of α-tubulin and consequently hinder the aggresome pathway in MM cells [4, 5]. HDAC6 binds ubiquitinated misfolded proteins and dynein in order to transfer the cargo to the aggresome along the MTs [6–8]. Tubacin-mediated increases in the acetylation of tubulin disrupted HDAC6 binding with dynein, and this resulted in the accumulation of polyubiquitinated misfolded proteins that contribute to the bortezomib-mediated apoptosis of MM cells [5]. The effect of tubacin had not been tested in ALL cells.

In our laboratory, tubacin was found to suppress proliferation of a variety of ALL cell lines, with IC50s ranging from 1.3 μM to 2 μM. AlamarBlue assays verified that the tubacin IC50 in Jurkat cells was approximately 2 μM. Our investigation found that

tubacin induced apoptosis, as indicated by the presence of PARP cleavage. Furthermore, our team found that tubacin sufficed to inhibit the aggresome pathway, leading to an accumulation of polyubiquitinated misfolded protein and apoptosis after twelve hours of treatment; however, the JNK/SAP kinases did not play a role in the tubacin-mediated apoptotic signals in ALL cells [9].

Increased levels of tubulin acetylation have been reported to inhibit the Na^+/K^+-ATPase pump, creating an ion imbalance that stimulates the release of Ca^{2+} from the ER to the cytosol and eventually activates caspases involved in apoptosis [10–13]. We examined whether tubacin may induce the same effect, contributing to apoptosis in ALL cells. We found that the levels of acetylation started increasing as early as 30 minutes after tubacin treatment in ALL cells [9]. In the cytosol, we also observed decreased levels of K^+ after six hours of tubacin treatment and increased Ca^{2+} and PARP cleavage after twelve hours of tubacin treatment. These results suggest that tubacin inhibits the Na^+/K^+-ATPase pump, further contributing to apoptosis. In a different study, apoptotic insults led to impaired Na^+/K^+-pump activity as a mechanism of neuronal death, due to a combination of energy deficiency and production of reactive oxygen species [14]. Based on previous reports, we see the need to study potential tubacin-mediated mitochondrial stress mechanisms that lead to apoptosis in ALL cells. Furthermore, since our results did not demonstrate that tubacin increased phosphorylation of JNK/SAP kinases, as seen with myeloma cells [15], activation of alternative signaling pathways warrant examination.

In order to determine whether tubacin directly affects the ATPase pump, we examined the direct *ex vivo* Na^+/K^+-ATPase enzymatic activity. We found that ouabain directly inhibits Na^+/K^+-ATPase enzymatic activity. Tubacin was also capable of inhibiting the Na^+/K^+-ATPase, though through an indirect mechanism. Tubacin-mediated HDAC6 inhibition may alter membrane fluidity [16, 17], leading to the inhibition of the Na^+/K^+-ATPase pump.

Our laboratory also performed drug combination studies with tubacin along with vincristine or bortezomib and found that combined treatment decreased the viability of cells more than tubacin alone. We also found that tubacin suppresses leukemic progression in NOD/SCID mice injected with Nalm-6 cells expressing luciferase. Together, these results suggest that tubacin can act as an agent to potentiate the effect of standard chemotherapy drugs against ALL.

New drugs that overcome resistance to the standard chemotherapy against acute leukemia are needed. XX-650-23 and tubacin may be used as reference compounds to synthesize potential chemotherapeutic agents with low toxicity and greater specificity effects against leukemic cells.

3-2 References

1. Pui C. H., Carrol W.L., Meshinchi S, Arceci R. J. Biology, risk stratification, and therapy of pediatric acute leukemias: an update. J. Clin. Oncol. 2011; 29(5):551–565.

2. Crans-Vargas, H. N., Landaw, E. M., Bhatia, S., Sandusky, G., Moore, T. B., Sakamoto, K. M. Expression of cyclic adenosine monophosphate response-element binding protein in acute leukemia. Blood 2002; 99(7):2617–2619.

3. Shankar, D. B., Cheng, J. C., Kinjo, K., Federman, N., Moore, T. B., Gill, A., Rao N. P., Landaw, E. M., Sakamoto, K. M. The role of CREB as a proto-oncogene in hematopoiesis and in acute myeloid leukemia. Cancer Cell 2005; 7(4):351–362.

4. Haggarty, S. J., Koeller, K. M., Wong, J. C., Grozinger, C. M., Scheiber, S. L. Domain-selective small-Molecule inhibitor of histone deacetylase 6 (HDAC6)-mediated tubulin deacetylation. PNAS 2003; 100:389–4394.

5. Hideshima, T., Bradner, J. E., Wong, J., Chauhan, D., Richardson, P., Schreiber, S.T., Anderson, K. C. Small-molecule inhibition of proteasome and aggresome function induces synergistic antitumor activity in multiple myeloma. PNAS 2005; 102:8567–8572.

6. Aldana-Masangkay, G. I., Sakamoto, K. M. The Role of HDAC6 in Cancer. J. Biomed and Biotech. 2011; 2011:875824.

7. Rodriguez-Gonzalez, A., Lin, T., Ikeda, A. L., Simms-Waldrip, T., Fu, C., Sakamoto, K. M. Role of the aggresome pathway in cancer: targeting histone deacetylase 6- dependent protein degradation. Cancer Res. 2008; 68:2557–2560.

8. Kawaguchi, Y., Kovacs, J. J., McLaurin, A., Vance, J. M., Ito, A., Yao, T. P. The deacetylase HDAC6 regulates aggresome formation and cell viability in response to misfolded protein stress. Cell 2003; 115:727–738.

9. Aldana-Masangkay, G. I., Rodriguez-Gonzalez, A., Lin, T., Ikeda, A. K., Hsieh, Y.-T., Kim, Y. –M., Lomenick, B., Okemoto, K., Landaw, E. M., Wang, D., Mazitschek, R., Bradner, J. E., Sakamoto, K. M. Tubacin suppresses proliferation and induces apoptosis of acute lymphoblastic leukemia cells. Leuk. Lymphoma 2011; 52(8):1544–1555.

10. Santander, V. S., Bisig, C. G., Purro, S. A., Casale, C. H., Arce, C. A., Barra, H. S. Tubulin must be acetylated in order to form a complex with membrane / K^+-ATPase and to inhibit its enzyme activity. Mol. Cell Biochem. 2006; 291:167–174.

11. Fujiki, Y., Hubbard, A. L., Fowler, S., Lazarow, P. B. Isolation of intracellular membranes by means of sodium carbonate treatment: application to endoplasmic reticulum. J. Cell Biol. 1892; 93:97–102.

12. Hughes, F. M., Bortner, C. D., Purdy, G. D., Cidlowski, J. A. Intracellular K+ suppresses the activation of apoptosis in lymphocytes. Biol. Chem. 1997; 272:30567–30576.

13. Raghavendra, P. B., Sreenivasan, Y., Ramesh, G. T., Manna, S. K. Cardiac glycoside induces cell death via FasL by activating calcineurin and NF-AT, but apoptosis initially proceeds through activation of caspases. Apoptosis 2007; 12:307–318.

14. Wang, X. Q., Xiao, A. Y., Sheline, C., Krzystztof , H., Yang, A., Golberg, M. P. Choi, D. W., Yu, S. P. Apoptotic insults impair Na^+, K^+-ATPase activity as a mechanism of neuronal death mediated by concurrent ATP deficiency and oxidant stress. J. Cell Sci. 2003; 116:2099–2110.

15. Aldana-Masangkay, G. I., Rodriguez-Gonzalez, A., Lin, T., Ikeda, A. K., Hsieh, Y-T., Kim, Y.-M., Lomenick, B., Okemoto, K., Landaw, E. M., Wang, D., Mazitschek, R., Bradner, J. E., Sakamoto, K. M. Tubacin suppresses proliferation and induces apoptosis of acute lymphoblastic leukemia cells. Leuk. Lymphoma 2011; 52:1544–1555.

16. Carew, J. S., Giles, F. J., Nawrocki, S. T. Histone deacetylase inhibitors: Mechanisms of cell death and promise in combination cancer therapy. Cancer Lett. 2008; 269:7–17.

17. Koksoy, A. A., Na+,K+-ATPase: a review. J. Ankara Med. Sch. 2002; 24:73–82.